THE EFFECT OF SQUISH ON TURBULENCE IN SPARK IGNITION ENGINE COMBUSTION CHAMBERS

by

R. ANTON

THESIS: Submitted in fulfillment of the requirements for the award of Master of Science of Loughborough University of Technology.

SUPERVISOR: Dr. G.G. LUCAS

February 1978

ACKNOLEDGEMENTS

The author wishes to acknoledge the helpful advice given by Dr G.G. Lucas who supervised this work.

The sponsorship of the project by the Ford Motor Company and the Science Research Council were greatly appreciated.

The author also wishes to thank for the assistance given by the technical staff of the Department of Transport Technology of Loughborough University of Technology.

S U M M A R Y

The thesis is concerned with the study of the effects of squish on the turbulence structure in the combustion chamber of a spark ignition engine.

Existing hot wire anemometry calibration techniques have been studied and an improved version developed.

A data acquisition and processing system has been developed whereby the raw data is digitised and processed by a Hewlett Packard computer, thus making possible the analysis of a large number of cycles.

The data acquisition system fulfills the requirement of perfect synchronisation with the crank rotation to ensure the accurate location of every event in the engine cycle.

Nine combustion chambers have been tested. One was a datum chamber with no squish and the rest featured increasing squish areas ranging from 5 to 20%. Two locations of each of these were studied: all in one place and equally divided into two areas.

The mean air velocity, turbulence intensity, relative turbulence intensity and macro scales of turbulence have been calculated for everyone of these chambers. The probe position and engine speed were altered to create a complete image of the flow structure in the combustion chamber.

It was found that the intake jet creates a strong body swirl motion in the combustion chamber. This persists during the compression stroke and is only broken up if large squish areas are present.

It was also found that the effect of squish on the turbulence level is to increase the frequency of rotation of the eddies.

The eddy size does not alter but more eddies are created and they have faster rotational motions.

NOTATION

I_o – probe current at ambient conditions

I – probe current during engine tests

V_W – voltage across wire

V_B – bridge voltage

R_W – wire operating resistance

R_L – wire element operating resistance

R_1 – resistance in bridge arm in series with probe arm = 50Ω

R_C – total conductor resistance in the leads and probe body

A – wire crossectional area

A_X – surface area of wire element

A_S – surface area of wire

T_W – wire operating temperature

T_g – gas temperature

T_L – wire element temperature

T_S – temperature of the surroundings

T_f – film temperature

T_o – ambient temperature

T_{μ} – prong temperature

Q_{sup} – heat supplied to the wire

Q_C – heat loss through conduction

Q_e – heat loss through convection

Q_r – heat loss through radiation

n – polythropic index of compression

c_p – gas specific heat at constant pressure

c_v – gas specific heat at constant volume

R – Universal gas constant

d – wire diameter

l - wire length

h - convection heat transfer coefficent

Re - Reynolds Number

NU - Nusselt Number

U - Instantaneous gas velocity

$\bar{U}$ - average gas velocity

u - instantaneous air velocity fluctuation

$\bar{u}$ - turbulence intensity

$R(i)$ - relative turbulence intensity

$R_I(i)$ - non stationary autocorrelation coefficient

$T(i)$ - time macro scale of turbulence

$L(i)$ - length macro scale of turbulence

ΔP - pressure drop in calibration tunnel

P_o - ambient pressure

λ_w - air thermal conductivity at hot wire temperature

λ_g - air thermal conductivity at gas temperature

λ_L - thermal conductivity of wire element at its temperature

λ_H - thermal conductivity of the wire material at the temperature of the prongs

σ - Stefan Boltzmann's constant 5.693 x 10 J/m sec K^4

ϵ - wire emissity = 0.1

α - thermal coefficent of resistance for wire material

ρ - gas density

μ - gas dynamic viscosity

γ - ratio of specific heats = 1.4

LIST OF FIGURES

All figures for a particular section appear at the end of the section in which they are refered to.

INDEX OF CONTENTS

CHAPTER 1

INTRODUCTION

INTRODUCTION

A great deal of work has been done in recent years to improve the operation of spark ignition engines.

Legislation limiting the amount of exhaust pollutants has been adopted in many countries. At the same time the energy crisis created the advent of an energy conscious society in which governments are taking serious steps towards limiting the fuel consumption of passenger vehicles.

Consequently the motor manufactuers and the research organisations focused their attention on the combustion process in internal combustion engines.

Lean mixture running is an obvious answer to the problems outlined above. This would guarantee low fuel consumption figures and clean exhaust gases. However most engines are reluctant to run smoothly on lean mixtures and sometimes special combustion systems have to be developed.

One answer is the stratified charge engine which has the ability to run on lean mixtures at the expense of increased mechanical complication. High compression ratios in conjunction with lean mixtures has also been known to give good results. Another trend of thought is to enhance the turbulence level in the combustion chamber. Various turbulence promoters or high turbulence combustion chambers have been tried with various degrees of success. One of the best known methods of increasing the turbulence level is squish. It is a feature of many production engines and in some of these it features the ability to run on lean mixtures.

However the mechanism through which squish generates turbulence is not completely understood. It is not clear which of the air flow parameters are affected by a squish configuration. The turbulence intensity or the time or length scales can be affected separately or all at the same time. It is also accepted that there is an optimum degree of squish at which a particular combustion chamber performs best. This is based only on empirical experience and no satisfactory theoretical explanation of the process involved has yet been found.

Consequently this study was envisaged with the following goals:

- The measurement of the average velocities in combustion chambers differing only by the degree of squish built in and the precise location of these velocities within the engine cycle.
- The measurement of the turbulence intensities in the combustion chambers and their location in the cycle.
- The calculation of the turbulence scales for every combustion chamber and their precise location in the engine cycle.

To answer these problems the obvious research tool is the hot wire anemometer. A number of research reports have been published, outlining the use of hot wire anemometry systems to measure the turbulence levels of the air trapped inside the combustion chamber of an internal combustion engine.

This report is a continuation of a previous study by James(6) in which the turbulent flow in the combustion chamber and the effect of the compression ratio have been studied.

A data acquisition and processing system has been developed and one of its benefits is that it can be used with other types of engine related research work.

The investigation of the flow in the combustion chamber using a hot wire probe in a motored engine is hardly likely to give all the answers to the problems outlined above. This has to be backed by comparative studies in fired engines which will relate the air flow pattern to the combustion response. This work is currently under way and a report will follow at a later date.

The thesis contains a review of the best known flow measurement techniques emphasising the principle and characteristics of the hot wire anemometer.

This is preceded by a survey of the reports covering the areas of measurement techniques and investigation of turbulence in general and squish in particular.

A description of the test rig and the associated instrumentation is given in Chapter (6). A detailed presentation of the problems related to the use of hot wire anemometry systems in unsteady flows follows.

This is followed by a description of the data acquisition system. The development of this took a large proportion of the time devoted to the experimental work.

The main part of the thesis finishes with the discussion of the results and the conclusions and recommendations for further work.

The appendices follow dealing with the experimental procedure, the evaluation of the polytropic index of expansion, and a listing of the computer programs used in the calibration process and in reducing the data.

A list of references is given at the end of the thesis.

CHAPTER 2

LITERATURE SURVEY

Literature Survey

There is a sizeable amount of information covering flow measurement techniques applicable to the gas motion in engine combustion chambers.

The detectors as well as the techniques vary from water models to hot wire anemometry systems.

Huebner and McDonald (9) used a large scale water model to arrive at a number of maps of the flow inside the clearance volume above the piston. Although the fluid used was incompressible and the speed was low (60-80 rpm), the velocity distribution trends show a number of interesting features. The most important of these is the general decrease in flow velocity in the centre of the combustion chamber.

Daneyshar et al (35) used a water analogy rig to study the characteristics of the fluid flow in the cylinder of an engine. He observed the development of rolling vortices as the piston scrapes the cylinder wall. These increase in size as the piston approaches T.D.C. However, the regularity of their shape is destroyed, as the engine speed increases, to such an extent that the vortex motion becomes insignificant at high engine speeds.

The work of Ohigashi et al(33,34)led to the conclusion that the combustion during one cycle had very little effect on the mixture velocity during the following cycle. It thus follows that hot wire measurements in motored engines are good representations of the mixture motion prior to ignition. A modified form of electric discharge anemometry was used for their tests. This was based on the fact that the path of an electric discharge moves in the direction of the flow of a gas stream. If a probe, then detects the arrival of the discharge, the gas velocity would be a function of the time elapsed between the beginning of the discharge and its arrival at the detection point.

One of the earliest comprehensive studies on gas motion in engine combustion chambers was done by Semenov (1958) (26). He placed a hot wire probe in the combustion chamber of an engine to study the effects of various parameters as : engine speed, throttling, compression ratio on the flow velocity. Also the probe was traversed across the combustion chamber. The conclusion of his work was that the nature of the air motion in the combustion chamber is largely due to the jet motion of the flow past the inlet valve. This jet sets up large velocity gradients which lead to a high and persisting degree of turbulence. During compression the jet action disappears but it leaves behind a turbulent gas motion. It was also found that most of the turbulent energy was limited to frequencies below 1000 Hz.

Semenov concluded that the turbulence levels do not vary greatly during compression and expansion and that the turbulence intensities do not vary much at the locations in the combustion chamber where measurements have been taken. His calibration technique compensated for the pressure and temperature changes by reducing the probe current at high temperature and pressure conditions to a current at ambient conditions. The air velocity was then derived from calibrations at ambient conditions. The relationship used was

$$I_o = K(\rho, T_g) \cdot I$$

where $K(\rho, T)$ is the coefficient of reduction which is dependent of the density and temperature of the gas.

Hassan (22) used a constant temperature anemometry system to study the heat transfer in an internal combustion engine. An analytical calibration technique was developed, which catered for the changes in pressure and temperature of the cylinder gas.

Horvatin and Hussmann (7) studied the charge motion in a high swirl type of combustion chamber. An analytical calibration procedure was used. A result of this work was a separate paper by Horvatin (20) which looked in considerable detail at the characteristics of hot wires used in flows of varying temperatures and pressures. He used a heat balance to arrive at a relationship also found by Davies and Fisher (18)

$$I^2\left[\frac{dR_W}{dx}\right]_x = \lambda_w A \frac{d^2T_W}{dx^2} + \pi d \sigma \left[T_W - \left(T_g + \eta_r \frac{U^2}{2c_p}\right)\right]$$

where

η_r is a recovery factor

c_p is the specific heat of the gas

However the merit of the work consists in the detailed analysis of errors that follows. The effects of the changes in the cold resistance are examined and the article suggests that a 3% error in the measurement of R_o can lead to an error in excess of 10% in the calculation of velocity. Also it was pointed out that if the prong temperatures are disregarded the errors in the evaluation of velocities are between 5 and 15%. On the other hand the measurement of the prong temperatures with only a 10% accuracy reduces the maximum error in the air velocity down to 1.5%

Winsor and Patterson (28) used a hot wire anemometer to measure the turbulence characteristics of the flow in an engine equipped with a shrouded inlet valve. The conclusions outlined the fact that the turbulence in the combustion chamber was isotropic and homogeneous and was not affected by the volumetric efficiency. The velocities were found to increase with the engine speed and the turbulence levels decreased during the compression stroke. The report also evaluates the suitability of 5μm and 10 μm wires for engine work. It was found that their response was practically identical and it was outlined that by using 10μm wires one has the advantage of better endurance.

Salama (23) used a hot wire to study the cyclic variation in gas velocity and the turbulence structure in spark ignition engines. A digital data acquistion process was used. Two commercially available types of combustion chambers were used namely wedge and Heron.

It was found that while the general characteristics in gas velocites are similar for most shapes of combustion chambers, the turbulence characteristics are mainly function of inlet, tract and combustion chamber shape. Salama, also carried out an evaluation of the turbulence scales from which it was found that at high engine speeds, the frequency of eddy rotation increased along with the turbulence intensity. An analysis of the effects of shrouded valves was carried out and it was concluded that while the velocities imparted continued well into the compression stroke the eddy frequencies did not change much as a result. By traversing the probe across the combustion chamber it was found that there is a zone, in the centre where the flow is statistically steady. It was also found that the squish components develop along the wedge wall of the combustion chamber rather than as single jets perpendicular to the cylinder axis. The calibration procedure was based on the relationship found by Davis and Fisher. (18) The same technique was also used by Hassan and Dent (10). The relationship used was based on a comprehensive heat balance for the hot wire. The mass flow past the wire was related to the convective heat transfer coefficient by

$$h=c_f \rho \frac{c_v \lambda_w}{\pi \cdot \lambda_g}$$

where ρ = airdensity at the free stream temperature

c_v = specific heat at constant volume

c_f = skin friction coefficient. This was defined as follows:

$$c_f=1.4\,Re^{-0.5} \quad \text{when} \quad 40<Re<1000$$

and

$$c_f=2.6\,Re^{-0.666} \quad \text{when} \quad 0<Re<50$$

James (6) studied the turbulent flow in the combustion chamber by comparing a disctype chamber with a squish chamber. It was found that most of the turbulent energy was contained below 1000 Hz. The data was analysed by passing the anemometer voltage through a bank of filters. Thus the analysis led to an evaluation of the velocity and turbulence components at various frequencies. It was found that the flow fluctuations in the cylindrical combustion chamber were much lower than those in the squish chamber. The calibration technique used is discussed in detail in Chapter (5) because this work is based on the same procedure.

Lancaster (27) used a triaxial hot wire probe to resolve the velocities in their cartesian components. The data was analysed using a digital data acquistion and processing system.

A number of parameters were altered to study their effect on the charge motion. These were: volumetric efficiency, engine speed, compression ratio and intake geometry. The gas velocities were found to increase with the engine speed and volumetric efficiency. The compression ratio did not have any effect on the velocity levels. The analysis of the data obtained shows that only 20% of the flow energy is contained at frequencies above 1000 Hz and only 2% above 5kHz. It was found that the in cylinder turbulence at TDC near compression is isotropic and is determined by the intake jet flow. To reduce the data Lancaster used a heat balance for the hot wire. He investigated the suitability and the allowances that have to be made when calibrating at ambient conditions for flows at high temperatures and pressures. These are discussed in more detail in Chapter (5).

Witze (30) used a hot wire anemometry system to measure the spatial distribution and engine speed dependence of turbulent air motion in an I.C. engine. This was used in conjunction with a high speed digital data acquisition and processing system. It was observed that both the mean velocity and the turbulence intensity vary with the engine speed. However the relative turbulence intensity stays practically constant during induction and compression.

Also the time and length scales of turbulence are only dependent on the chamber geometry. It was noted that the turbulence production by a squish volume would appear to be insignificant when compared to the compression stroke enhancement of intake generated turbulence. Witze states that the turbulence structure is not homogeneous in the clearance volume but he adds that it is not certain whether the degree of turbulence variation that exists is large enough to be significant to the mixing and flame preparation process.

An interesting point was raised by some private communication with P.O.Witze. This refers to some of his earlier work on hot wire measurements in I.C.engines. The air velocities were observed to peak at TDC of the compression stroke and again at about 30 after TDC. It was initially suggested that this rise was due to the effect of the squish area present in the combustion chamber. Later, however it was found that imperfect sealing of the probe at the combustion chamber wall can lead to this sort of result.

Witze used a calibration formula based on the relationship published by Collis and Williams. This was

$$U = \left[\frac{V_e^2}{b\left[\left(T_w - T_g\right)/T_g\right]^{0.17}\left(T_w - T_g\right)} - a/b\left(T_w + T_g\right)^{0.8} \right]^{\frac{1}{n}}$$

where a, b and n are constants determined from calibration.

The above survey lists the trends of thought concerning turbulence measurements in I.C. engines. It underlines that the hot wire anemometer is an accepted tool in this process and outlines some conclusions which are generally agreed upon.

However there are a number of phenomena not fully understood which led to inconsistent results. Thus there is scope for further research especially in the investigation of squish which generated a number of puzzling results and conflicting theories.

CHAPTER 3

FLOW MEASUREMENT TECHNIQUES

Flow measurement techniques.

Throughout the years numerous techniques have been used to detect the characteristics of fluid flows generally.

However, a relatively small number of these can be applied to the investigation of the fluctuating flow which exists in an engine combustion chamber.

Broadly speaking the various techniques fall in one of the following two categories according to the detector position relative to the fluid:

- The detection is made visible (to the eye or through some apparatus) by the use of a tracer introduced in the flow and which moves with the fluid under investigation. The detector (eye or apparatus) is situated outside the flow and does not interfere with it in any way.
- The flow characteristics are detected by a sensor introduced in the fluid and use is made of some change in the mechanical, physical or chemical properties of the sensor.

The following discussion of the available techniques will refer solely to the methods used in the past to detect the flow characteristics in engine combustion chambers.

Optical Methods

1. Particle track photography

When using this method, tiny particles are supplied to the incoming charge and their paths are recorded cinemato graphically or using flash photography. In both cases the speed of the moving fluid is found by relating the trace left by the particle on the film, to the exposure speed.

When the fluid is air and the particles are solid, in other words they have higher specific gravity one must allow for their different density.

Although the use of smoke or some coloured gas is generally favoured in steady state fluid dynamics studies, the mixing of these tracker fluids with the air makes any observation very difficult in engine work.

2. Light refraction by density variations

The variation in density of a fluid affects its refraction properties. These changes are used in techniques such as the Schlieren and the Shadowgraph methods.

A density gradient in a gas acts as a lens and it can change the path and alter the wavelength of a beam of light passing through.

Thus the Schlieren technique gives a visual image of the density gradients in the fluid, and this is identical to the physical vorteces existing in the fluid under study.

The shadowgraph method detects the gradient of the density change and hence it is used where extremely sharp density variations occur. It is used mostly in the study of shock waves.

Interferometry methods will give quantitative results evaluating the refractive index of the gas which is proportional to its density. This can then be related to the velocity of the gas.

3. Laser anemonetry

This is based on the principle that a laser beam is scattered in all directions from particles in a fluid flow. The particle velocity causes this scatter to be frequency shifted. By combining scattered laser rays from two incident beams an interference phenomenon occurs, and the resultant beat frequency (Doppler frequency) is proportional to the particle velocity.

There is more than one mode of operation of a laser anemometry system. However all of these are based on the pick up of the Doppler frequency.

When aiming the two convergent laser beams at a volume in the flow this appears (on a miniaturised scale) fringed. Where a particle crosses the light and dark fringes it will emit light pulses at a frequency dependent upon its velocity. This is the Doppler frequency which is detected by a photo-detector. Fig 3.1

The system requires that the flow is seeded with particles of sufficient size to allow the intensity of the scattered light to be detected. At the same time they must be light enough to represent the instantaneous velocity of the fluid.

The advantage of using the laser Doppler anemometer is that the measurements are not affected by the changes in density, pressure or temperature of the fluid under consideration and no calibration is required. However the velocity readings are not taken at one point because of the finite size of the beam.

The use of optical methods will normally yield qualitative results which will be a very good complement to any quantitative study.

Such methods however, when applied to engine studies suffer from either of the two following disadvantages.

1. The observations are made through windows which distort the light passing through them. This is due to the fact that either the windows are curved to follow the shape of the cylinder or that their material distorts or absorbs certain wavelengths.

2. The changes in density of the fluid are not only due to the flow but to the motion of the piston as well. This makes a comparative cycle analysis very difficult.

3. Their frequency response can be limited.

Detector Methods

There is a number of conditions that a detector must fulfil so that it can accurately and reliably measure the flow characteristics of a fluid:

These are:

1) The disturbance it causes to the flow must be minimal. Thus the detector and its mounting system must be very small so that it does not induce large velocity variations in its vicinity.

2) When measuring turbulence the detector must be smaller than the dimensions of the micro scales.

3) It must feature a high frequency response. The sensor must be able to respond quickly to sudden changes in the flow conditions. This must be matched with high sensitivity so that even small variations can be detected.

4) The instrument must be dynamically stable and free from response drift.

5) A highly desirable property which only a few instruments posses is a good directional sensitivity. Normally this can be obtained at the cost of increased complexity in the data acquisition process.

The only instrument that meets these requirements with any degree of success is the anemometer. This can be of one of a number of types which are listed below:

1. The laser Doppler anemometer.

2. The electric discharge anemometer.

3. The hot film anemometer.

4. The hot wire anemometer.

1. The principle of operation of the laser Doppler anemometer has already been mentioned in the previous chapter.

2. The electric discharge anemometer makes use of the fact thát air is not a perfect insulator and will allow the flow of minute currents if an electric field is created between two very close electrodes. This feeble current depends on the shape and gap of the electrodes, the characteristics of the electric field, the nature of the gas, the pressure, temperature, humidity and velocity. If all these characteristics, excluding the velocity, are kept constant, the characteristics of the discharge between the electrodes can be related to the velocity of the flow.

However, in an engine cylinder the temperature and pressure of the gas change with the crankshaft rotation and therefore difficulties are likely to arise if this method was used in engine studies.

Nevertheless the electric discharge anemometer is a good instrument to use in the study of steady state flows.

The hot wire and hot film anemometers are based essentially on the same principle, the only difference being the size and shape of the sensor. These two methods will be discussed under a common heading which refers to hot wire anemometry since this was the method used in this study.

The Hot Wire Anemometer

The operation of the hot wire anemometer is based on the heat loss from a very fine heated wire cooled by the surrounding fluid. The heat loss rate is proportional to the velocity of the fluid. The reduction in temperature causes a reduction of the wire resistance which in turn is sensed by a feedback circuit which is part of the hot wire anemometry system.

There are two modes of operation of a hot wire anemometer.

a) constant current.

b) constant temperature.

Each of these modes uses the wire sensor as an arm of a Wheatstone Bridge. Fig 3.2

In a constant current operation mode the probe is powered by a constant current from a power source with high internal resistance. Thus the current which passes through it is independent of any change in resistance of the probe. However, when the resistance of the probe changes because of the heat loss, the resulting bridge unbalance is detected, amplified and displayed on the anemometer meter.

The DC component of the bridge unbalance voltage is a measure of the mean velocity of the flow. Similarly the AC component is a measure of the velocity fluctuations about the mean.

However the system suffers from a number of disadvantages. The inherent thermal inertia of the wire can only be partially compensated by electrical circuitry. This can lead to the critical situation where in a flow with large velocity fluctuations the wire could be burned because it cannot recover to the nominal operating condition. Also the compensating network must allow for the thermal inertia of the wire at all temperatures. However, since these vary with the mean flow velocity it follows that the network settings must be adjusted every time the mean velocity changes. This is because the network time constant must equal the wire time constant at all times.

These drawbacks and its inherent low frequency response makes the constant current operation unsuitable for studies of highly turbulent flows.

The constant temperature mode overcomes the disadvantages of the constant current operation.

The technique in this case is to maintain the sensor at a constant temperature and to detect the current passing through it. This is then related to the heat loss and hence the flow velocity. As already mentioned the probe is an arm of a wheatstone bridge. When the bridge is in balance there is a voltage across its vertical diagonal. When the balance is upset by a change in the temperature of the sensor the result will be a change in its resistance. Following this the voltage which is generated across the bridge horizontal diagonal is amplified by theservo amplifier and supplied to the vertical diagonal. Thus an increase in flow velocity will cause a higher rate of heat loss and will lead to a decrease in the wire resistance. The amplifier will increase the bridge voltage thus increasing the probe current which in turn would heat the wire bringing its resistance back to the initial value. The process will reverse if the flow velocity decreases.

Although termed as constant temperature or constant resistance anemometer it can be seen that neither of these quantities remain rigorously constant. The small variations are essential for the operation of the system.

This mode of operation offers a high frequency response and is particularly suitable for high speed flows with high velocity fluctuations.

The sensor is normally a very fine wire suspended between two prongs. However, the film probes have a higher mechanical strength and they tend to be used in hostile environments but the operation is essentially the same. Their frequency response is somewhat lower than that of a hot wire sensor .

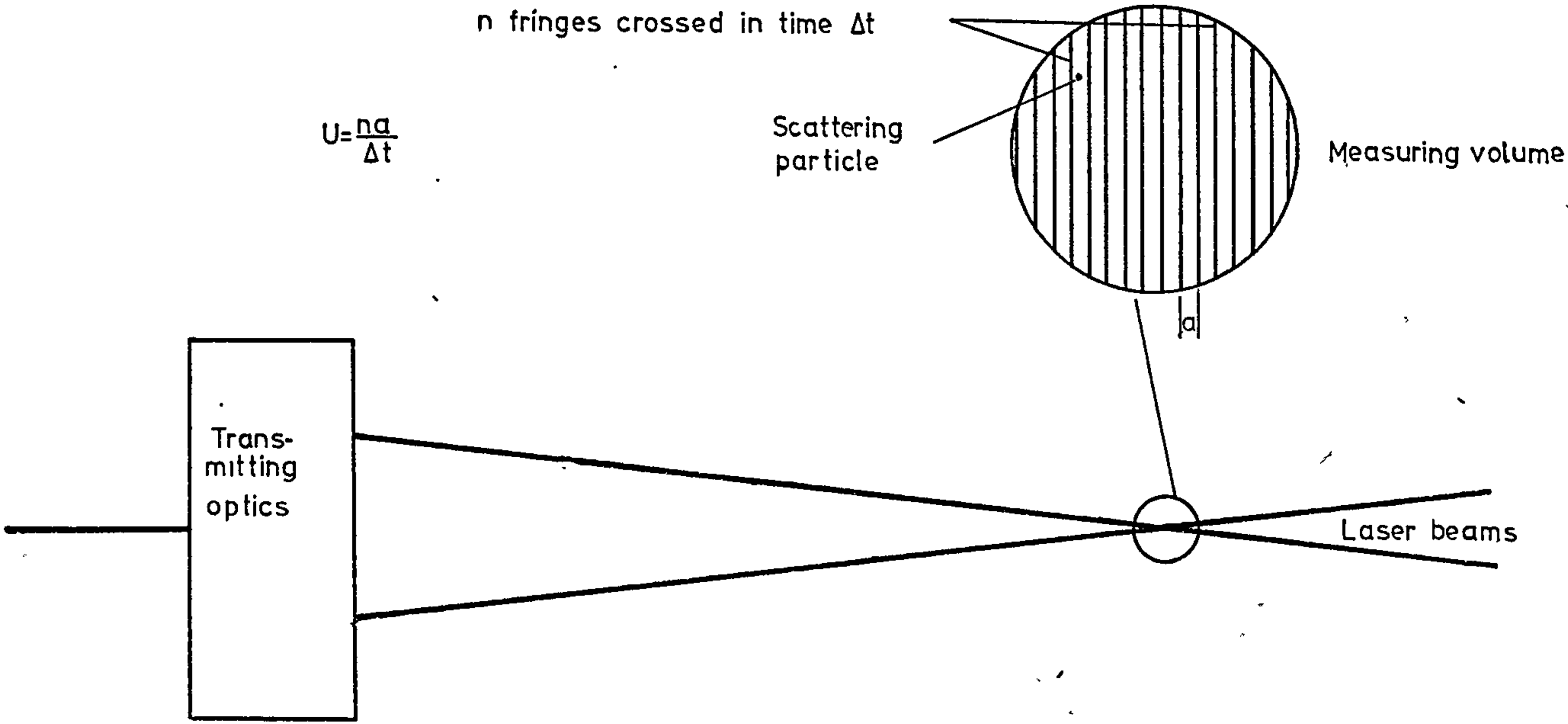

FIG 3·1 PRINCIPLE OF THE LASER-DOPPLER ANEMOMETER

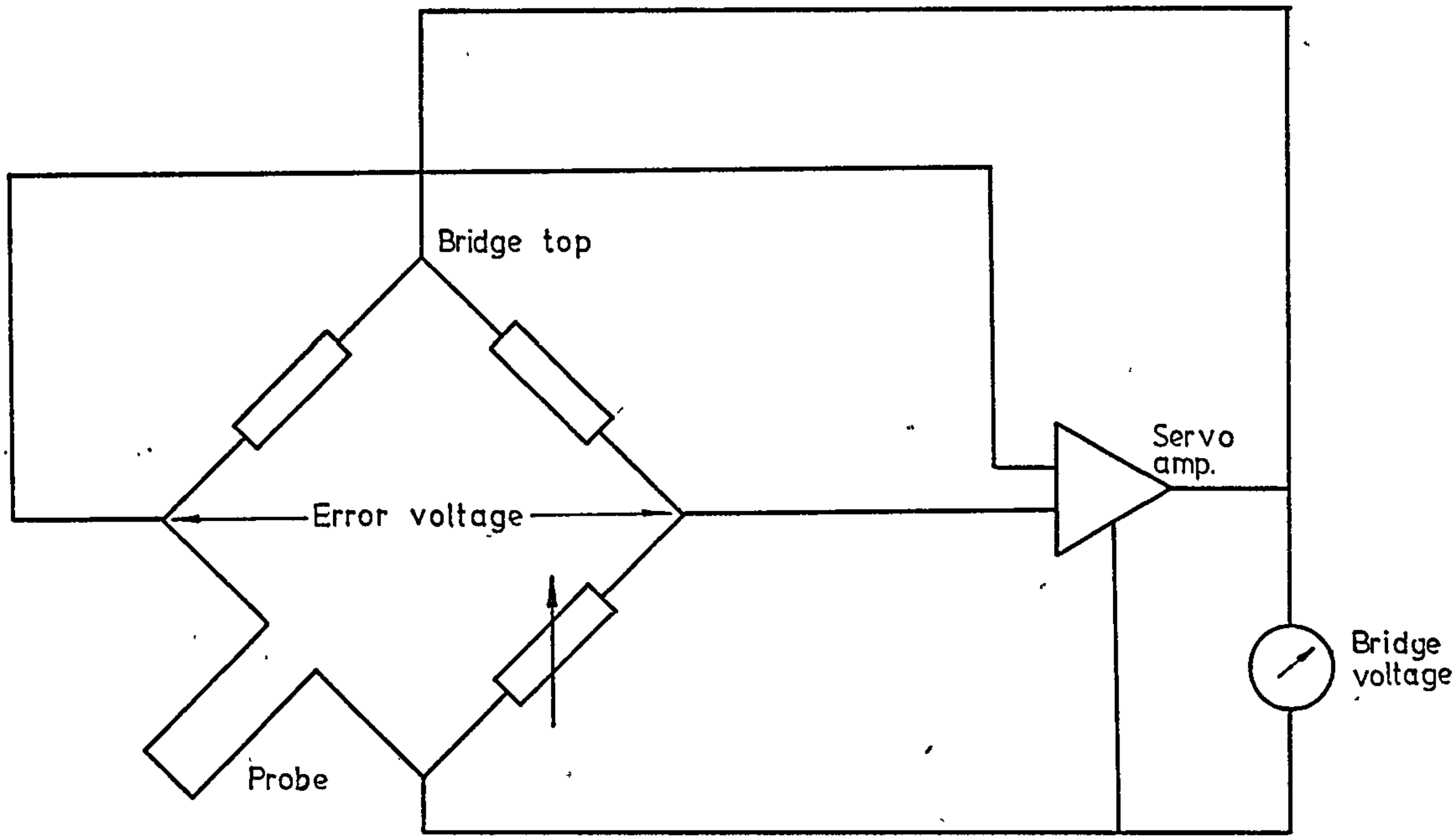

FIG 3.2 PRINCIPLE OF THE HOT WIRE ANEMOMETER

CHAPTER 4

CONSTANT TEMPERATURE ANEMOMETRY SYSTEMS AND THEIR CHARACTERISTICS

Constant Temperature Anemometry Systems and their Characteristics

The hot wire anemometer in unsteady flows

Hot Wire anemometry systems have been used for many years to investigate the characteristics of steady flows. Recently their characteristics encouraged more and more research workers to use them in the study of unsteady flows.

James (6) reviews the basic operational characteristics of a hot wire anemometer. He outlined the importance of the closed loop feedback circuitry which greatly enhances the frequency response of the instrument. It is noted that the frequency response of a circuit containing the hot wire probe in an open loop system is limited to about 1000 HZ . The time constant of the probe in this configuration only depends on the magnitude of the temperature and resistance changes it undergoes.

However, by employing a feedback technique, the frequency response of the system can be increased by a factor of several hundreds.

In practical terms the successful operation of the feedback system depends on the damping factor of the system. If the gain is extremely high and the damping factor approaches zero, the system becomes unstable when subjected to velocity charges.

Thus, when measuring high velocities and using high amplifier gains for high frequency response there is a danger of transition to unstable oscillations. To avoid this the anemometer used (D.I.S.A. 55D01) was equipped with an adjustable inductor in series with the probe. When properly adjusted this ensured that the damping factor of the system is set above the threshold value which could make the system unstable.

During the early stages of the work the damping factor setting otherwise known as the L. and Q. compensation, was set at ambient conditions for maximum frequency response. This was done by feeding square wave electrical disturbances into the amplifier which caused the wire resistance to vary. The anemometer response was monitored on an oscilloscope and the L and Q. controls were set so that the output did not feature any trace of inherent instability. In ambient conditions this procedure led to a gain setting of 8. However when introduced in the engine cylinder the wires soon broke for no apparent reason. This was explained by the fact that in the engine cylinder the wire is subjected to much more severe disturbing factors than in ambient conditions. This would make the circuitry unstable although the response was adequate at ambient conditions. A new L and Q compensation procedure was tried where the amplifier gain was set for the maximum frequency response needed which was 6500 HZ . This allowed the gain to be turned down to 4. Following this the wire life was extended appreciably, which proves that no instability occured when the probe was inserted in the cylinder. Fig 4.1

The anemometer voltage was observed to drift during the first hour of operation. Following this the test runs were performed only after an initial warm up period of at least one hour.

Hot Wire Probe.

The hot wire probe was especially manufactured by DISA ELECTRONIK and it can accommodate two wires at an angle of 90^{o} to each other. However only one of these was used during the tests.

The wire material was a Pt - 10% Rh alloy which is suitable for operation at high temperatures. This is an important factor since it is essential to operate at wire temperatures at least 100°C above the temperature of the surrounding gas. Normal working temperatures were in the region of 835°K.

The wire diameter was 10 μm and its length was approximately 2 mm. The length was measured every time it was renewed by using a calibrated enlarger. When replacing a broken wire, the new one was always welded on so that it was slightly slack. This was done to improve its endurance to mechanical vibrations transmitted through the prongs. After fitting, the new wire had to be annealed. This was necessary to avoid the increase in its cold resistance after every run. To achieve this the wire was gradually heated up by altering the decades on the front panel of the anemometer. This procedure took about 5 minutes after which the wire was gradually cooled down. Following this no resistance increase was observed.

Oscillations caused by bridge unbalance

Oscillations caused by inadequate amplifier bandwidth

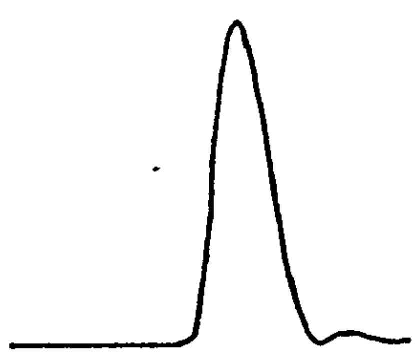

Oscillations obtained at optimum adjustment

FIG 4.1

CHAPTER 5

HOT WIRE PROBE CALIBRATION

Hot wire probe calibration

Heat balance of hot wire

The calibration procedures necessary for the successful use of hot wire anemometers are normally quite complex. This is because a large number of factors have to be taken into account.

When applied to air flow measurements in engine cylinders the process is further complicated by the fact that the gas temperature and pressure undergo large variations which influence the response of the hot wire. Thus normal calibration procedures where a known air velocity is related to the anemometer bridge output voltage would give erroneous results.

Consequently the present work was based on an analytical heat balance of the hot wire which takes into account the variation of the gas characteristics with the temperature and pressure. The procedure is largely based on the work of James(6) which proved it to be suitable for flow measurements in engine combustion chambers.

In arriving at the final correlation James made a number of assumptions when setting up the heat balance of a wire element dx. It was assumed that the wire element loses heat by the following processes:

a) by convective heat transfer to the normal air flow Q_e

b) by conduction along the wire Q_c

c) by radiation to the surroundings Q_r

It was also assumed that:

a) The radial temperature variation in the wire is small

b) The wire element surface temperature is constant

c) The element resistance and hence its temperature is constant along its length.

The heat balance would then be:

Q supplied = Qe + Qc + Qr

or

$$I^2R_L = A_x h(T_L - T_g) + A\frac{d}{dx}(\lambda_L T_L) + A_x \epsilon_T (T_L^4 - T_S^4)\sigma$$

where

I = bridge current

Ax = πddx - surface area of element

h = heat convection constant

Tg = gas temperature

$A = \frac{\pi d^2}{4}$ = wire crossectional area (d= 0.00001 m)

λ_L = thermal conductivity of wire material at temperature T_L

σ = Stefan Boltzmann constant =

= 5.693×10^{-8} J/m·sec°K^4

ϵ = surface emissivity of the wire which was evaluated by James and found to be 0.1

T_S = temperature of surroundings

The above equation was then integrated over the complete wire length and in doing this a number of further assumptions had to be made. James listed these as follows:

1. The average wire operating resistance R_W, and temperature T_W, are constant along the wire length.

2. The thermal conductivity of the wire material is constant along its length.

3. Heat conduction losses to the two prongs occur at both ends of the wire and are of equal magnitude.

The heat balance for the entire hot wire is then

$$I^2R_W = A_S h(T_W - T_g) + 2\lambda_W A\frac{dT_W}{dx} + A_S \epsilon_T (T_W^4 - T_S^4)\sigma$$

where

A_S = $\pi d l$, l = wire length.

λ_H = thermal conductivity of the wire material at the temperature of the prong tip T_H. After compiling data quoting λ_H at various temperatures the following relationship emerged.

$\lambda_H = 3.02 \times 10^3 + 4.819 \times 10^{-3} \times (T_H - 290)$ Watts/m°K

T_W = wire operating temperature.

The above equation has to be related to a convective heat transfer relationship to link up the two phenomena which are related by a hot wire anemometry system.

1. Heat convection — to the air stream
2. Compensation of the heat loss by increasing the voltage across the wire.

The correlation that was used, following James' work was an empirical relationship found by Collis and Williams (1) where the Nusselt number and the Reynolds number are related. This relationship also takes into account the temperature loading of the wire as shown below

$$Nu = \left(a + bRe^{m}\right)\left(\frac{T_f}{T_g}\right)^{0.17}$$

The constants a, b and m depend on the Reynolds number range and Collis and Williams quote the following figures

	$0.02 < Re < 44$	$44 < Re < 140$
n	0.45	0.51
a	0.24	0.0
b	0.56	0.48

Thus from the anemometer voltage data for a certain air velocity the corresponding Nusselt number can be established as follows:

$$Nu = \frac{hd}{\lambda_g}$$

where

$$\lambda_g = 2.41 \times 10^{-2} (1 + 0.00317t - 0.0000021t^2) \text{ J/m sec °K} =$$

$=$ the air thermal conductivity at the film temperature

and

$$t = T_f - 273$$

$$T_f = \frac{T_w + T_g}{2} = \text{film temperature}$$

From the relationship that defines the Nusselt number

$$h = \frac{Nu\lambda_g}{d}$$

This can be replaced in the heat balance of the wire, resulting in

$$\frac{V_w^2}{R_w} = A_s \frac{Nu\lambda_g}{d}(T_w - T_g) + 2\lambda_H A \frac{dT_w}{dx} + A_s \epsilon_T \sigma (T_w^4 - T_g^4)$$

Thus the Nusselt number can be isolated

$$Nu = \frac{\frac{V_w^2}{R_w} - 2\lambda_H A \frac{dT_w}{dx} - A_s \epsilon_T \sigma (T_w^4 - T_g^4)}{\frac{A_s \lambda_g}{d}(T_w - T_g)}$$

or

$$Nu = \frac{Q_{supp} - Q_c - Q_r}{\pi \lambda_g l (T_w - T_g)}$$

Going back to the formula quoted by Collis and Williams

$$Nu \left(\frac{T_f}{T_g}\right)^{-0.17} = a + bRe^m$$

and using the formula of definition of the Reynolds number

$$Re = \frac{\rho U d}{\mu}$$

where

$\rho =$ air density at the film temperature

$\mu =$ air dynamic viscosity at the film temperature

The air velocity can be obtained by straightforward substitution.

$$\left[\frac{Nu\left(\frac{T_g}{T_f}\right)^{0.17} - a}{b}\right]^{\frac{1}{m}} = \frac{\rho U d}{\mu}$$

or

$$U = \left[\frac{1}{b} Nu\left(\frac{T_g}{T_f}\right)^{0.17} - \frac{a}{b}\right]^{\frac{1}{m}} \frac{\mu}{\rho d} \qquad (1)$$

Heat supplied to the wire

The current passing through the wire will create a certain amount of heat which is then dissipated by convection, conduction and radiation. Thus

$$Q \text{ supp} = \frac{V_W^2}{R_W}$$

where

V_W is the voltage across the wire.

However V_W is difficult to establish and a more useful expression would be in terms of the current through the wire

$$V_W = I \cdot R_W$$

This current would be the same in the half of the bridge which contains the wire and would cause the bridge imbalance voltage.

Thus

$$I = \frac{V_B}{R_W + R_1 + R_C}$$

where

V_B = Bridge voltage

R_1 = $50\,\Omega$ = resistance in bridge arm in series with probe arm

R_C = total conductor resistance in the leads and probe body = $1.5\,\Omega$.

Hence

$$Q \text{ supp} = I^2 \cdot R_W = \frac{V_B^2 R_W}{(R_W + R_1 + R_C)^2}$$

The operating resistance was assumed to vary linearly with the difference in temperature between the wire and T_o. This is now a universally accepted practice.

Thus:

$$R_W = R_o \cdot (1 + \alpha \cdot (T_W - T_o))$$

where

R_o = wire cold resistance

α = temperature coefficient of resistence for wire material.

T_o = temperature at which R_o is determined

The manufacturer quotes approximate figures for α, but the experience of many research workers shows that its value can vary greatly from one wire batch to another. For the Pt – 10%Rh wire used for this work this value was found experimentally.

Evaluation of the thermal coefficient of resistence for the

Pt - Rh wire

Test run 1

$R_o = 4.84\,\Omega$ $\quad$ $T_o = 18^{\circ}C$

$T_w (^{\circ}C)$	$R_W (\Omega)$	$T_w - T_o$	$\frac{R_w}{R_o} - 1$
20	4.86	2	0.004
30	4.93	12	0.018
40	5.02	22	0.037
50	5.07	32	0.047
60	5.13	42	0.06
70	5.21	52	0.076
80	5.27	62	0.088
90	5.34	72	0.103
100	5.41	82	0.117
110	5.48	92	0.132
120	5.54	102	0.144
130	5.62	112	0.161
140	5.7	122	0.177
150	5.78	132	0.194
160	5.85	142	0.208
170	5.92	152	0.223
180	5.0	162	0.239
190	6.07	172	0.254
200	6.16	182	0.272

Estimated α = 0.001466.

Test run No. 2

Tw (°C)	Rw (Ω)	Tw - To	$\frac{Rw}{Ro} - 1$
30	4.93	8	0.012
40	4.99	18	0.024
50	5.07	28	0.041
60	5.14	38	0.055
70	5.21	48	0.0698
80	5.28	58	0.084
90	5.35	68	0.098
100	5.42	78	0.113
110	5.5	88	0.129
120	5.57	98	0.143
130	5.63	108	0.156
140	5.7	118	0.170
150	5.77	128	0.1848
160	5.85	138	0.201
170	5.92	148	0.215
180	6.0	158	0.232
190	6.08	168	0.248
200	6.15	178	0.262
210	6.22	188	0.277

Ro = 4.87Ω ; To = 22°C

Estimated α = 0.001455

Temperature measured on Comark electronic thermometer.

Resistance measured on anemometer decades.

The probe was heated in an oven from the ambient temperature up to 200°C and the resistance of the wire was measured at intervals of 10°C. The test was then repeated to check the figures obtained. By plotting $\frac{Rw}{Ro} - 1$ against $(T_W - To)$ a straight line was obtained. The slope of this line gave the value of α which in this case was found to be 0.001474 Fig 5.1.

Heat loss through Conduction

In many cases the end conduction losses into the probe prongs have been ignored on the basis that they are extremely small. However, while this is certainly true for high air velocities, the error due to the end conduction losses at low air velocities is significant. In the present work where flow reversals and low velocities are often encountered it was considered important to allow for these losses, particularly since they are a function of velocity.

To evaluate the end conduction losses one needs to know the temperature gradient in the wire in the vicinity of the prongs. Provided this is known then:

$$Qc = 2 \cdot \lambda_H \cdot A \cdot \frac{dT_W}{dx}$$

this allows for the two prongs.

The determination of the temperature gradient factor can be done through a complicated iteration process, which was used by James (6). However a different method was used in this work, where the heat loss to the prongs is measured and related to the temperature gradient in the wire.

To achieve this, the probe equipped with a thermocouple on one of the prongs was introduced into a vacuum sealed flask and the air was evacuated. Thus the probe functioned in an environment of high vacuum. Fig 5.2, 5.4

Assuming that the radiation from the wire is negligible and that convection does not exist if there is no fluid then the bridge unbalance would only be caused by the heat loss into the probe prongs. During the test run the overheat ratio of the probe introduced in vacuum was varied from 1 to 1.9 and the bridge voltage and prong temperatures were recorded. In the end a correlation was drawn between the heat supplied to the wire, equal to the heat lost through the prongs, and the temperature difference between the wire and the prongs.

During the engine tests the prong temperature was recorded so that the heat loss through conduction at any point in the engine cycle could be evaluated.

The calibration in vacuum was repeated with two different wires and the results were found to be within 5% of each other. A third order polynomial was fitted to the data relating the heat loss to the temperature difference between the wire and the prong. This was found to be: (Fig 53)

$$Q_c = 0.14264 \cdot 10^{-2} + 0.32763 \cdot 10^{-5} \cdot \Delta T + 0.7251 \cdot 10^{-7} (\Delta T)^2 + 0.51078 \cdot 10^{-10} \cdot (\Delta T)^3$$

where $\Delta T = T_W - T_H$

Heat loss through radiation

Normally the radiation losses are small enough to be negligible but since the velocities measured were expected to be fairly low it was decided to allow for them. Again the evaluation of the radiation losses is based entirely on the work of James (6). He underlines that the only type of radiation worth taking into account is the radiation loss between the hot wire and the surrounding solid surfaces. Also in his work it was estimated that the value for the emissivity of the wire material is on average equal to 0.1.

Measurement of end conduction losses. - Run 1.

To = 20.5°C Ro = 5.33Ω

Rw (Ω)	Bridge Voltage (V)	Prong Temperature (°C)
5.33	0.288	24.2
5.5	0.488	24.3
5.7	0.642	24.8
5.9	0.798	25.0
6.1	0.900	25.2
6.3	1.034	25.9
6.5	1.136	26.0
6.7	1.201	26.3
6.9	1.298	26.8
7.1	1.396	27.0
7.3	1.467	27.5
7.5	1.536	28.0
7.7	1.596	28.2
7.9	1.666	28.8
8.1	1.730	29.1
8.3	1.794	29.6
8.5	1.864	30.0
8.7	1.898	30.3
8.9	1.996	31.0
9.1	2.034	31.3
9.3	2.098	31.7
9.5	2.162	32.1
9.7	2.197	32.6
9.9	2.266	33.0
10.1	2.299	33.5
10.3	2.368	34.0
10.5	2.409	34.5

Measurement of end conduction losses Run 2.

To = 25.0°C Ro = 4.8 Ω

Rw (Ω)	Bridge Voltage (V)	Prong Temperature (°C)
4.805	0.234	24.05
4.975	0.464	24.2
5.175	0.684	24.4
5.375	0.862	24.6
5.575	0.983	24.75
5.775	1.098	25.10
5.975	1.237	25.35
6.175	1.340	25.64
6.375	1.432	26.96
6.575	1.532	26.26
6.775	1.598	27.67
6.975	1.688	27.07
7.175	1.764	27.50
7.375	1.835	27.95
7.575	1.898	28.35
7.775	1.974	28.75
7.975	2.063	29.15
8.175	2.132	29.53
8.375	2.188	29.92
8.575	2.264	30.30
8.775	2.3	30.70
8.975	2.345	31.15

Thus the heat loss through radiation will be

$$Q_r = A_S \cdot \epsilon \cdot \sigma \cdot (T_W^4 - T_g^4)$$

<u>Nusselt - Reynolds number correlations.</u>

The relationship published by Collis and Williams

$$Nu = (a + bRe^m) \cdot \left(\frac{T_f}{T_g}\right)^{0.17}$$

was first used in the form shown above but the calibration results were found to be rather poor, with the estimated velocities being approximately 30% in excess of the real velocities.

It was also noted that a number of research workers criticised the above relationship on the grounds that it was arrived at by using wires with a very high aspect ratio, ranging from 2000 to 8600 which would minimise the end conduction losses. The wires used in the present work had aspect ratios of about 200.

Thus it was decided to run an iteration procedure where a best fit could be found to a set of calibration results. This is a procedure similar to that quoted by Lancaster (27) and it was applied to two arrays containing the $Nu\left(\frac{T_f}{T_g}\right)^{-0.17}$ and Re^m terms respectively. The results were the appropriate constants a and b.

Initially m was set up at 0.4 and a first order polynomial was fitted to the data, using a least squares routine. Consequently the coefficients a and b were calculated and the corresponding velocities would result from the formula (1). These were compared with the real velocities and the error was evaluated in the process. Following this m was incremented by 0.01 and the procedure was repeated. It was thus possible to choose a combination of coefficients which gave a minimum error. Incidentally, these coefficients were found to vary in a rather narrow range but certain combinations could lead to large errors.

Once a, b and m were found the calibration process was completed.

Experimental calibration procedure.

The actual calibration technique was to insert the probe into a calibration wind tunnel and to record the air velocities and the bridge voltages. The calibration tunnel was in fact a Venturi tube with a throat diameter of 1 inch. The air velocity in the measuring section was given by: (Fig 5.5)

$$U=\sqrt{\frac{2\gamma}{\gamma-1}RT_o\left[1-\left(1-\frac{\Delta P}{P_o}\right)^{\frac{\gamma-1}{\gamma}}\right]}$$

where

γ = 1.4

R = gas constant

To = ambient temperature

Po = ambient pressure

ΔP = pressure drop in the Venturi throat.

The pressure drop in the throat of the tunnel was measured using a Furness micro manometer which is able to measure extremely low pressure drops (0.1 mm water). This provided for accurate calibration at extremely low air velocities which did not require the use of special equipment built just for that purpose.

Having overcome the problems of the correlation between the experimental calibration and the theoretical one and having found the appropriate calibration constants one more factor remained unaccounted for. The calibration was performed at ambient pressures and temperatures but there was no guarantee that this would hold at the temperatures and pressures encountered in the cylinder. However a survey of the literature showed that experiments performed in high temperature and/or high pressure rigs proved that the values of the calibration constants are not affected by these changes provided that the calibration embraced a wide range of the Nu - Re numbers. One way of doing this would be to build a rig with a measuring section that can allow a temperature and/or pressure increase. The air velocities and bridge voltages would be noted and included in the calibration iteration alongside with the ambient data.

Another method would be to calibrate the wire at a number of overheat ratios varying the sensor temperature as suggested by Lancaster (27). This would lead to an increase in the range of Nu - Re numbers that are included in the calibration data. Fig 5.6

Calibration runs were performed at overheat ratios ranging from 1.5 to 1.95 and the data was prepared for iteration. This procedure was followed every time a wire was calibrated although, it was found that generally the data from calibration runs at different overheat ratios on the same wire tend to overlap. This is in agreement with the conclusions of other research workers who found that no correction of the ambient conditions calibration runs is necessary to cater for the increased temperature and pressure within the cylirder, provided the calibration is based on a heat balance of the wire.

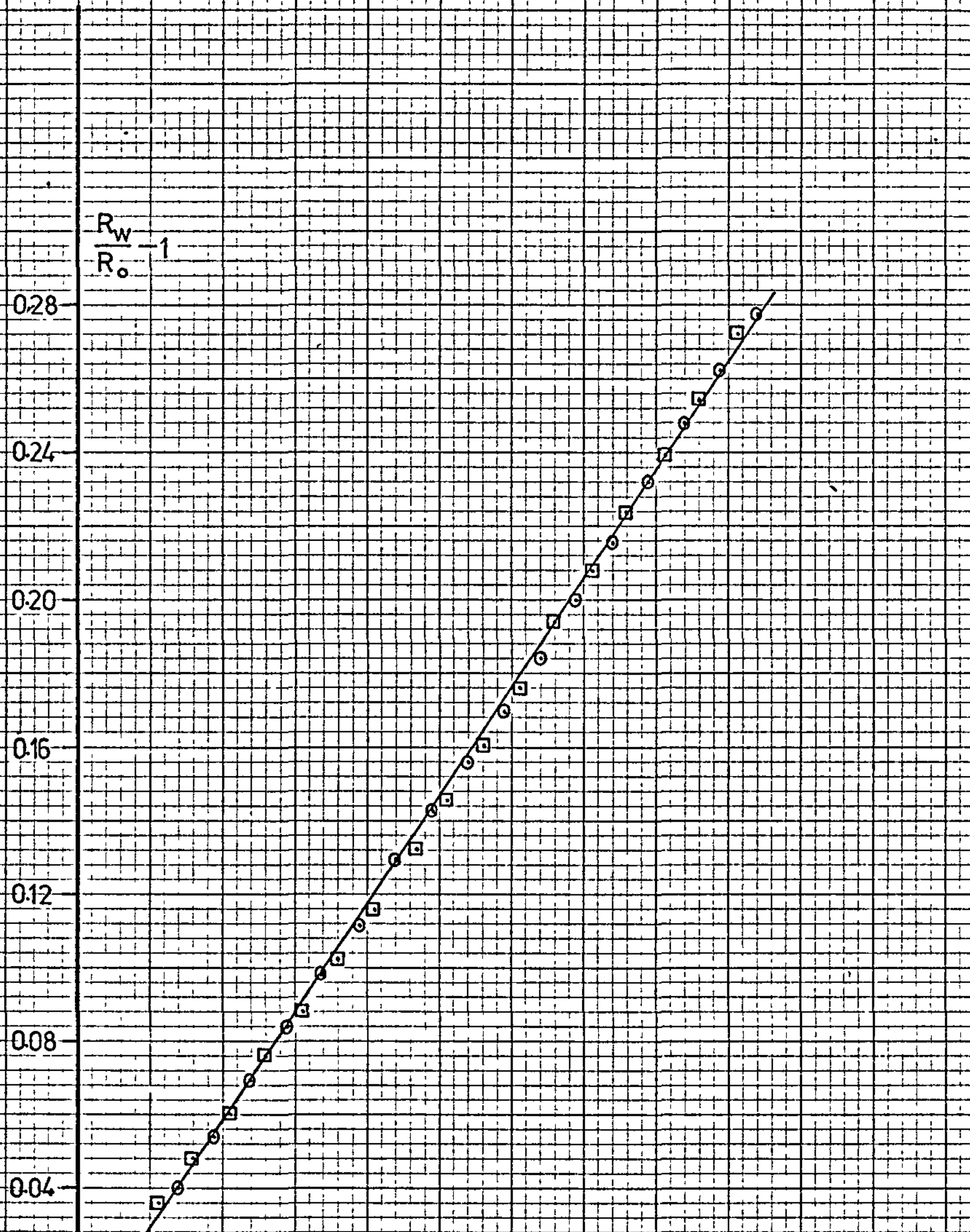

FIG 5.1 TEMPERATURE COEFFICIENT OF RESISTANCE

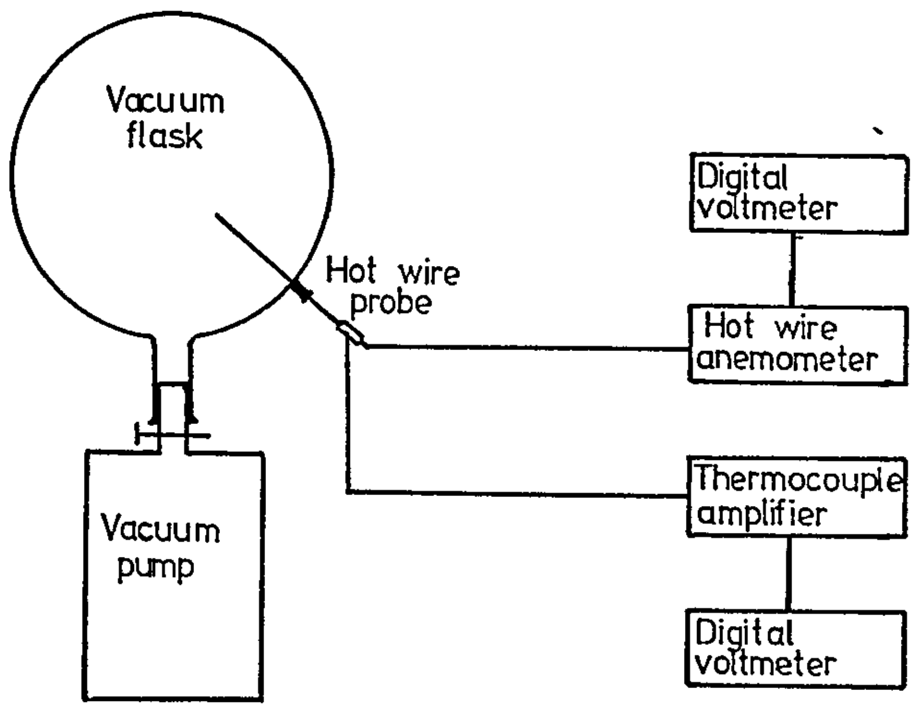

FIG 5.2 HEAT CONDUCTION LOSS MEASUREMENT

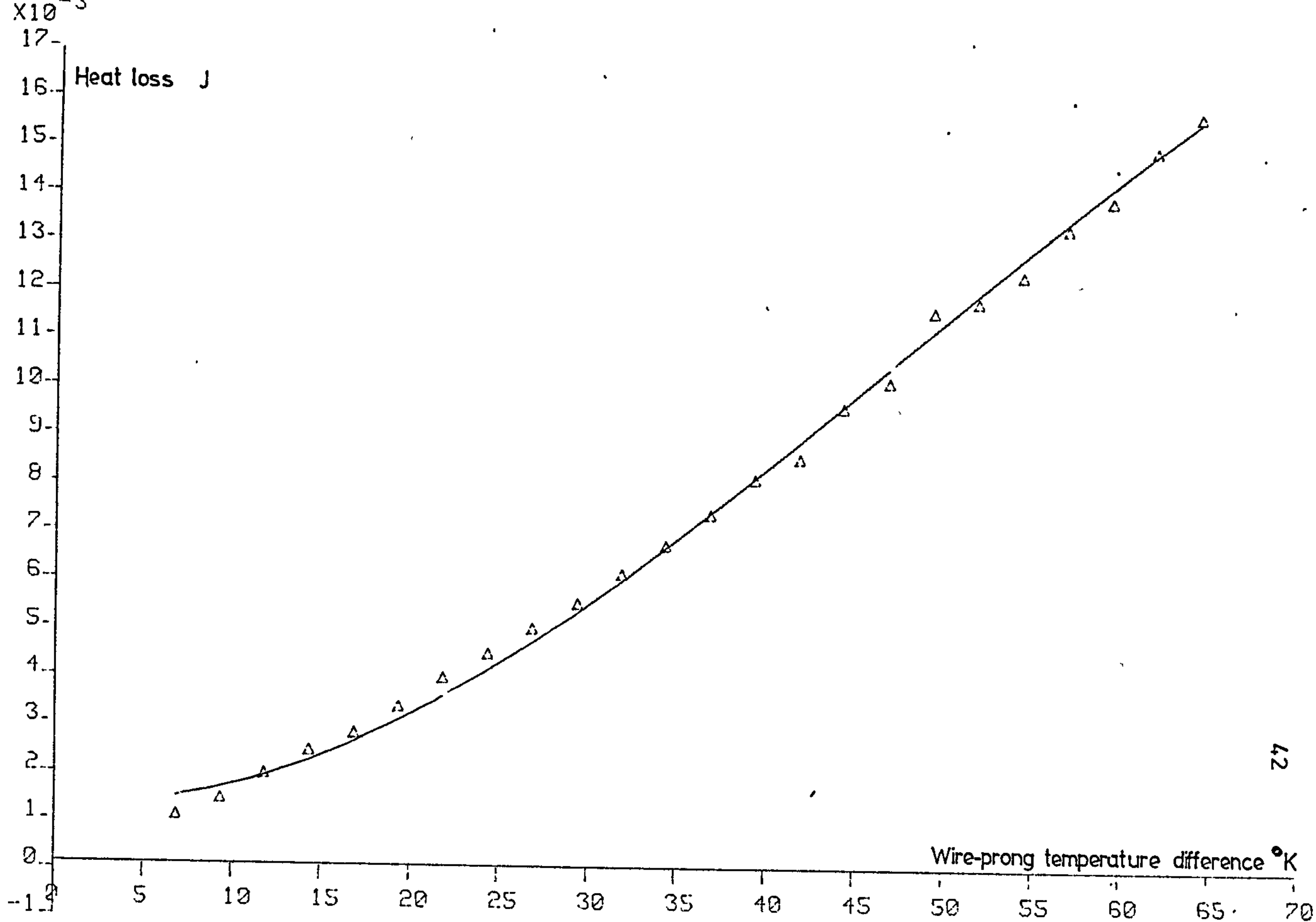

FIG 5.3 HEAT CONDUCTION LOSS

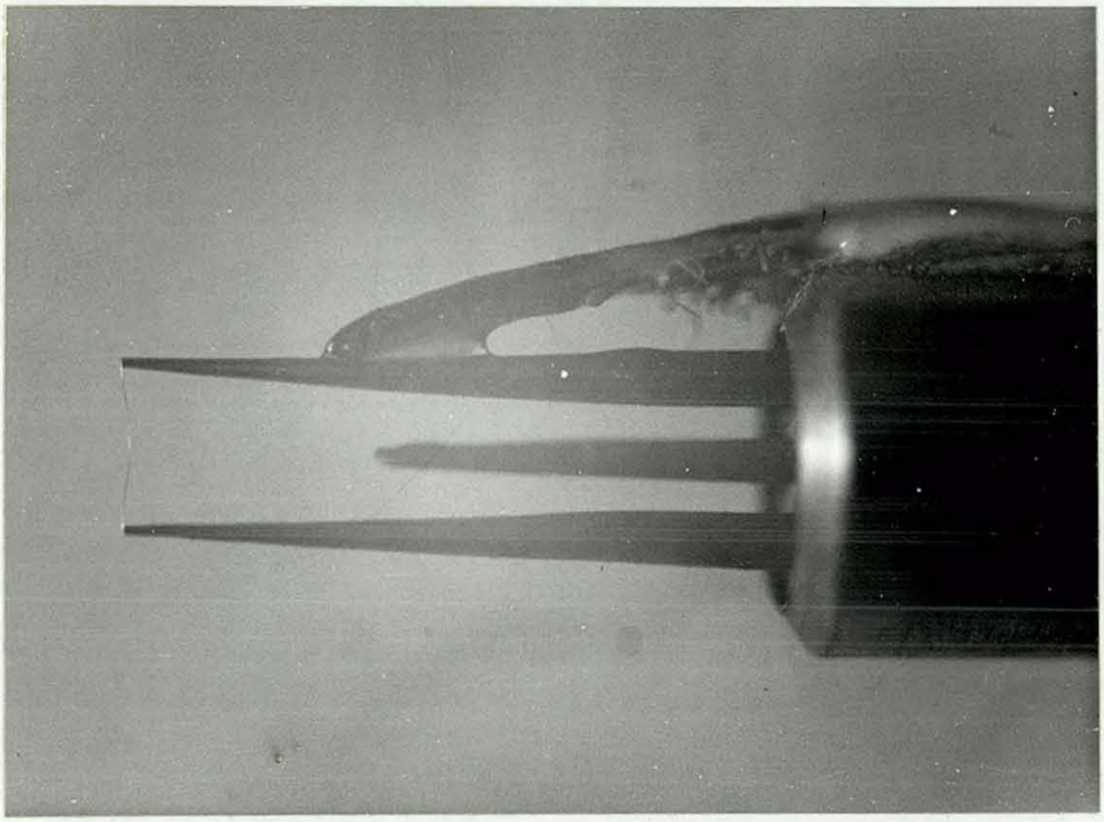

FIG 5.4 HOT WIRE PROBE

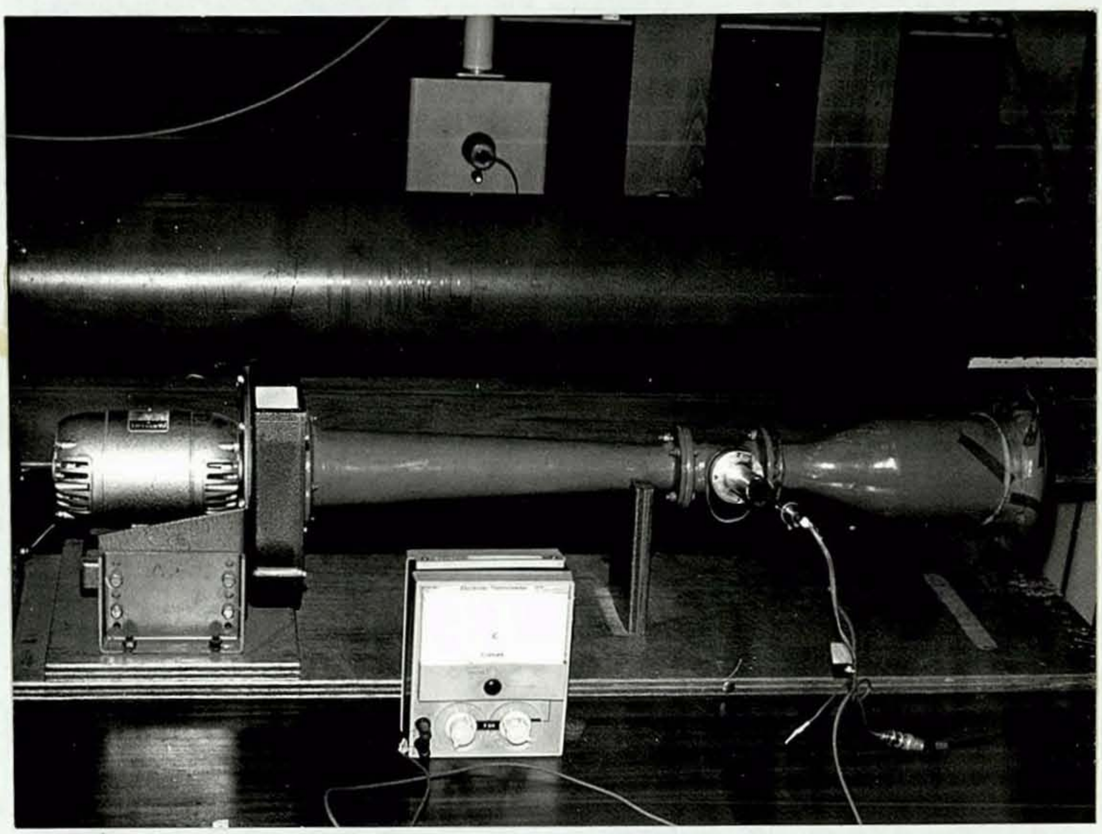

FIG 5.5 HOT WIRE PROBE CALIBRATION RIG

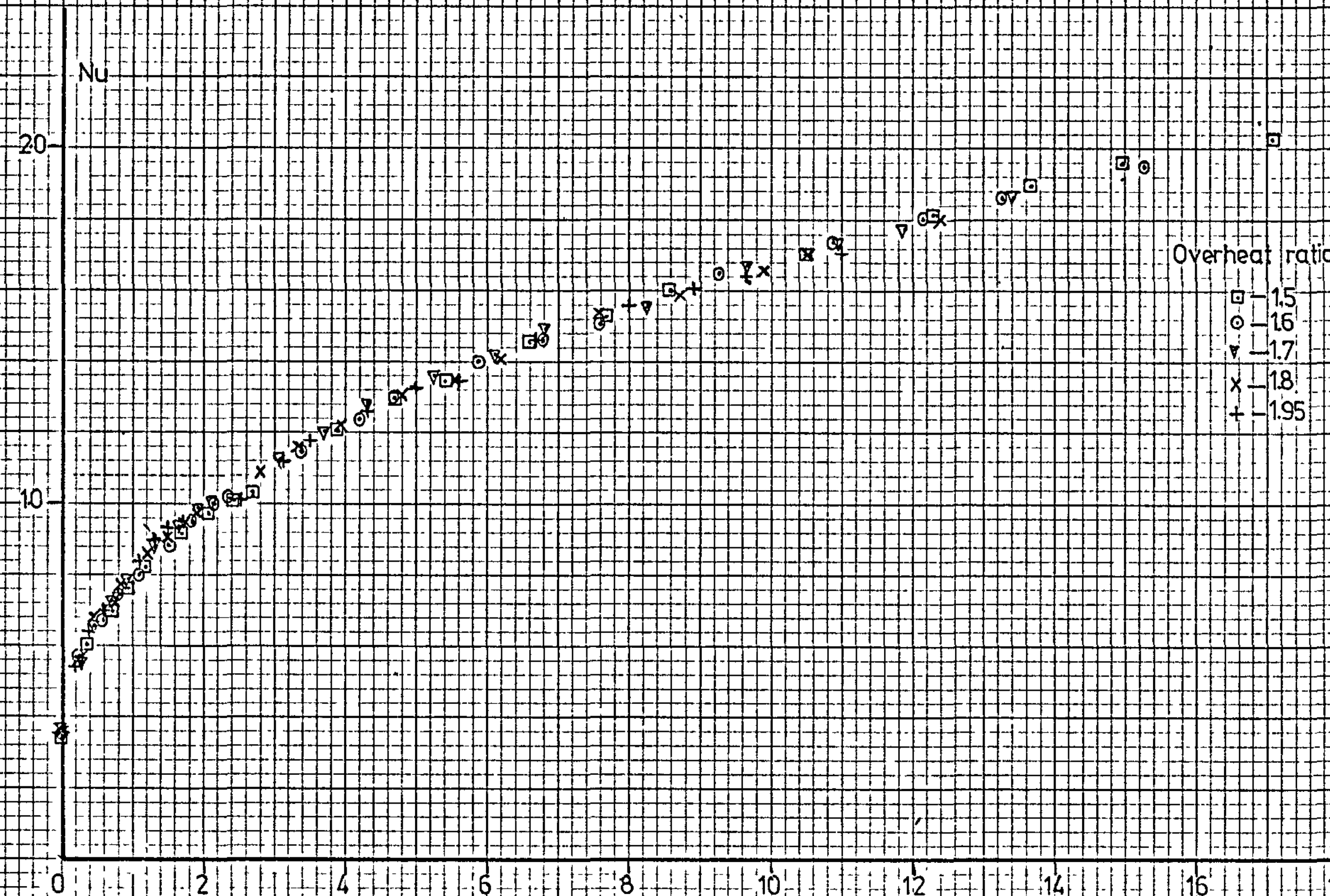

FIG. 5.6 NU-RE NUMBER CORELATION

CHAPTER 6

ENGINE RIG AND INSTRUMENTATION

Engine Rig and Instrumentation

Engine

The tests described in this report were performed on a Petter single cylinder engine suitably converted from diesel to spark ignition configuration. This involved the reduction of the compression ratio and the blanking off of the orifice of the precombustion chamber in the cylinder head that this engine features. Fig 6.1

The top of the piston was raised so that it was level with the top surface of the engine block. The combustion chamber was situated in a place sandwiched between the block and the cylinder head. Fig 6.3, 6.4

Nine combustion chamber configurations were investigated ranging from zero squish which was essentially a pancake type (Fig 6.5) chamber to 20% squish (5%, 10%, 15%, 20%). For every squish percentage the squish area was located in two alternative positions.

1) all in one place on one side of the combustion chamber Fig 6.7.
2) equally divided between two adjoining quadrants of the combustion chamber forming a V shape. Fig 6.6

The thickness of the squish plates varied with the degree of squish so that the compression ratio could be kept constant.

Cylinder head gaskets were used on both sides of the squish plates. Their thickness was taken into account when calculating the volume of the combustion chamber.

The engine specification was:

Bore	80.112 mm
Stroke	110.0 mm
Cubic capacity	555 cc.
Connecting rod length	232 mm.
Compression ratio	8.5:1
I.V.A.	4.5° BTDC
I.V.C.	35.5° ABDC
E.V.O.	35.5° BBDC
E.V.C.	4.5° ATDC

Maximum recommended speed 2000 rpm.

The combustion chamber heights were as follows:

0% squish	13.12 mm.
5% "	13.81 mm.
10% "	14.58 mm.
15% "	15.44 mm.
20% "	16.40 mm.

The engine was fitted with a new low clearance set of rings before testing commenced. Consequently it was run in (by motoring it) after which it was dismantled and the piston, piston rings and liners were scrupulously cleaned. The oil was then flushed out so that the tests were performed on a dry engine. This was so that no oil contamination of the probe would occur.

Out of all the auxiliary systems, the fuel, cooling and exhaust systems were removed and only the oil pump with its feed to the crankshaft and camshaft journals was kept. This was necessary in order to provide for easy cylinder head removal which had to be performed every time a new squish plate was tested.

The intake manifold consisted ofa short length of pipe with a micronic filter at the end.

The intake filter, together with the dry running of the engine and disconnection of the oil feeds to the rocker shaft was a probe protection measure which proved well worthwhile.

The engine was motored by a variable speed 10 HP. dc. electric motor powered by a Ward Leonard generating set.

Probe Traverse

The probe traverse was mounted on one side of each squish plate.Fig 68.

Since the cylinder head removal was made extremely easy, the design of the traverse did not incorporate an advance mechanism. Instead, all the attention was concentrated on the sealing of the probe at the combustion chamber wall.

When running a test the probe was inserted and positioned in the combustion chamber with the cylinder head removed and then this was placed in position. When a change in probe position was required the cylinder head was removed. This proved to be simple and convenient avoiding complicated probe advance systems.

The design used enabled the probe to be located at any point along the axis of the combustion chamber while it could be rotated about its own axis.

The probe location with the cylinder head removed has the added bonus of providing for the accurate radial and directional location of the probe.Fig 6.9

Signal Recording.

The signals were recorded on a Samagamo 3500, 16 track, F M tape recorder. The recording speed was 60 ips with four channels being used at any one time.Fig 6.10, 6.2

1. Top dead centre marker
2. Crank Angle marker.
3. Anemometer output signal.
4. Pressure signal.

The anemometer and pressure signals had to be attenuated by a factor of 8 and 3 respectively in order to be accommodated within the input voltage band required by the tape recorder(1.5V)

Pressure Measurement

The cylinder pressures were measured using a Southern Instruments Type G3 0 1 inductance type pressure transducer. This was used in conjunction with the Southern Instruments E7A F M system. The pressure changes were used by the system to vary the inductance of the transducer. This, in turn controls an oscillator and its frequency will change accordingly. The oscillator is coupled to an amplifier whose output is proportional to the oscillator frequency. Thus the output voltage is proportional to the pressure applied to the transducer.Fig 6.11

The calibration of the transducer was performed using high pressure nitrogen from a gas bottle. The line pressure was monitored on a Barnet test gauge and the output voltage was read off a digital voltmeter. As a check the calibration was repeated and the second set of readings matched closely the first as shown in the table. Fig 6.12

The pressure transducer was placed where the prechamber orifice was originally located.

As already mentioned the output had to be attenuated by a factor of 3 to match the voltage bandwidth of the tape recorder.

Gas Temperature Measurement

The measurement of the gas temperature in engine cylinders poses a requirement which is difficult to meet by any sort of temperature measuring instrument.

The gas temperature varies fast and within a wide range. This leads to the requirement for an instrument with a very small time constant and an extremely low thermal mass. A number of systems have been tried.

A chromel alumel junction has been manufactured from a 0.0076 in diameter thermocouple wire but this proved to be far too slow in response to be of any use. Next a BLH fast response thermocouple was tried. This was made of the same material but the diameter of the bead was only 0.001 in. While the response of this was considerably faster it still did not follow successfully the temperature changes in the cylinder.

Next the standard hot wire probe was used in conjunction with the anemometer operating in constant current mode. Essentially this was a resistance thermometer which proved to have an extremely fast response and could easily follow the temperatur changes of the gas.

The constant current mode was chosen since it is suitable

Pressure transducer calibration data.

Pressure (p.s.i.)	Output volts run 1.	Output volts run 2
0	0.02	0.01
20	0.356	0.385
40	0.836	0.835
60	1.29	1.23
80	1.725	1.72
100	2.164	2.18
120	2.6	2.63
140	3.04	3.07
160	3.5	3.50
180	3.94	4.0
200	4.37	4.37
220	4.83	4.85
240	5.31	5.28
260	5.73	5.76
280	6.20	6.22
300	6.60	6.7

for the wide band of temperature variations that occur in the case under study. While the constant temperature operation offers a higher frequency response it is only suitable for small temperature changes.

The only calibration involved is concerned with the determination of the temperature coefficient of resistance and which is covered in chapter 5 of this report.

Some errors might occur when the air velocities are very low but these become negligible as the air velocity increases. One important factor is the probe current which has to be low enough not to heat the wire to any significant degree. Such self heating effects would result in air velocity induced resistance changes being superimposed on the temperature induced resistance changes, thus leading toerroneous measurements. To avoid this the current was kept low and in fact two runs were performed using different probe currents. One run was performed using the probe current recommended by the manufacturer (DISA). This was 3.5 mA. A second run was then carried out using a probe current of 1.5 mA.Both these gave similar results.

Although the probe cannot follow the temperature changes on the advanced stages of the compression stroke, its performance during the intake stroke was considered adequate. This enabled a reading of the temperature at IVC to be taken from which the gas temperatures were calculated using the polytropic law (see appendix 1) Fig 6.13

As the anemometer output varied betweenl-10V this had to be attenuated by a factor of 8 in the same fashion as the air velocity measurements.

The pressure and temperature data are used to estimate other gas properties as well.

The air dynamic viscosity and the air conductivity were evaluated by James and were found to be given by:

$$\mu=(0.43868+5.13195y-1.31065y^2-0.668597y^3+0.922798y^4-0.342237y^5+0.042674y^6)\cdot 10^{5}\ \mathrm{Ns/m^2}$$

where

$$y = 0.001\ T_F$$

and

$$\lambda_g = 2.41 \times 10^{-2} + 7.6397\times10^{-5} T_F - 5.031\times10^{-8}\ T_F^{\ 2}$$

Note that all the gas properties are evaluated at the film temperature.

Prong Temperature.

The prong temperatures had to be measured so that the end conduction losses could be calculated.

A chromel alumel thermocouple was attached to one of the probe prongs being separated from the metal by a very small blob of araldite. This proved successful and the prong temperatures were recorded during the calibration runs and during the actual experimental runs. It was found that there was practically no change in the temperature readings from run to run, during the engine tests so the prong temperatures were not recorded in the later stages of this work.

The thermocouple output voltage was amplified using a thermocouple amplifier. The gain of this was set during the calibration runs at 10 mv/degree. Thus 0°C corresponded to 0V and 100°C to 1V. The thermocouple was calibrated in an oven which had a precision glass and mercury thermometer. The amplifier outputs were monitored on a digital voltmeter.

It was found that the prong temperatures vary only slightly due, no doubt, to the relatively high thermal mass of the probe prongs (116°- 120°C).

Top Dead Centre and Crank Angle Markers

Since the analysis of the anemometer output was going to be based on the average of the air velocities of a large number of cycles it was necessary to add the velocities at exactly the same points every cycle. Also since quantities such as the turbulence scales require readings taken at small time intervals apart it was necessary to take a large number of readings every cycle.

This, in practice, meant that readings of the anemometer output voltage had to be taken at every degree of crank rotation and that these were accurately located within the engine cycle.

To achieve this, a large diameter disc with 360 slots around its circumference had to be manufactured and bolted on to the engine flywheel. Fig 6.14.

A saddle type mounting was manufactured to house the actual pick ups. These involved a light source on one side of the slotted disc and a phototransistor on the other side.

Whenever the light fell on the phototransistor this would give an electric pulse which was then amplified and shaped by a separate circuit. The final result was a sharp, clean signal of 1V amplitude for every degree of crank rotation which was recorded synchronously with the anemometer output.

A similar technique was used to record the position of the top dead centre. A small disc with only one slot in it was (Fig 6.15) attached to the end of the camshaft and positioned so that the pulse it gave coincided with the top dead centre of the intake stroke. An identical channel to the one already described, of electronic circuitry served this purpose. This gave a signal at the beginning of every cycle which again was recorded synchronously with the crank angle marker and the anemometer output voltage.

Engine Speed Measurement

This system relied on the circuitry developed for the markers described above. It consisted of an identical photoelectric pick up which was triggered by 60 holes drilled concentrically with the 1^{o} slots, at equal intervals around the disc. The resulting pulses were fed into a frequency counter which gave a direct reading of the engine speed.

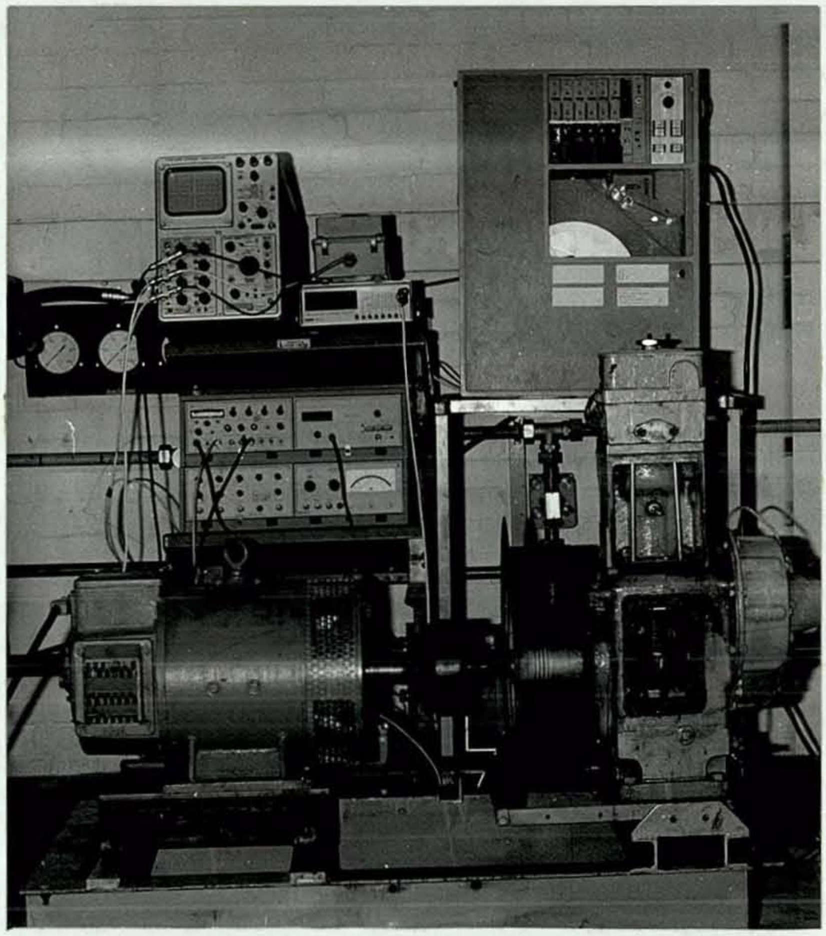

FIG 6.1 EXPERIMENTAL RIG

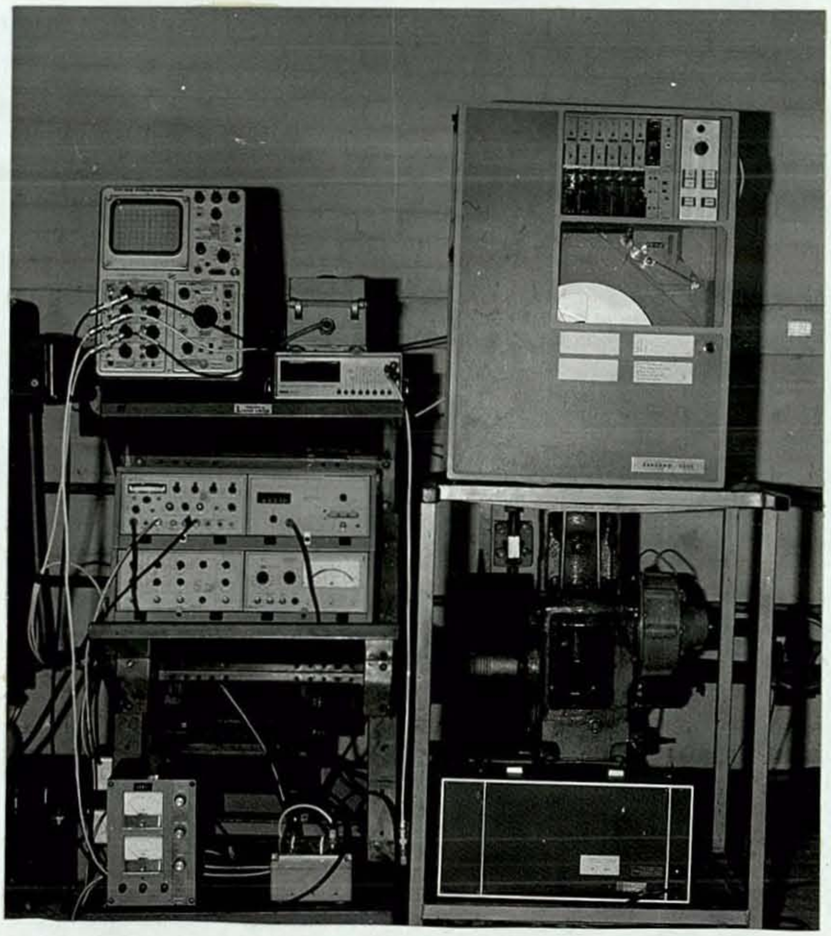

FIG 6.2 INSTRUMENTATION

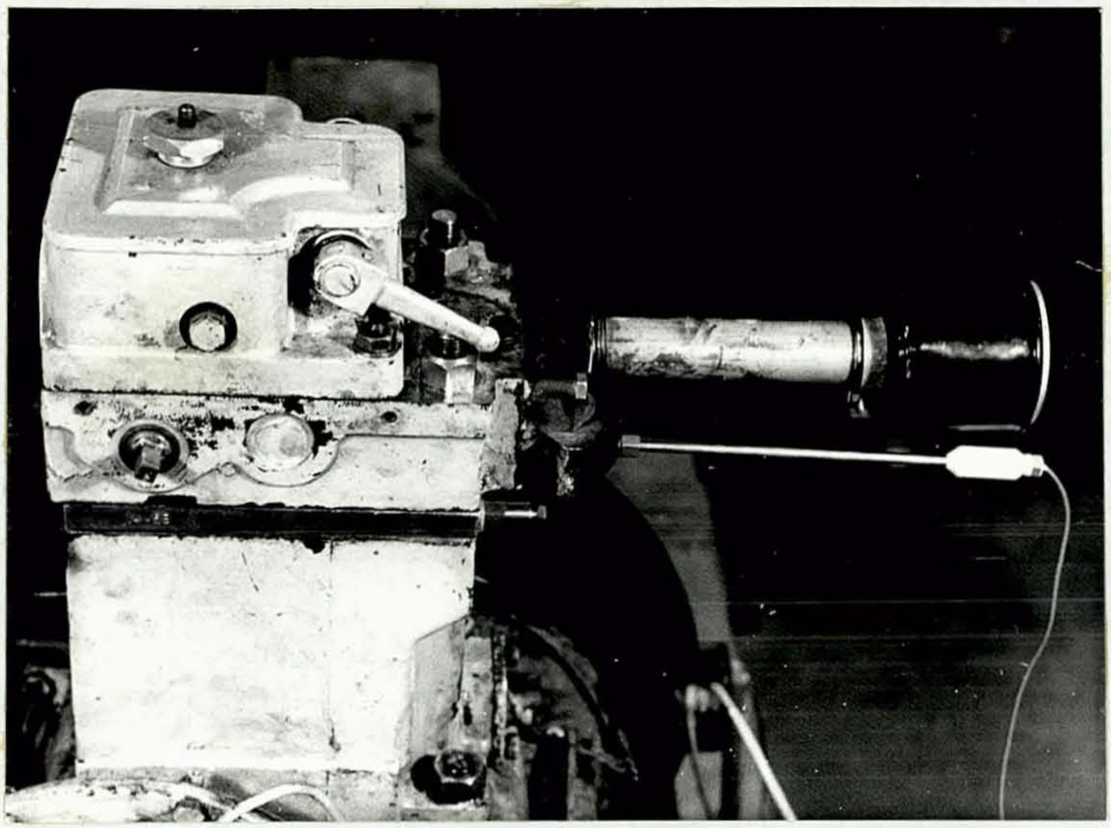

FIG 6.3 CYLINDER HEAD

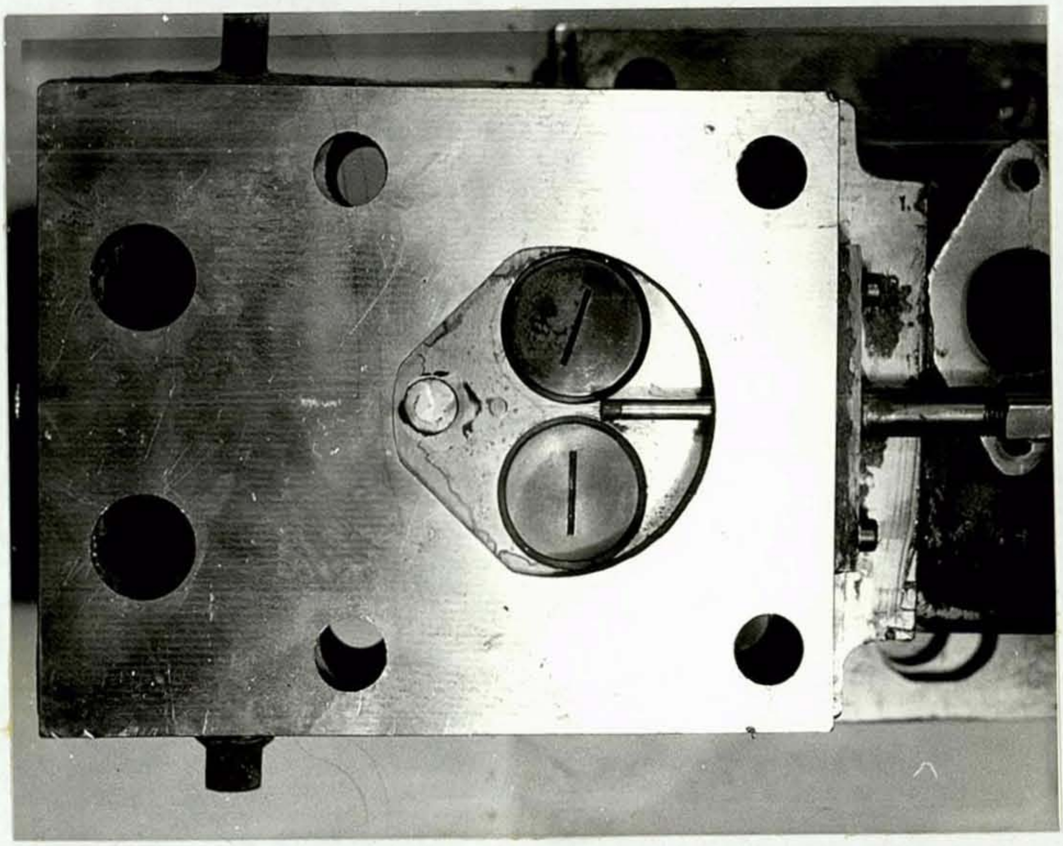

FIG 6.4 SQUISH COMBUSTION CHAMBER

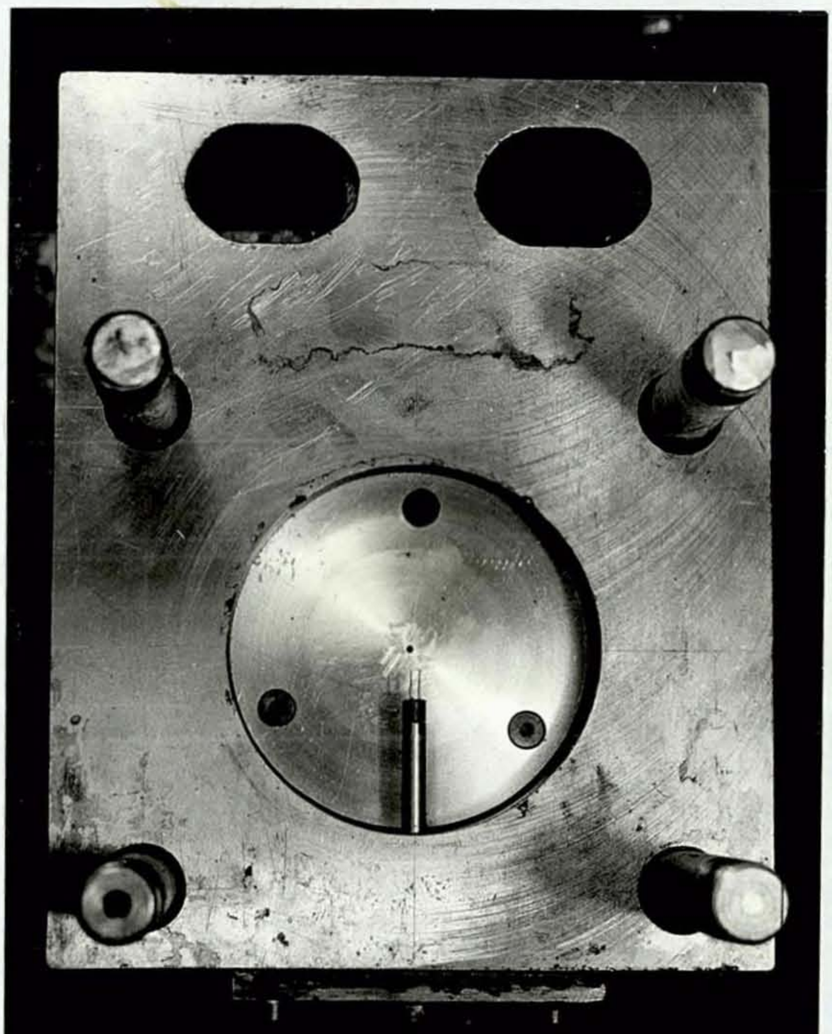

FIG 6.5 DATUM COMBUSTION CHAMBER

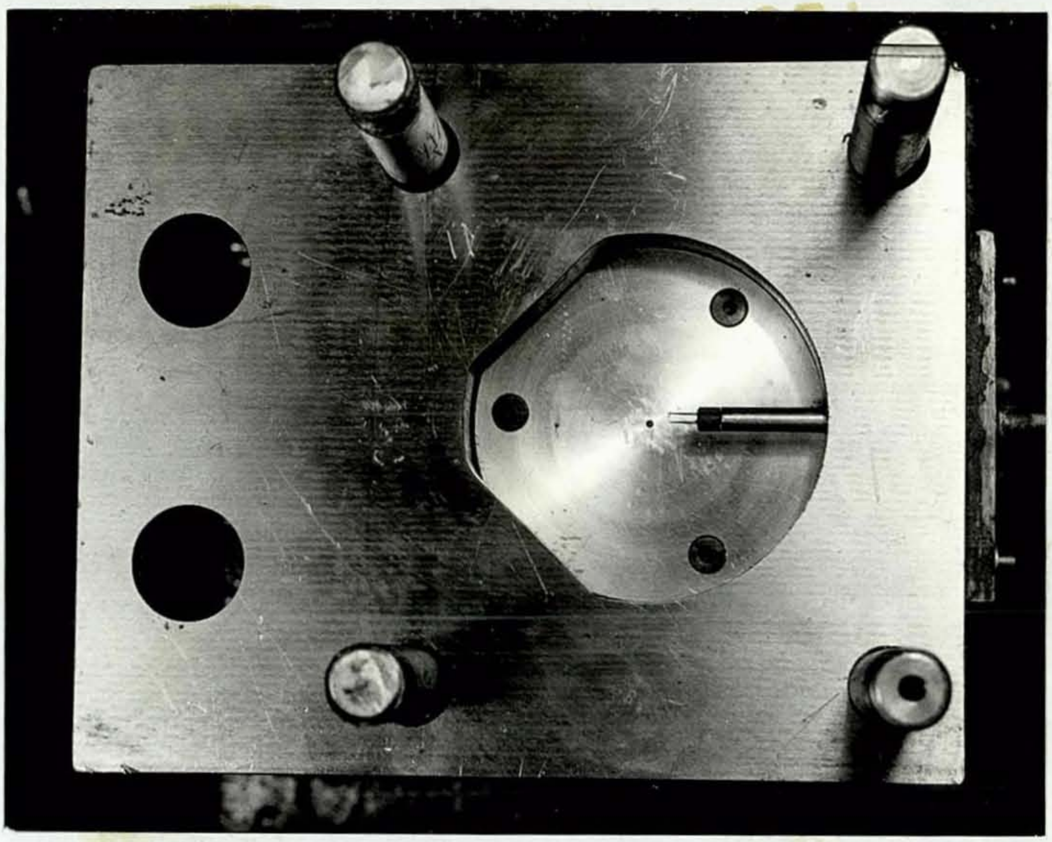

FIG 6.6 10% SQUISH IN TWO AREAS

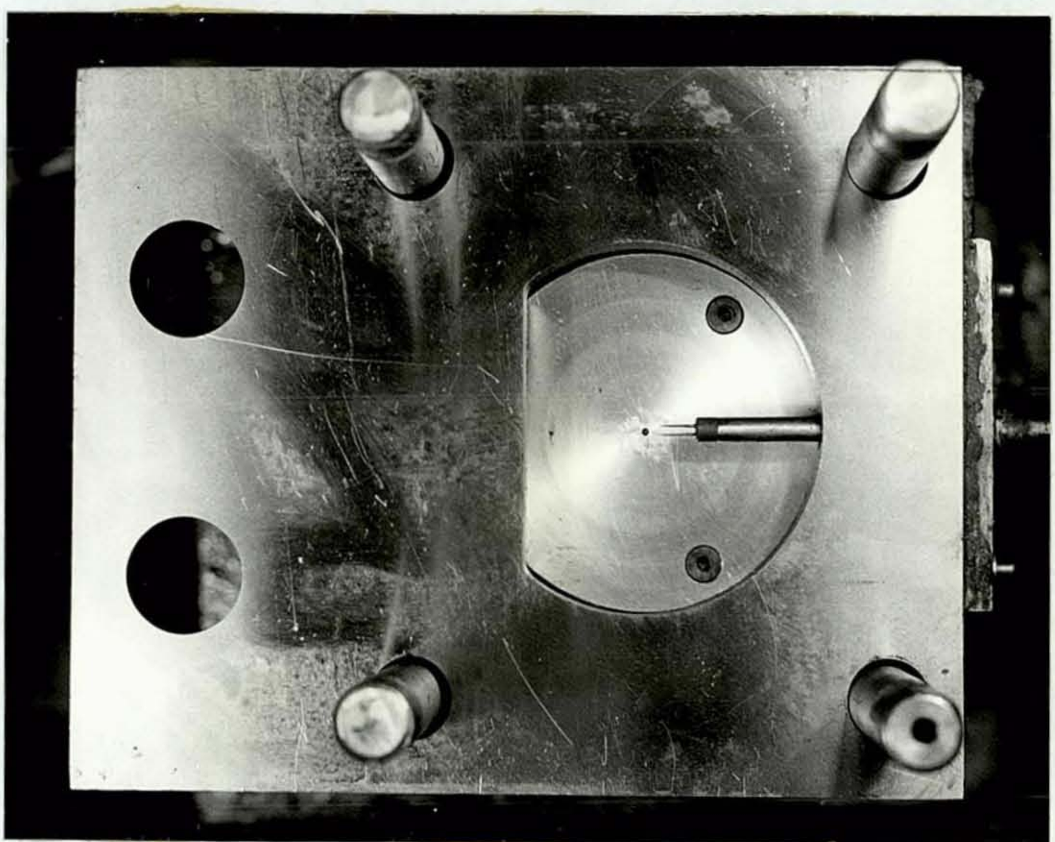

FIG 6.7 10% SQUISH IN ONE AREA

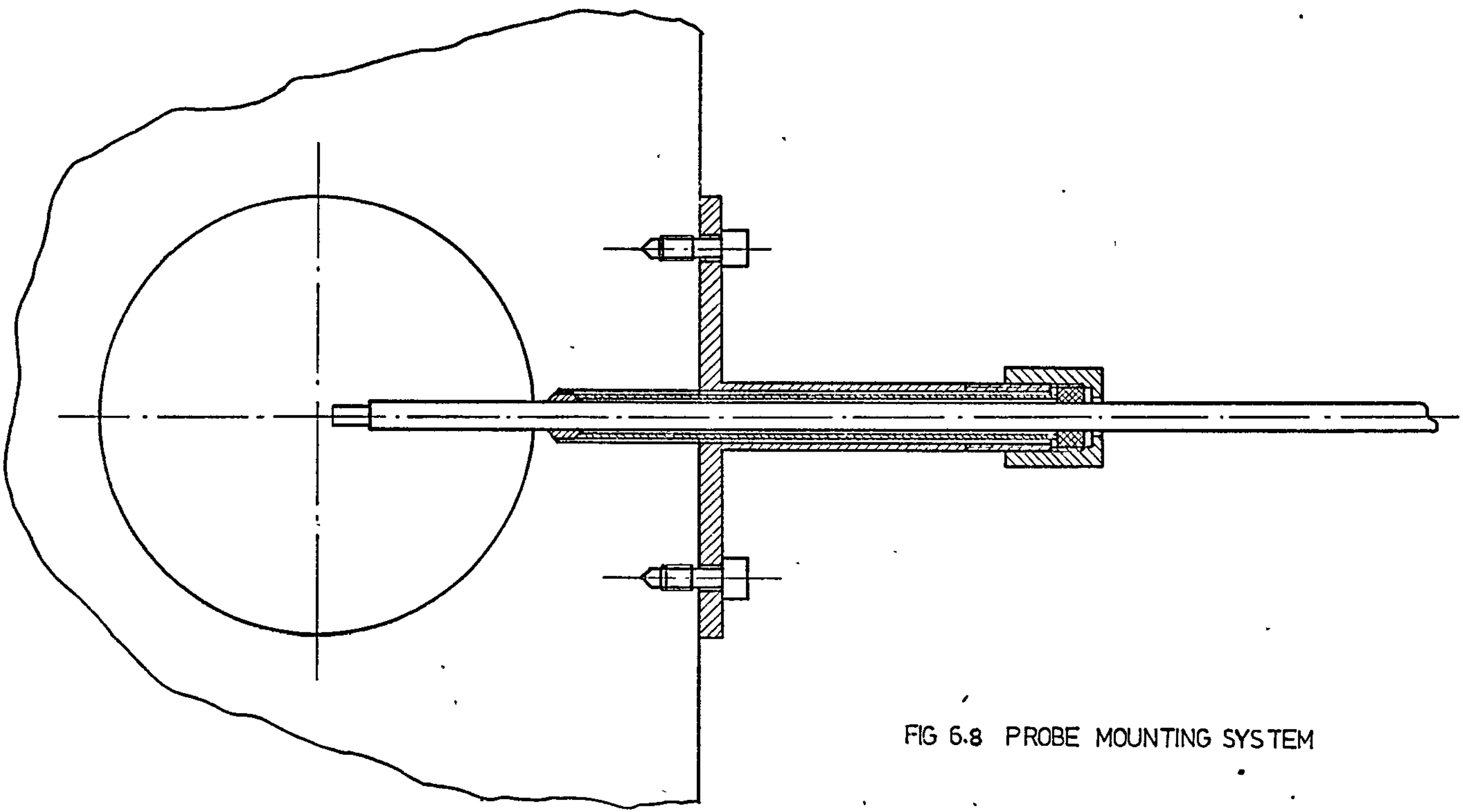

FIG 6.8 PROBE MOUNTING SYSTEM

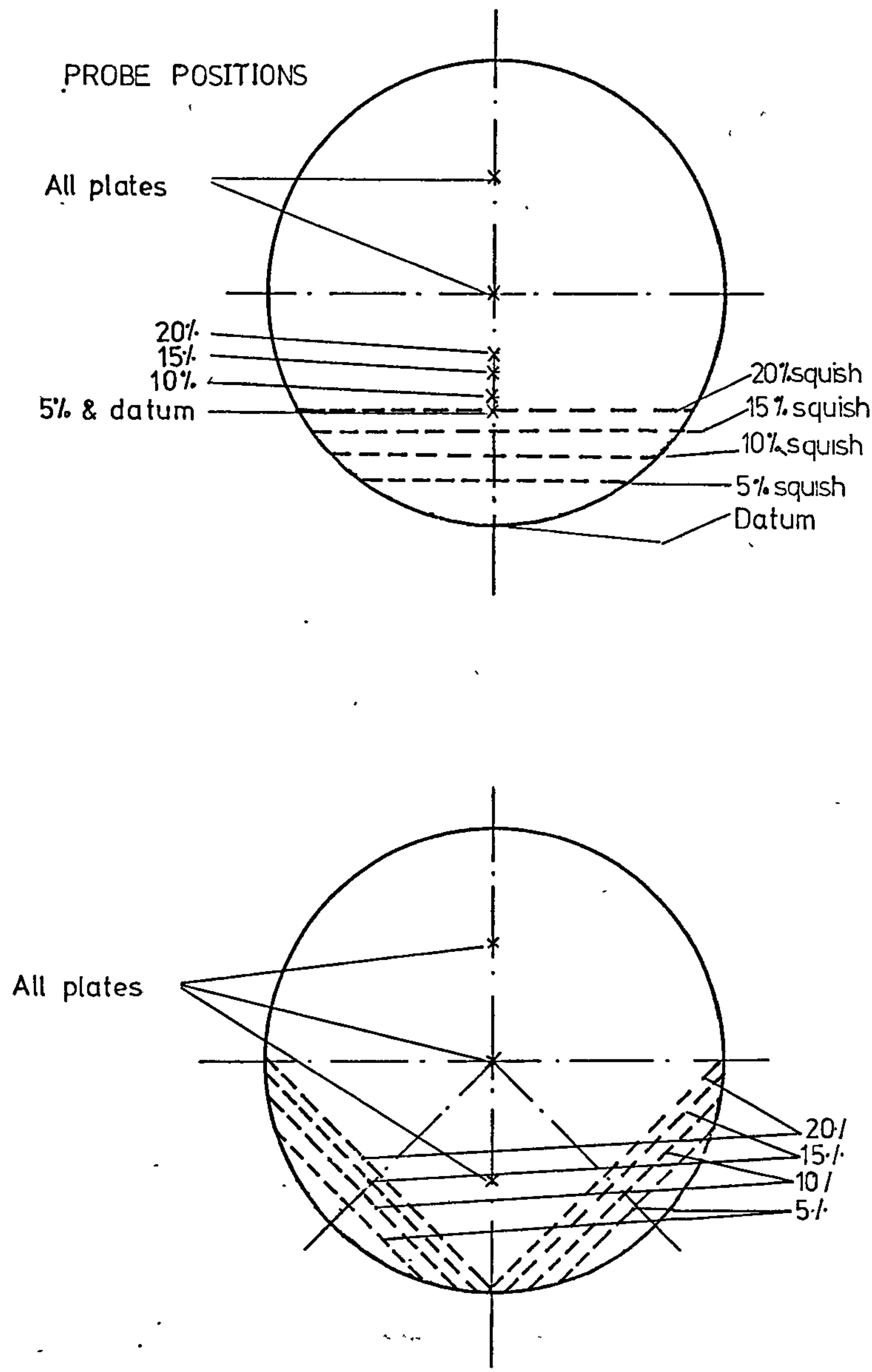

FIG 6.9 LOCATIONS OF SQUISH AREAS AND PROBE POSITIONS

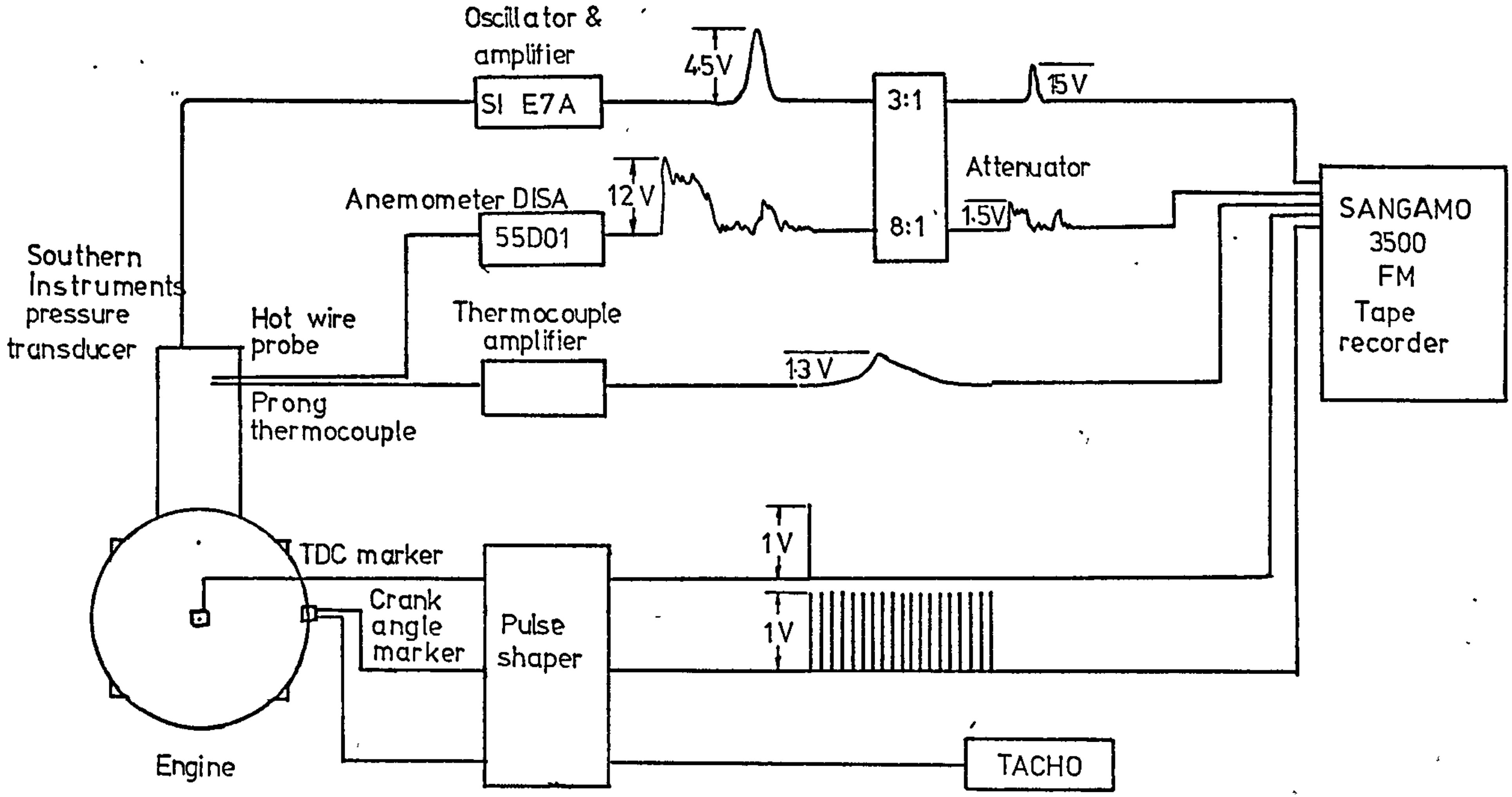

FIG 6.10 DATA ACQUISITION SYSTEM

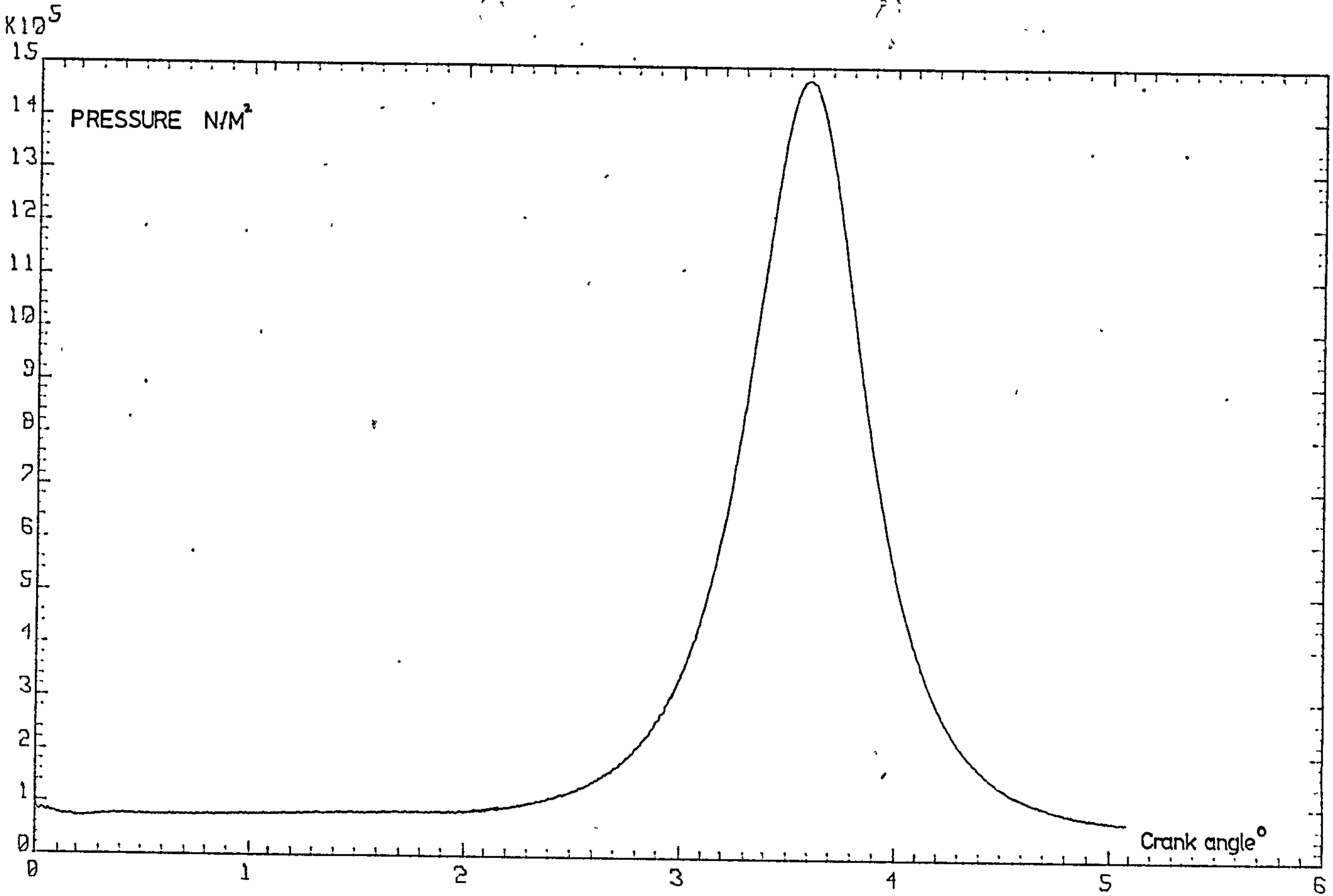

FIG 6.11 CYLINDER GAS PRESSURE

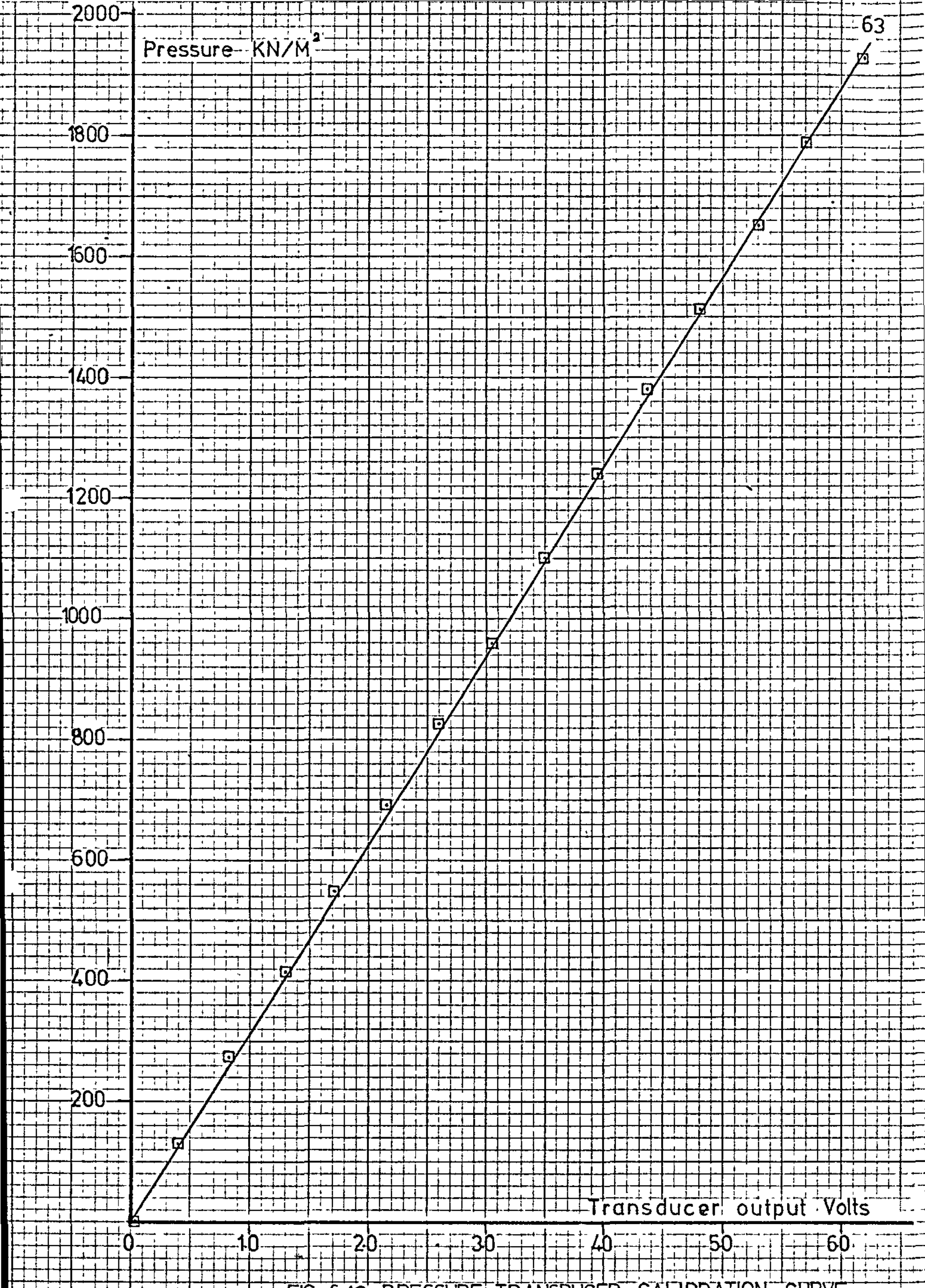

FIG 6.12 PRESSURE TRANSDUCER CALIBRATION CURVE

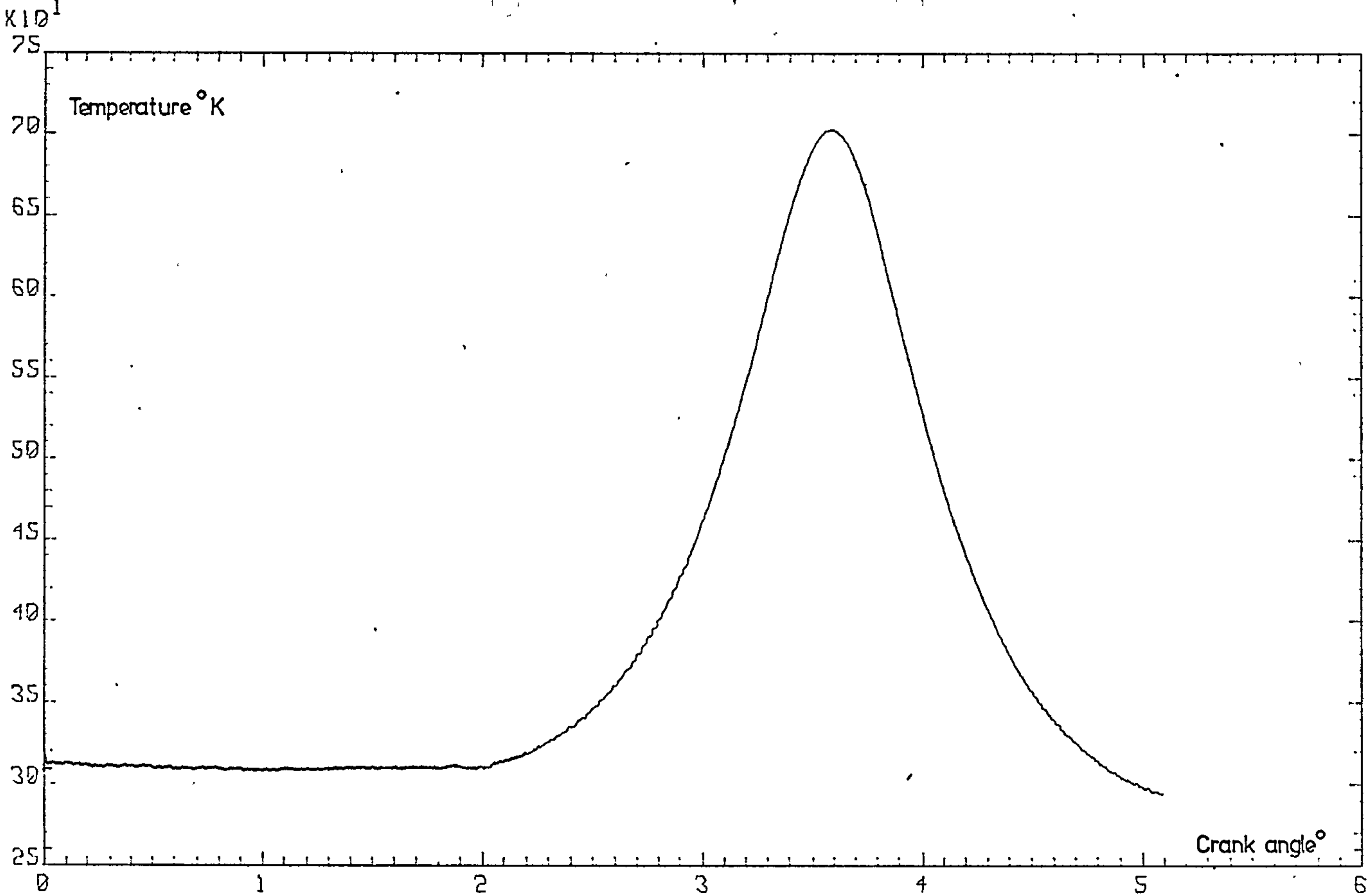

FIG 6.13 CYLINDER GAS TEMPERATURE

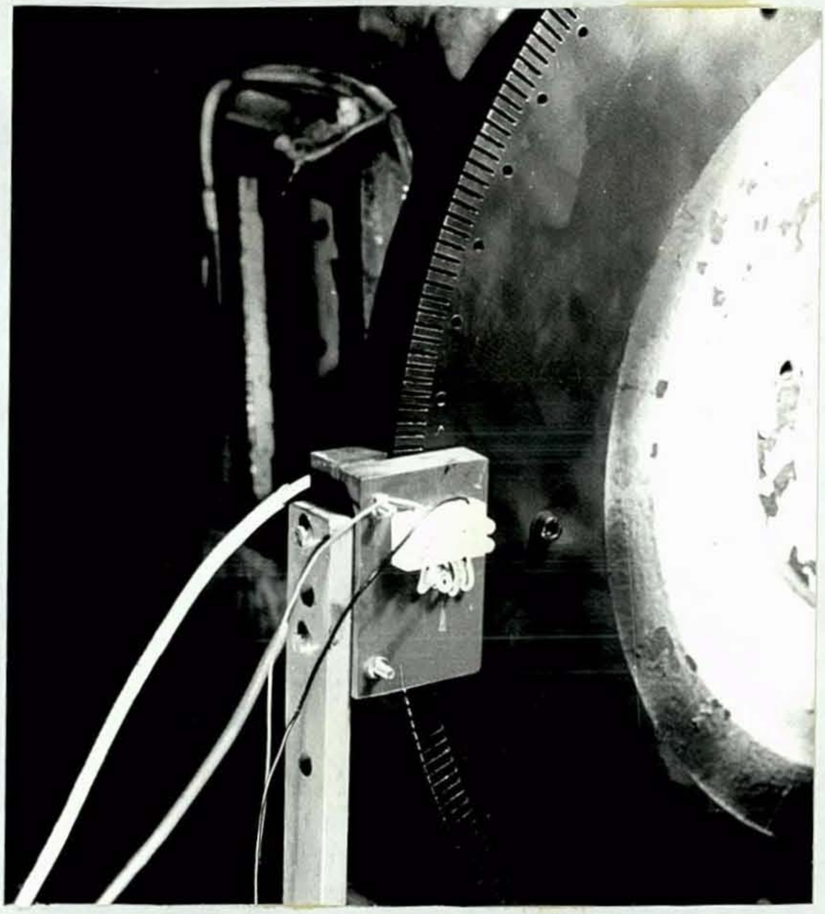

FIG 6.14 CRANK ANGLE MARKER DISC

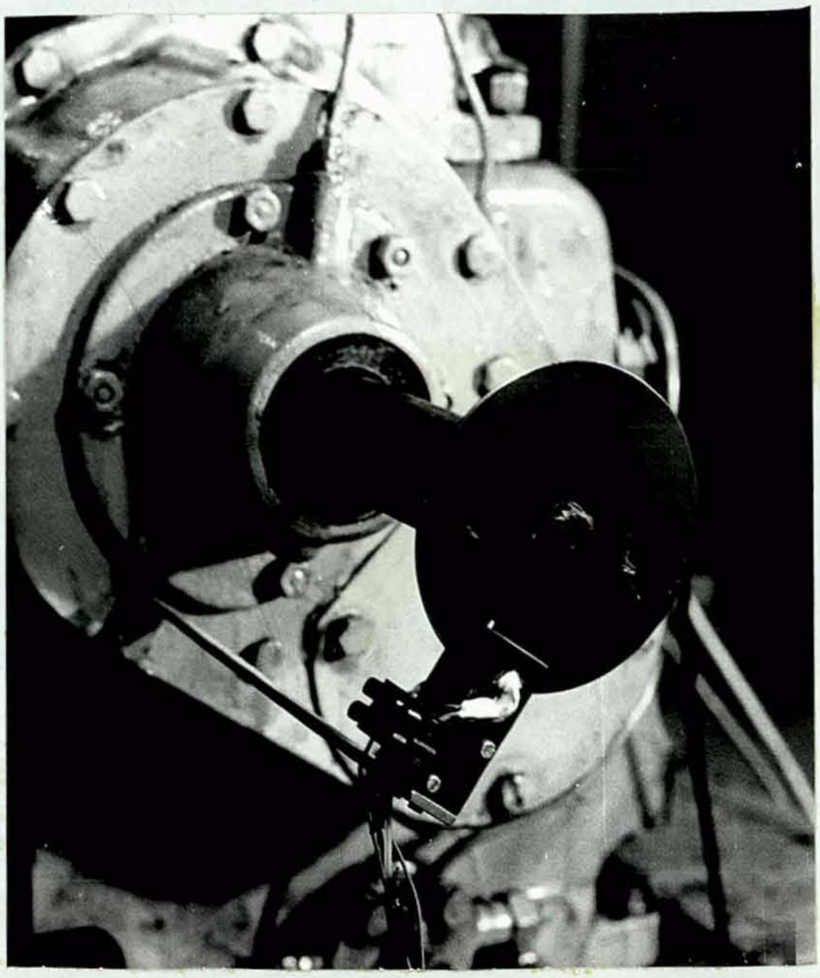

FIG 6.15 TDC MARKER DISC

CHAPTER 7

DATA ACQUISITION AND PROCESSING SYSTEM

Data acquisition system.

The motion of the air inside the combustion chamber of an engine is not a steady state phenomenon. The piston and valve positions alter all the time and this makes every point in the cycle a singular entity. Apart from this the engine cycles differ considerably from each other.

This situation leads to the requirement that the data acquisition system must be synchronous with the piston motion. In practical terms this means that it must be ensured that the anemometer output readings are taken at precisely the same points in every cycle investigated. Without this any comparison between cycles or any averaging of results would lead to doubtful results.

The experimental rig was equipped with a set of markers, one for the angle of crank rotation giving 360 equally spaced pulses per revolution, and one for the top dead centre position that gave a pulse at TDC of the intake stroke. These pulses were recorded simultaneously with the anemometer output signal and enablod the accurate location of every event during the engine cycle. The actual analysis of the recorded voltages was performed in two steps, each time using a digital computer.

In analogue form the recorded signal is difficult to analyse so it was desirable to digitise it. However the digitising rate had to be controlled to keep the synchronisation of the signal with the crank rotation.

This led to the use of a Hewlett Packard 2600 Digital Computer/Fourier Analyser equipped with the Hewlett Packard 5451A Analogue to Digital Converter and two Hewlett Packard magnetic tape units.Fig 7.1

Normally the data is read in by the ADC at a rate set by the user. The data is then stored on the magnetic tape in blocks that can be of various sizes, again set by the user. For this work a block size of 512 was used which meant that every block contained the data taken from 512 readings. The digitising process is initiated by a trigger which sets the beginning of every block of data.

The ADC which was used featured an external trigger facility on both the blocks of data converted and the digitising rate. Thus the top dead centre signal was fed into the data block trigger to ensure that the data was read in starting at TDC intake. Secondly the crank angle marker (1^{o} spaced) signals were fed into the external clock that controlled the digitising rate so that it gave one reading at precisely every degree of rotation.

This meant that after the digitising process, the data was stored on magnetic tape in individual blocks, each containing the part of one engine cycle stretching from 0^{o}-512^{o}. Every number in the data block corresponded to a precise position in the cycle (e.g. the 60th point corresponds to the output at 60^{o} after TDC intake).

For every probe location or engine speed examined 100 engine cycles were read in and stored.

After digitising the data this had to be processed to lead to air velocities, turbulence intensities, scales, etc. However the anemometer output does not vary linearly with the air velocity so a straight forward average of the data blocks obtained was not a suitable proposition. On the other hand the computer used for the digitising process can only handle a limited number of arithmetic operations and raising numbers to a real power is not one of these. It was therefore necessary to transfer the data to a larger digital computer which could meet these requirements. This was the ICL 1904S of the University Computer Centre. However the machine codes were not identical so the original tape had to be "translated" from Hewlett Packard code into ICL code. This process yielded a tape containing exactly the same information which would be read in by the tape units associated with the ICL 1904S comupter.

Processing of data

The data tape in ICL code was read into the computer so the air velocities were calculated (according to the calibration) at every point i in the cycle under investigation. This process involved the reading in of 512 anemometer output voltages per engine cycle (the exhaust stroke was excluded), the calculation of the corresponding air velocities and the storage of the results on a temporary data file. This process was repeated for a number of 100 engine cycles and the result was an equivalent copy of the data tape containing air velocities (rather than anemometer output voltages).

Following this the file was rewound and the first 512 instantaneous velocities U were read in. Consequently the second block of 512 velocities were read in and the values it contained were added to the corresponding values of the block previously read in. The procedure was repeated 100 times and the resulting block was divided by 100 value by value to yield the average air velocity U at every point i in the cycle.

$$\overline{U}(i) = \sum_{n=1}^{N} \frac{U(i)}{N}$$

where N is the total number of cycles averaged.

The next step was the calculation of the turbulence intensity values and for this the file containing the instantaneous velocity values was rewound and again read in block by block. The air velocity fluctuation about the average was calculated by using the following formula.

$$u(i) = \sqrt{\left[U(i) - \overline{U}(i)\right]^2}$$

These instantaneous variations of the air velocity were calculated at every point of every cycle under investigation. These fluctuations were averaged point by point correspondingly to yield the turbulence intensity.

$$\overline{u}(i) = \sum_{n=1}^{N} \frac{u(i)}{N}$$

The ratio of the turbulence intensity to the average velocity was calculated to find the relative turbulence intensity.

$$R(i) = \frac{\overline{u}(i)}{\overline{U}(i)}$$

The next step in the procedure was to calculate the turbulence macro scales. To make this possible the autocorrelation coefficient had to be established for every point in the cycle under investigation. The non stationary autocorrelation coefficient was defined as follows:

$$R_I(i) = \frac{1}{N} \sum_{n=1}^{N} \frac{u(i) \cdot u(I)}{\overline{u}(i) \cdot \overline{u}(I)}$$

where (i) is the angle at which the autocorrelation is evaluated and (I) is the angle about which it is calculated. Having found the value of the autocorrelation coefficient, the values of the turbulence scales can be then calculated. The time macro scale of turbulence is given by

$$T(i) = \frac{1}{W} \int_{i-I}^{0} R_I(i)\, di$$

where N is the engine speed in rad/s and i-I is the maximum lag angle involved in the calculation of R_I (i). The length macro scales result then simply by multiplying the time macro scales by their corresponding air mean velocity

$$L(i)=T(i)\cdot\bar{U}(i)$$

The calculation of the autocorrelation coefficient and time scales can take a large amount of computer time if the calculations involved take place at every degree of crank rotation or if the maximum lag angle is too large.

Hence a compromise had to be struck here between accuracy and efficiency. Reasonably good results were obtained by evaluating the autocorrelation coefficient at every 15 degrees of rotation with a maximum lag angle of 40°.

To achieve this the computer program read the file containing the instantaneous velocities in and for every engine cycle it evaluated the velocity fluctuations about the mean at the relevant points. A numerical integration was then carried out to find the time scales at every 15 degrees for every one of the 100 cycles involved. The macro scales corresponding to the same points in the cycle were then averaged to obtain the average time macro scales. This was then followed by the evaluation of the length scales which was a straight forward point by point multiplication of the time scales by the corresponding mean air velocities.

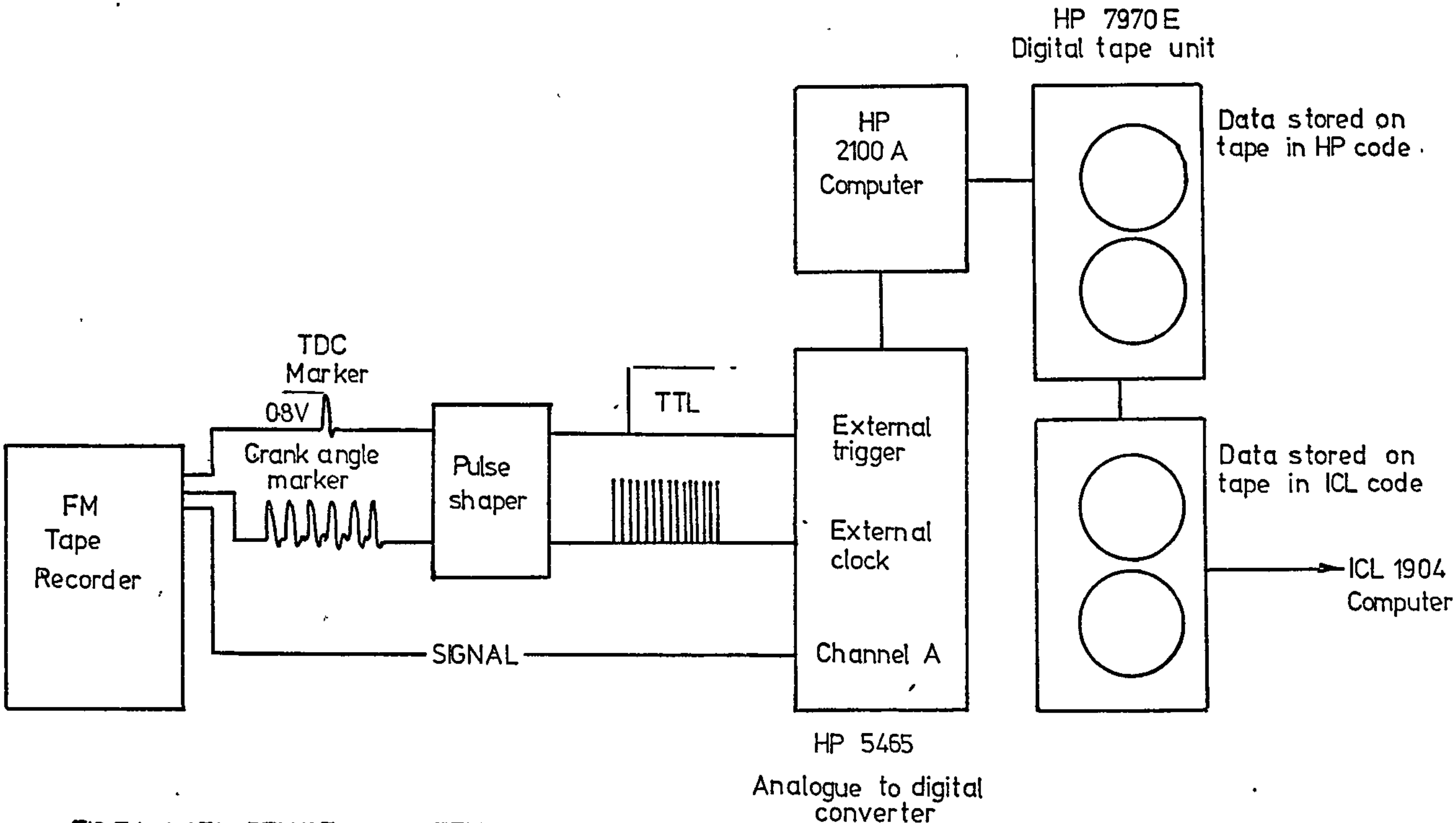

FIG 7.1 DATA REDUCTION SYSTEM

CHAPTER 8

RESULTS AND DISCUSSION

Results and Discussion

Gas velocities

The mean air velocity was observed to increase with the engine speed at all the probe positions in the combustion chamber and with all the chamber configurations. This proves that there is a velocity component related to the piston speed.Fig 8.1

The profile of the intake jet is dependent on the position in the combustion chamber. Next to the squish area one finds high air velocities until the piston reaches BDC. In this area strong and long lasting jets of air are detected. On the opposite side of the combustion chamber the peak air velocities are as high but they only last till approximately 100° ATDC. In the centre the intake jet lasts till approximately 150° ATDC. However the average air velocities are lower when compared to the values found at the extremities of the chamber. This proves that the intake imparts a swirling motion to the air. The charge is directed at the squish side of the combustion chamber on a path which follows an imaginary extension of the inlet tract. It then turns to follow the cylinder wall and sets the air in a rotational motion about the axis of the cylinder. This fact is proved by the low velocities found in the centre of the combustion chamber.Fig 8.2

The influence of squish at low engine speeds is quite marked. With small squish areas (up to 15% in 2 areas) the effect is high. The combustion chambers feature a region of high activity at the edge . However, increasing the amount of squish has the effect of increasing the mean air velocities in the centre of the combustion chamber. These are then comparable with the air velocities found at the extremities of the chamber. Squish areas bigger than 10% in one area create a local increase in air velocity in their vicinity but do not affect the rest of the chamber. At 750 rpm the only region affected by the squish velocites is the centre of the combustion chamber and the region situated opposite the squish area.

As the speed of the engine increases these transitions occur when smaller amounts of squish are present. At 1000 rpm the region of relative stagnation in the centre of the combustion chamber disappears after adding 15% squish in two areas. At 1500 rpm the charge motion is practically uniform after adding 20% squish in two areas. Large squish areas are of any consequence only at low engine speeds (750 rpm). Fig 8.3 – 8.8

As already mentioned in the centre of the combustion chamber the velocities are initially low but they increase rapidly when large squish areas are present.

In the region next to the squish area the air velocities are relatively high but do not vary as much with the amount of squish at any engine speed.

The situation is different at the opposite side of the combustion chamber. The air velocities increase initially and then decrease suddenly to very low values. The velocities increase yet again with increasing amounts of squish. This is thought to be due to the interaction between the intake induced swirl and the squish velocity. With low squish areas the charge has a body swirl motion carrying with it the squish velocity components. However with increasing squish this body motion is broken up and the resultant velocity is seen to drop significantly. Increasing the squish areas even further the squish motion becomes dominant but the velocities are always lower than those imparted by the body swirl motion. The effect is to create a more uniform velocity distribution.

It is worth mentioning that any change that takes place in the velocity profiles at the edge of the chamber is preceded by a similar change in the centre of the combustion chamber, but in a chamber with a lower squish area. Thus it follows that the spatial propagation of the squish velocities is enhanced by the magnitude of the squish area.

The test runs were carried out with the wire in a horizontal position. However a few tests were performed with both a vertical and a horizontal wire. This was done to put in evidence the vortices that was thought that exist in the vicinity of the cylinder wall. This region of transition from the cylinder wall boundary layer to the body of the charge is thought to have some significance in the general motion of the air in the combustion chamber. Fig 8.9.

These were tests performed in the datum chamber (disc) at 5 mm and 10 mm off the cylinder wall. Very high velocities were recorded at compression. Also extremely large eddies were detected by examining the macro length scales of turbulence. Fig 8.10–8.11

It is thought that these are due to a series of vortices that form at the cylinder wall right on top of the piston. As the piston moves down the bore small vortices are formed in its wake and these grow as the time lapses reaching the size of maximum $\frac{1}{4}$ of the bore size when the piston reaches BDC. Fig 8.12. The swirling motion of the charge sets the vortices situated on the crown of the piston in a rotational motion so that the result is a local swirling motion around an axis formed by the circumference of the piston. This chain of events always takes place and is only broken up in the vicinity of TDC if large squish areas are present. Salama (23) recorded high velocities when using a vertical wire but he thought that these are due to the squish components present due to the Heron chamber investigated. However in the present case the same phenomenon took place in a disc chamber with no squish areas which leads to the conclusions listed above.

Regarding the magnitude of the squish area it was found that when it was all concentrated in one place the resulting air velocities were more evenly distributed across the chamber. The air velocities were found to increase sharply in the vicinity of the top dead centre of the compression stroke. This applies to all the cases examined no matter what chamber shape or probe location was used at the time. It is thought that the ring vortex located on top of the piston travels up the bore with the piston. As this reaches TDC the vertical space above it becomes small and the air has a tendency to increase its velocity in the horizontal plane to conserve its momentum. This would enhance the swirl velocity of the ring vortex. These velocities would be picked up by a vertical wire, and if they are high enough, a horizontal wire would register them too.

Turbulence

It was found that the turbulence intensity profiles follow (Fig 8.13) closely the velocity profiles. It was found more useful to discuss the pattern followed by the relative turbulence intensity and the turbulence macro scales.

It was found that the effect of squish was to reduce slightly the level of the relative turbulence intensity. This occurs when the squish areas are small and no other change occurs if the squish areas are increased. Fig 8.14

Typical trends show that in the vicinity of the squish area and in the centre of the combustion chamber the level of the relative turbulence intensity does not vary at all with the amount of squish present in the combustion chamber. At the side of the combustion chamber opposite the squish area there is a slight decrease of the relative turbulence intensity with small amounts of squish (15% in two areas). Larger squish areas do not affect this level at all.

By comparing the relative turbulence intensity levels at the edge, centre and squish side of the combustion chamber a uniform turbulence structure was revealed. In the vicinity of the squish area the levels were very slightly lower than in the rest of the chamber. However the difference is not thought to be significant.

These facts prove that the squish areas do not affect the magnitude of the velocity fluctuations about the mean value of the air velocity.

Examining the turbulence macro length scales again the effect of squish was not obvious. The eddy sizes were found not to vary when low or moderate amounts of squish were present. However large squish areas were found to create large eddies. This increase in eddy size when large squish areas are present (15% in one area) is thought to be due to the body motion that is imparted to the change in this situation. Fig 8.15

When comparing the results found by traversing the probe across the combustion chamber it was found that the eddies were largest in the centre of the chamber. This relates well with the previous mention of low air velocities in the centre of the combustion chamber. Also it was observed that the eddies are smallest in the vicinity of the squish area.

So far the turbulence structure created in a squish combustion chamber seems hard to explain. The turbulent velocities are not affected and the spatial structure (eddies) of the turbulent flow does not seem to change with squish.

However this image changes when the macro time scales of turbulence are examined. In this case the effect of the squish areas is strong and easy to follow.

It was found that the macro time scales of turbulence decrease sharply with increasing squish. A minimum value is reached at all engine speeds when 10% - 15% squish in one area exists in the combustion chamber. A further increase of the squish area brings the time scales up again. This trend was maintained at all engine speeds and in all the positions examined in the combustion chamber. Fig 8.16 - 8.18

Taking these facts into account, an explanation for the action of squish can be given. Small or moderate amounts of squish enhance the turbulence level in the combustion chamber by creating more and faster revolving eddies. The eddy size does not change when the squish areas are altered but their motion does. The higher frequency of rotation of these vortices has two advantages:

- It will improve mixing of the charge
- It is likely to quicken the propagation of the flame front because of the quicker energy transfer between adjacent eddies.

The existance of an optimum degree of squish is obvious, because the time scales are seen to increase after 15% squish in one area. It is thought that at this point the squish motion involves such a large proportion of the available mass of air that the charge receives a body motion. This creates larger and slower eddies.

The centre of the combustion chamber offers again a mixed picture. The transition between the turbulent motion and the body motion occurs earlier (less squish) than at the extremities of the chamber. Also the eddy frequency is comparatively lower than at the extremities of the chamber. This again underlines the existance of a low activity area in the centre of the combustion chamber. The slow eddies will join early to form large eddies which have lower frequencies of rotation. Also the engine speed seems to affect the transition from turbulent to body motion in this area. The higher the engine speed the higher the squish needed for this transition to occur.

The region near the squish area shows the highest eddy frequency at all engine speeds and in all the chambers investigated.

When performing tests in the vicinity of the cylinder wall extremely large eddies were picked up. These showed a very low frquency of rotation. As already explained these are eddies created during the intake stroke when they grow to large sizes. The compression stroke damps out their motion due to the increase in viscosity of the air and the time lapsed from their formation.

All figures refer to horizontal wires unless otherwise stated.

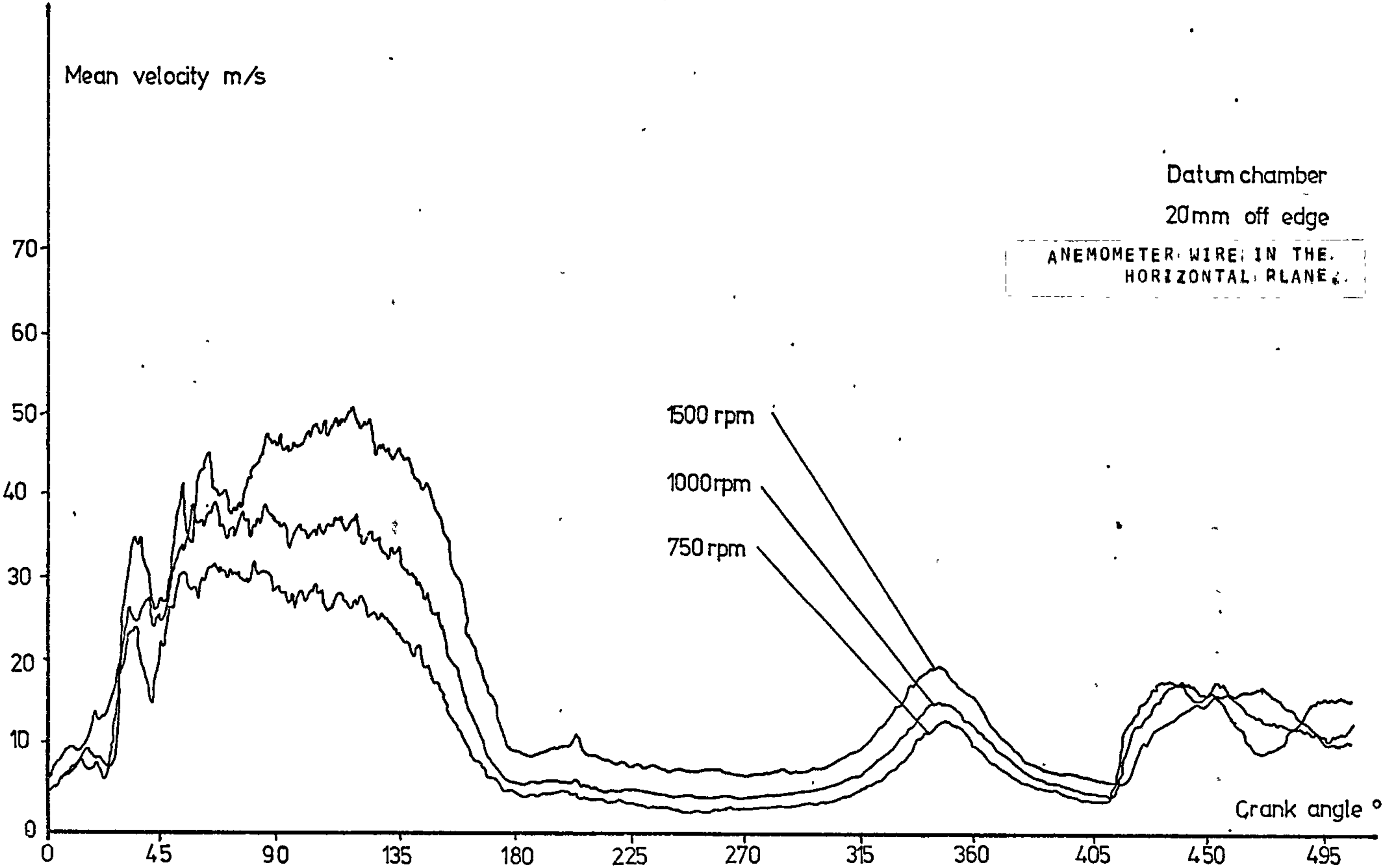

FIG8.1 INFLUENCE OF ENGINE SPED ON MEAN AIR VELOCITY

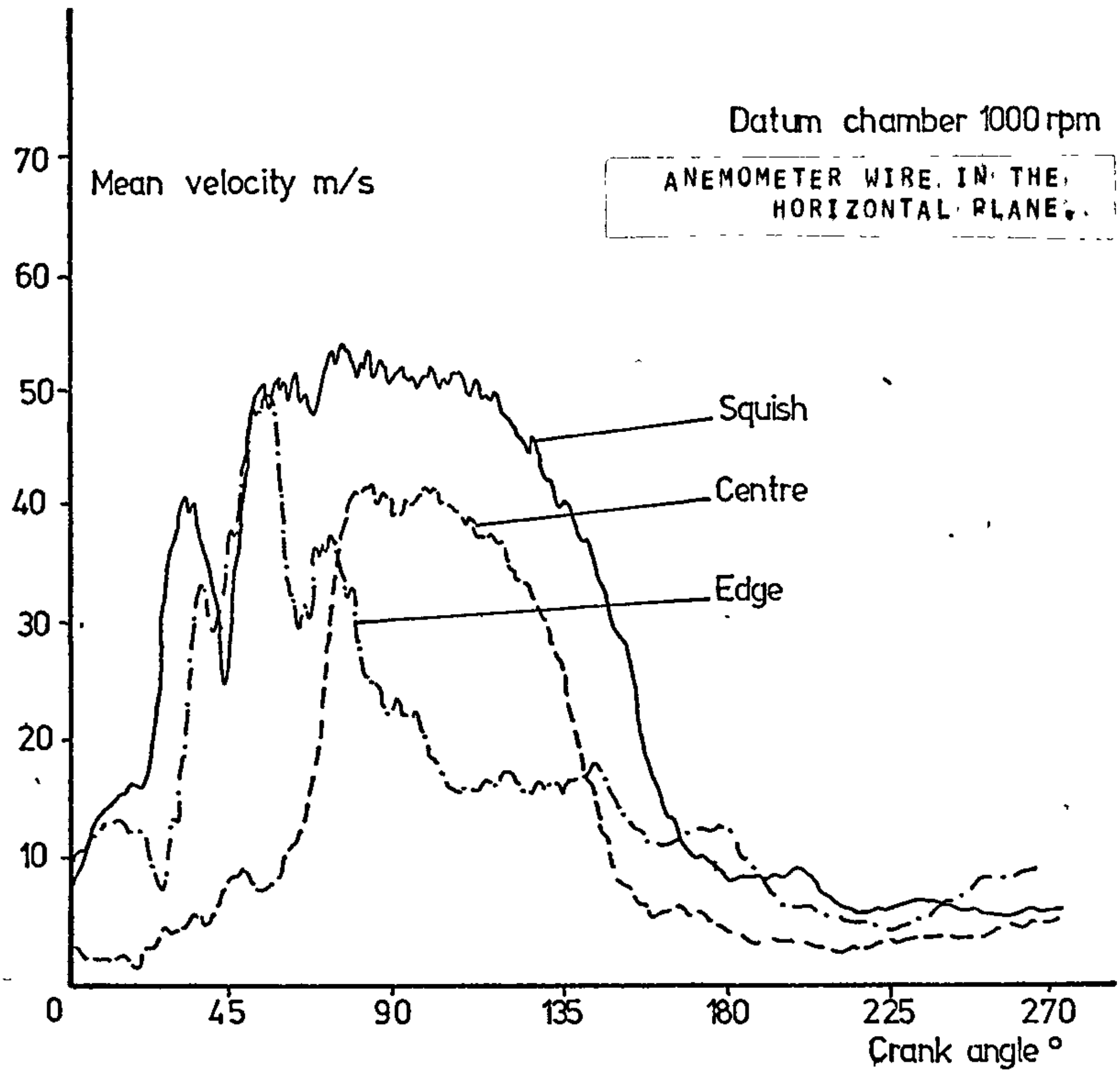

FIG 82 PROFILE OF INTAKE JET

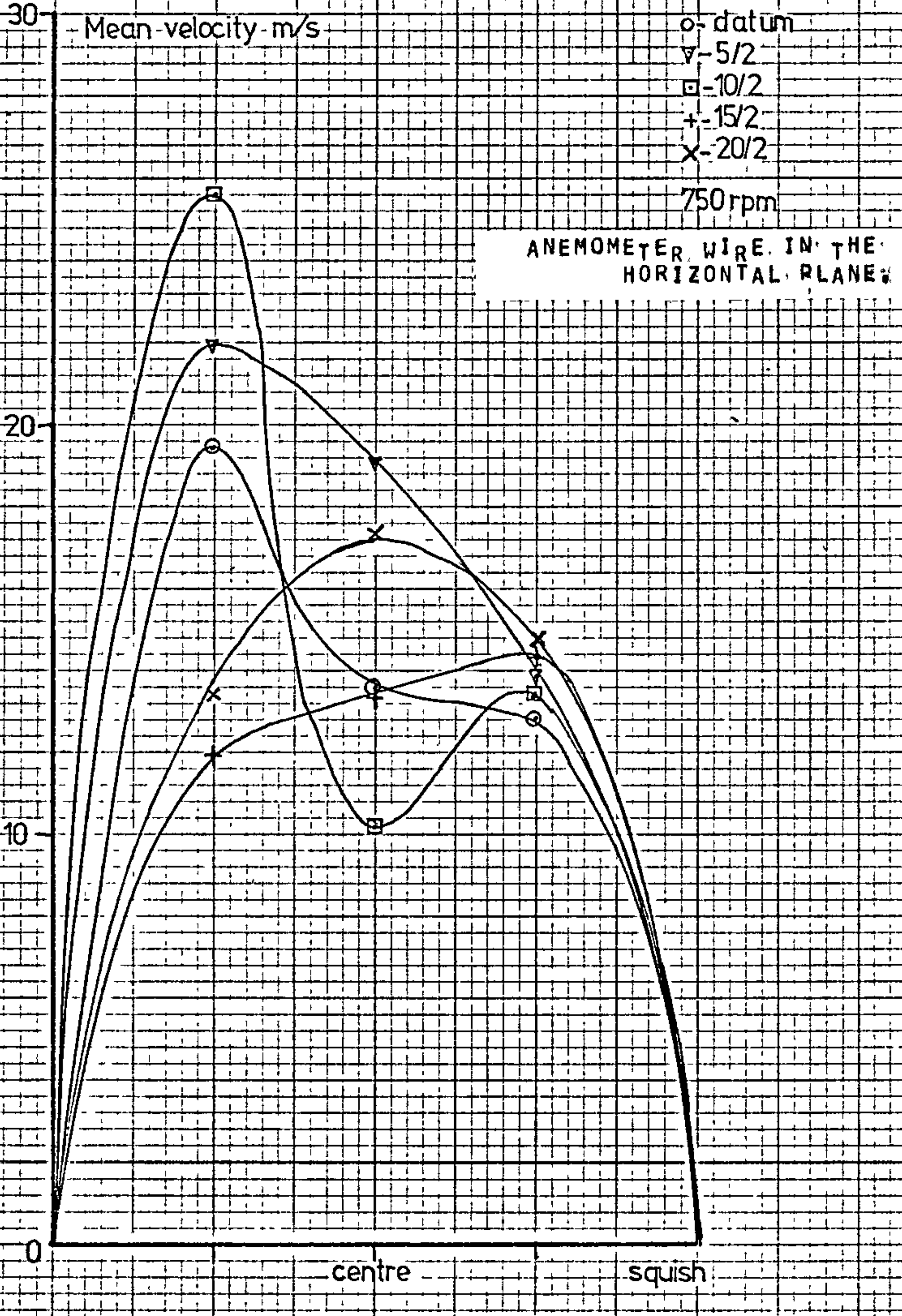

FIG83 MEAN VELOCITY DISTRIBUTION AT TDC

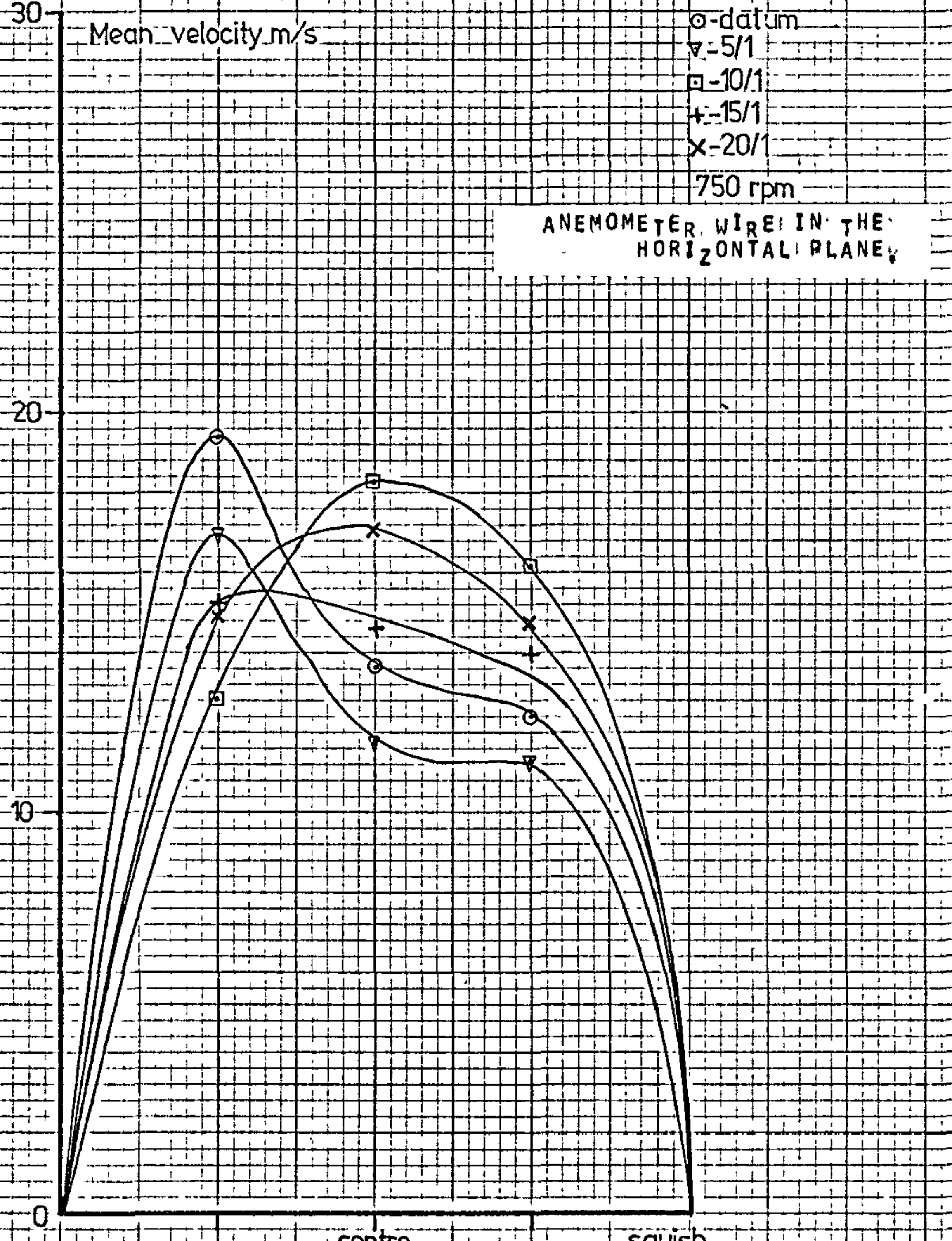

FIG 8.4 MEAN VELOCITY DISTRIBUTION AT TDC

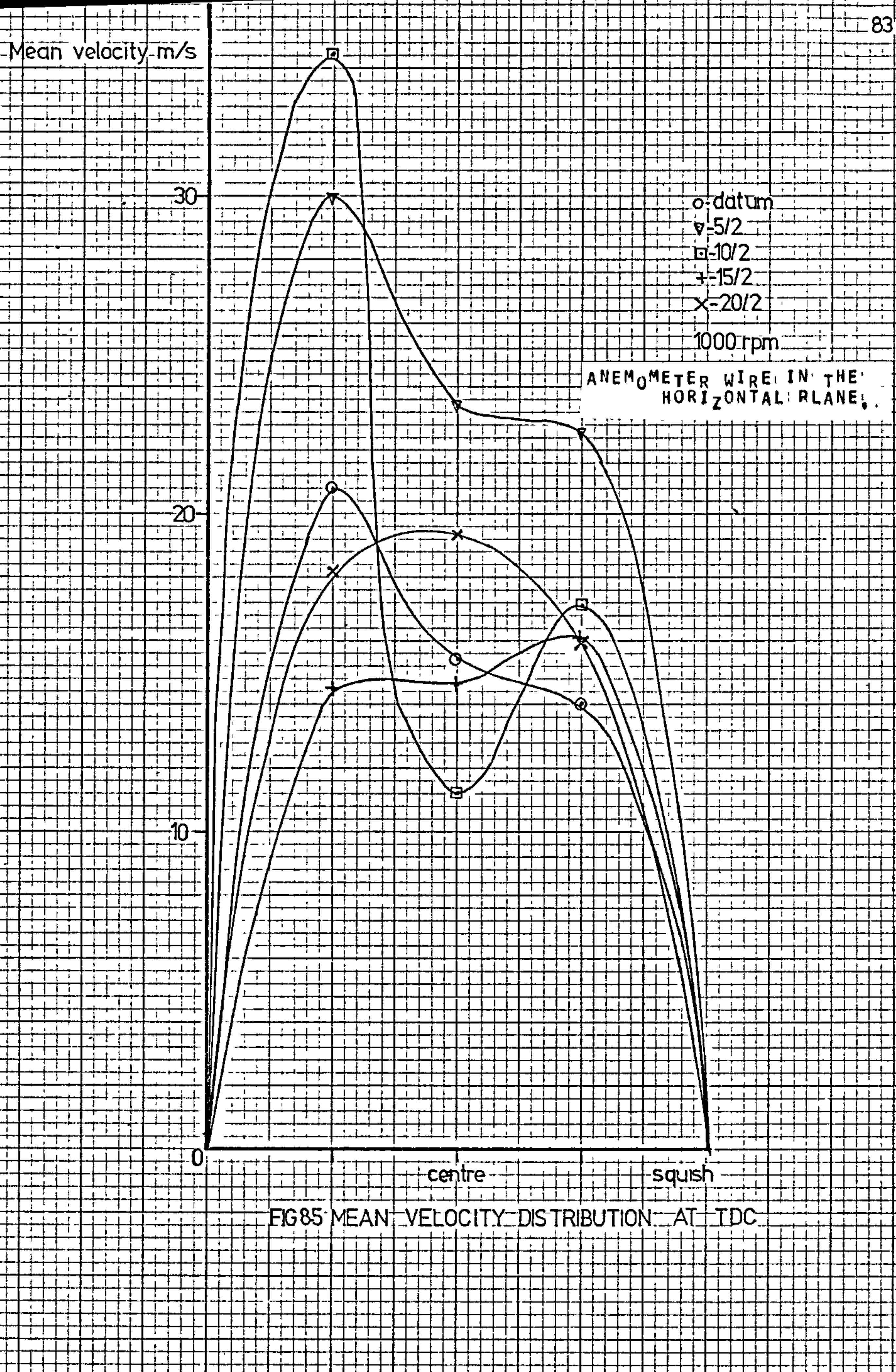

FIG 85 MEAN VELOCITY DISTRIBUTION AT TDC

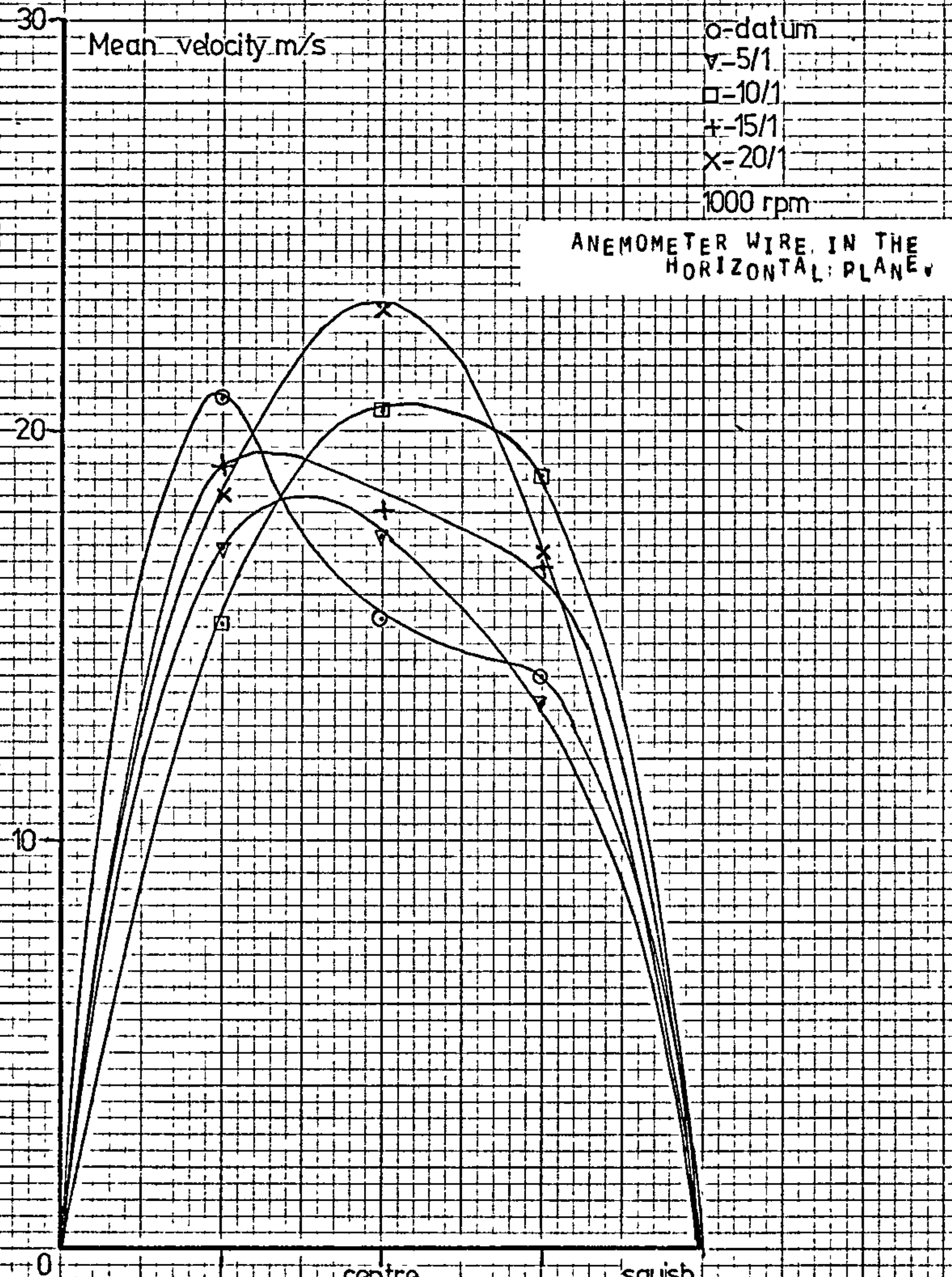

FIG 8.6 MEAN VELOCITY DISTRIBUTION AT TDC

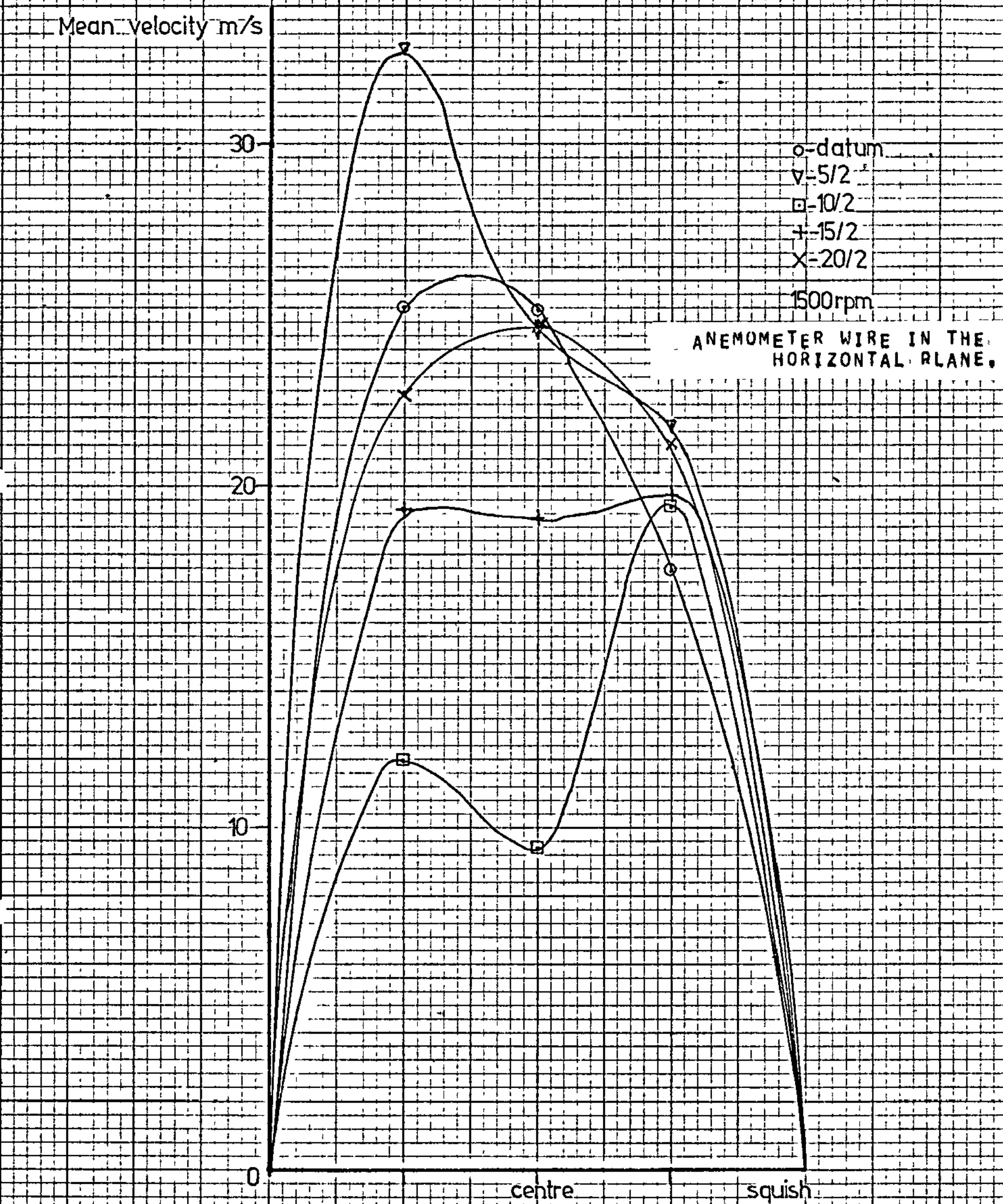

FIG 8.7 MEAN VELOCITY DISTRIBUTION AT TDC

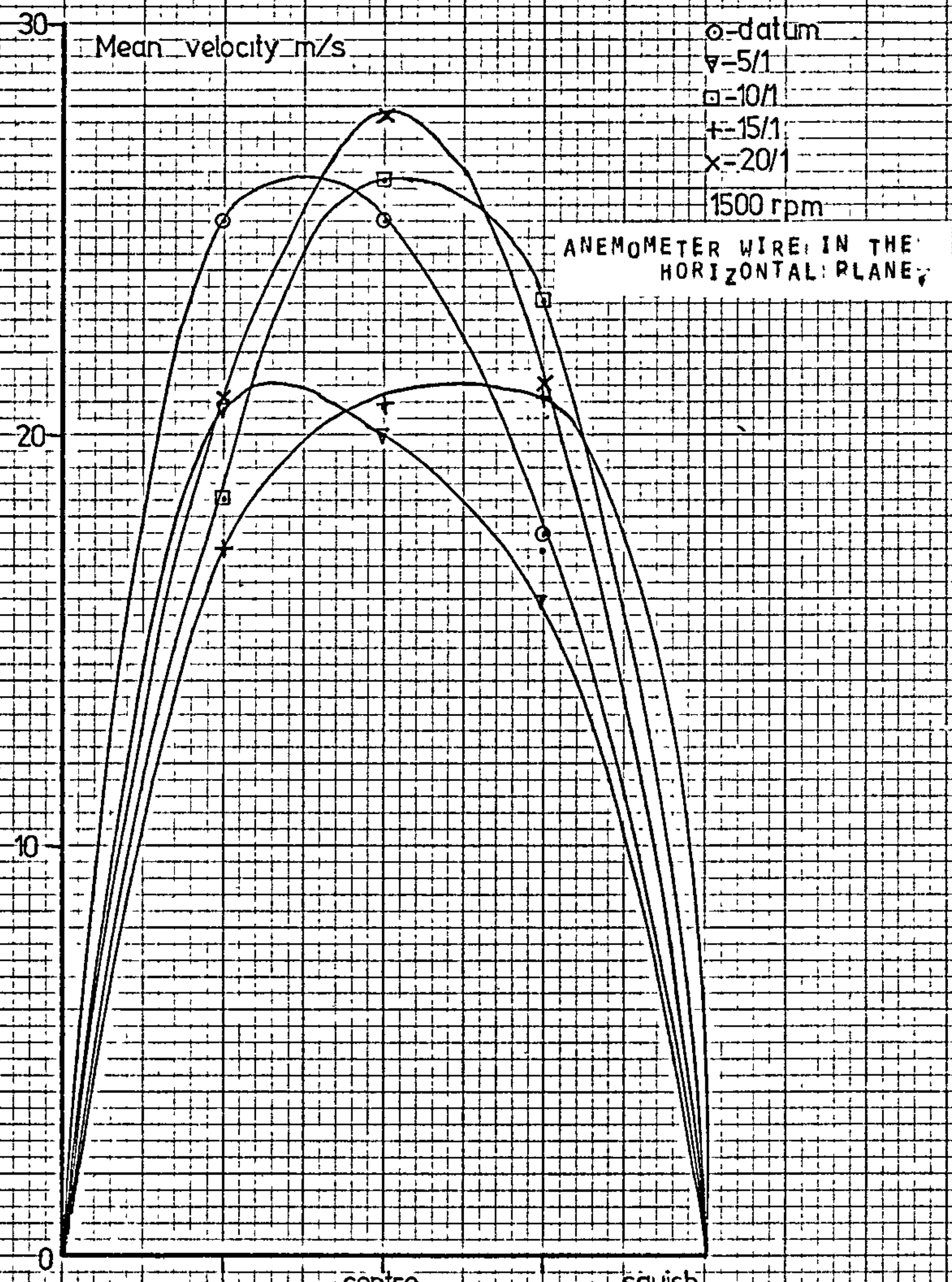

FIG8.8 MEAN VELOCITY DISTRIBUTION AT TDC

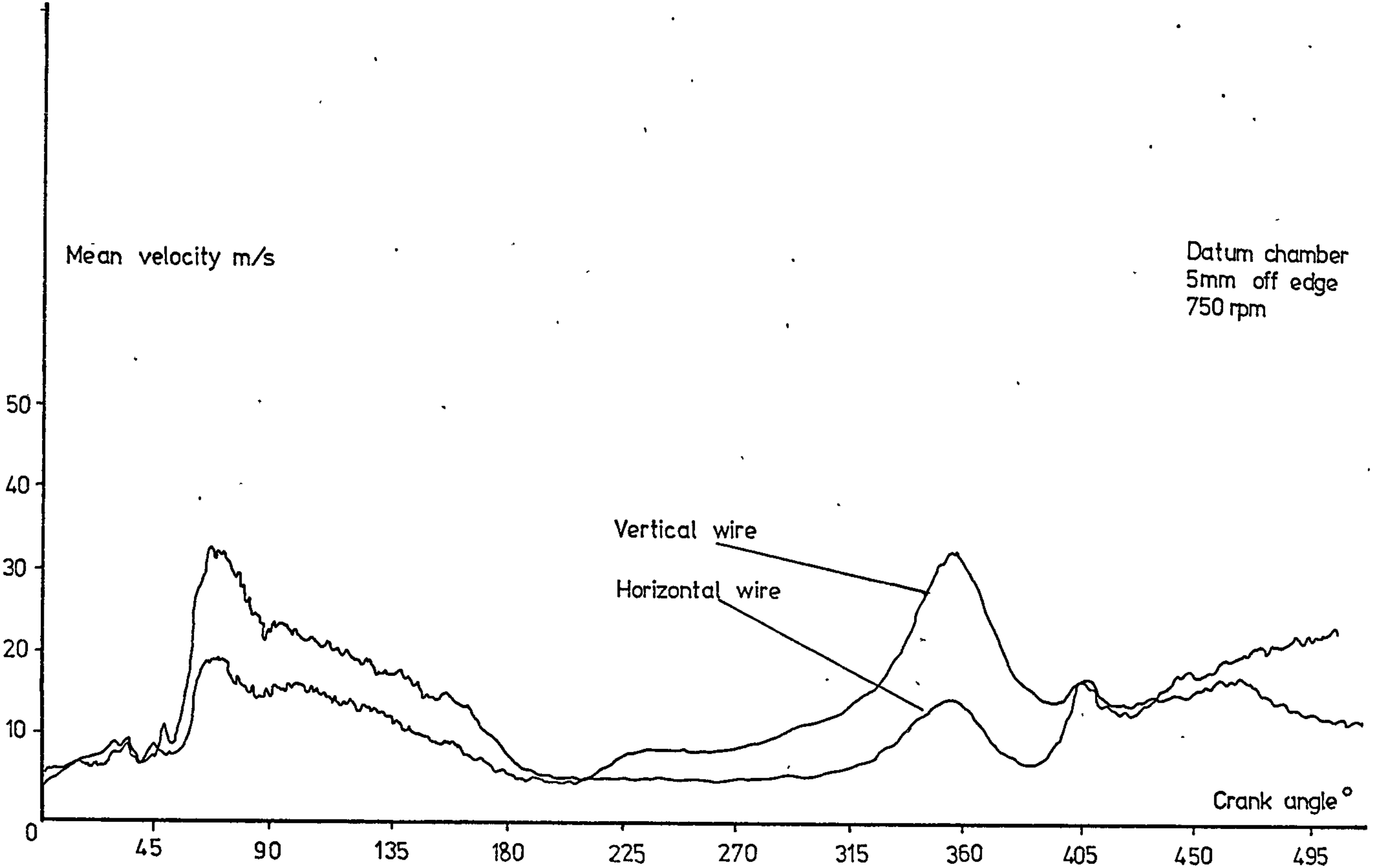

FIG89 INFLUENCE OF WIRE DIRECTION

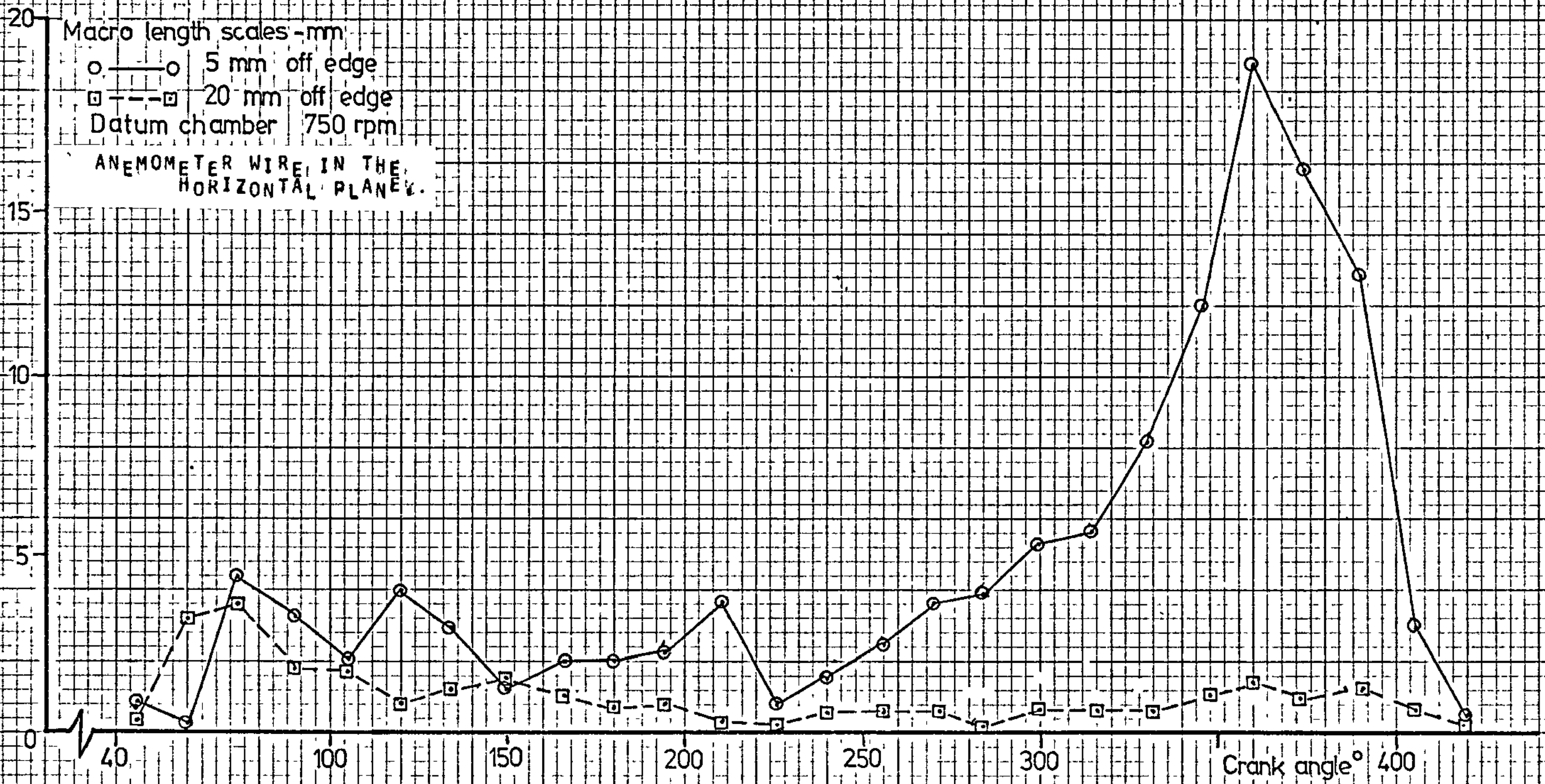

FIG8.10 MACRO LENGTH SCALES DISTRIBUTION

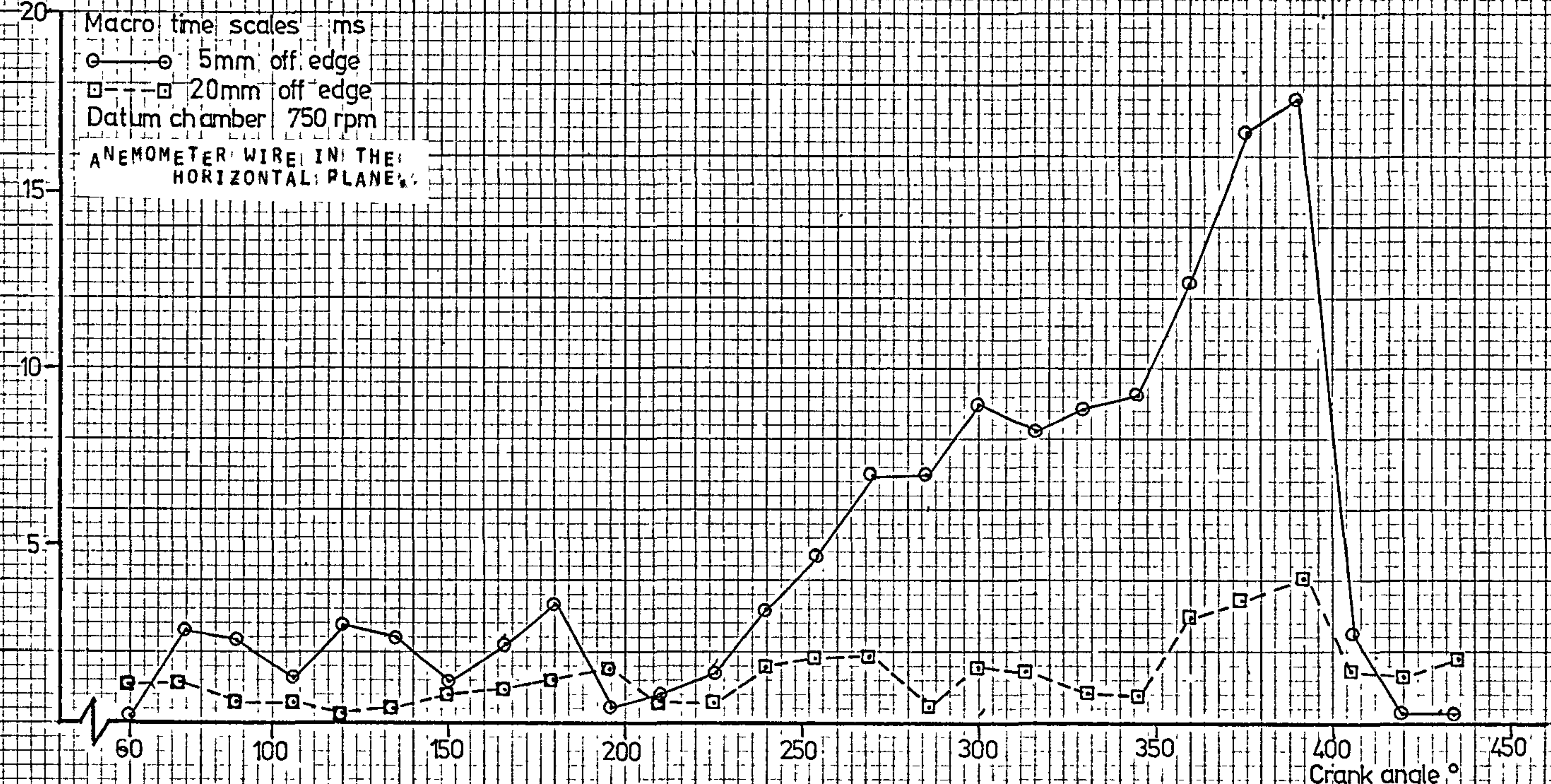

FIG8.11 MACRO TIME SCALES DISTRIBUTION

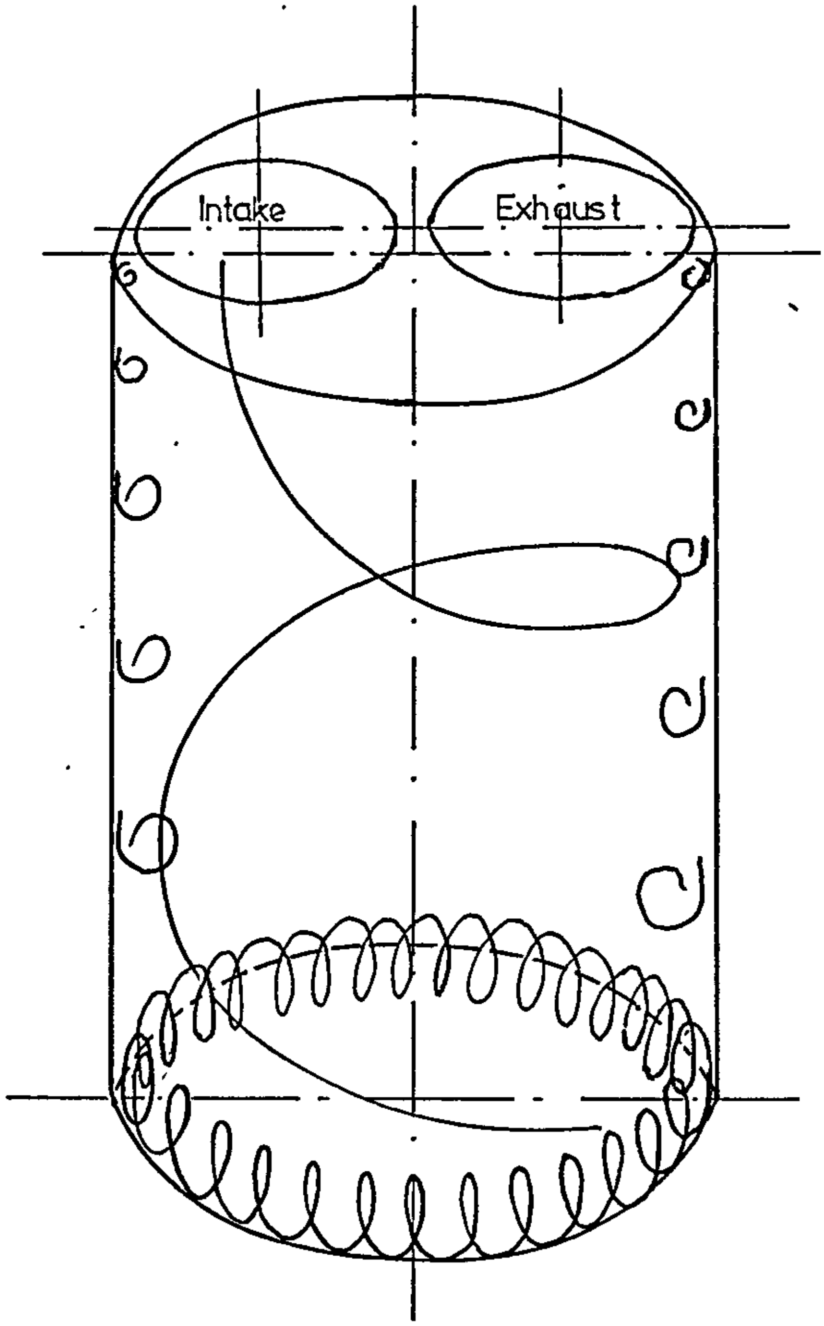

FIG 8.12 FLOW PATTERN OF CYLINDER GAS

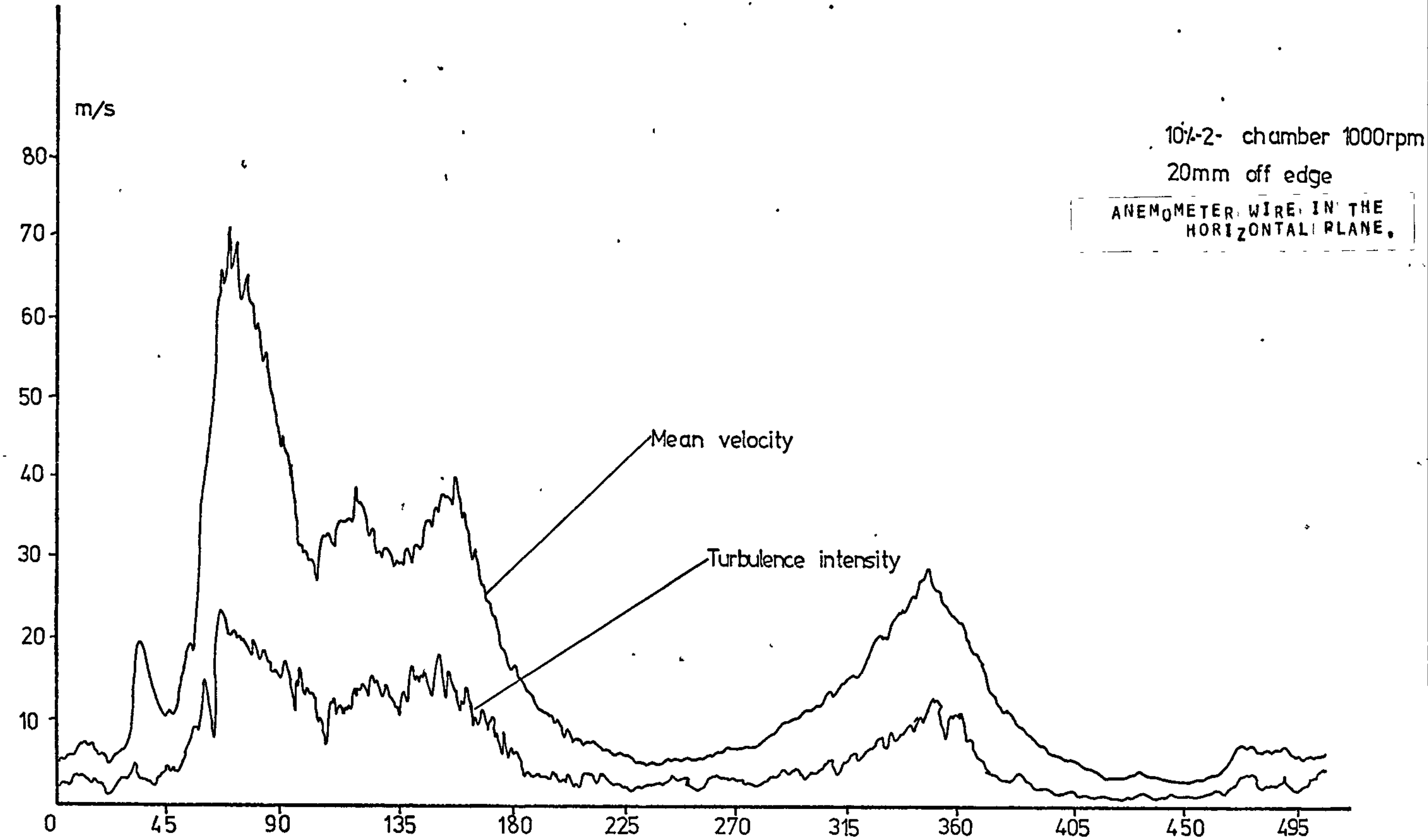

FIG8.13 MEAN VELOCITY-TURBULENCE INTENSITY DISTRIBUTION

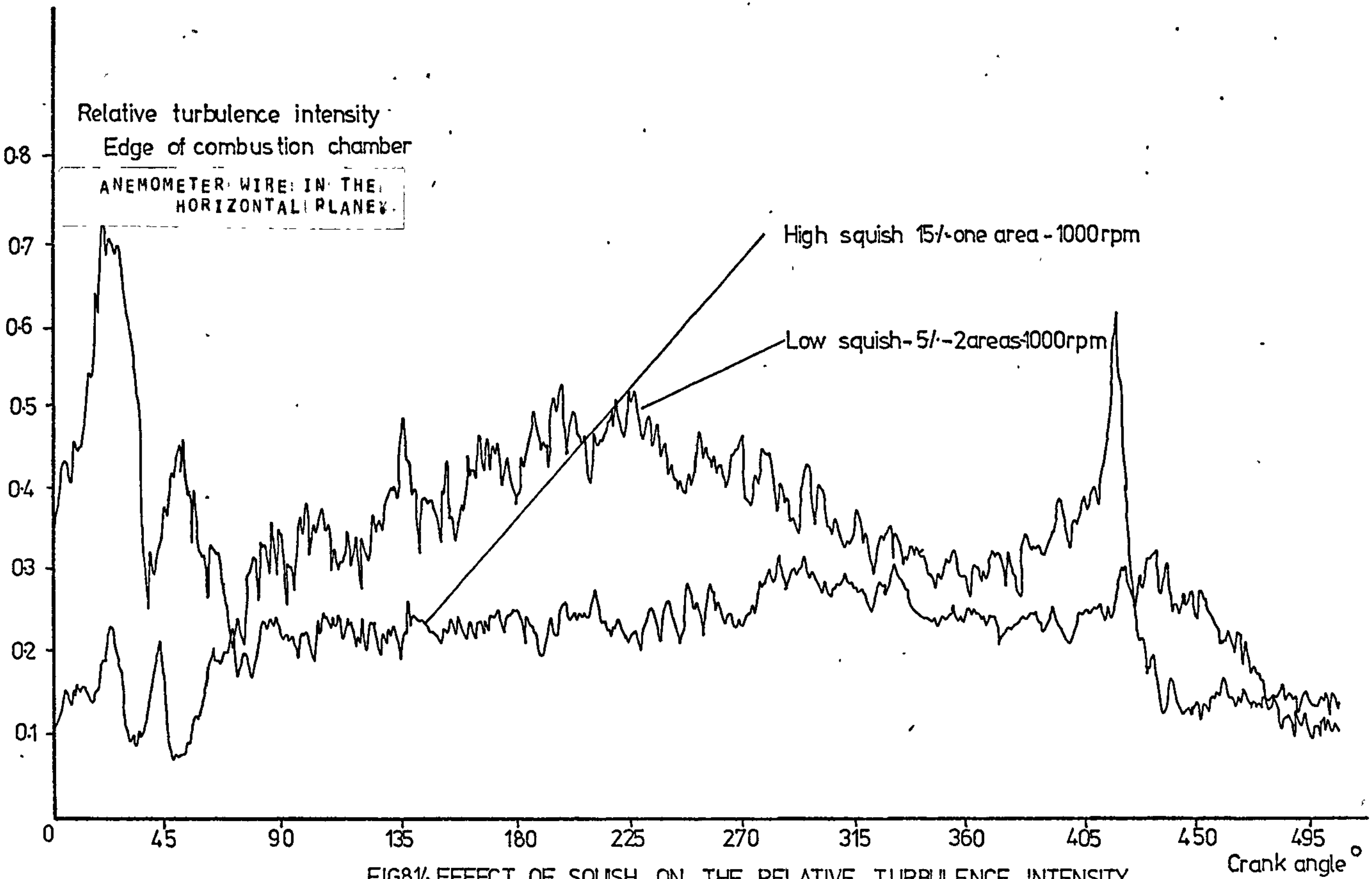

FIG8.14 EFFECT OF SQUISH ON THE RELATIVE TURBULENCE INTENSITY

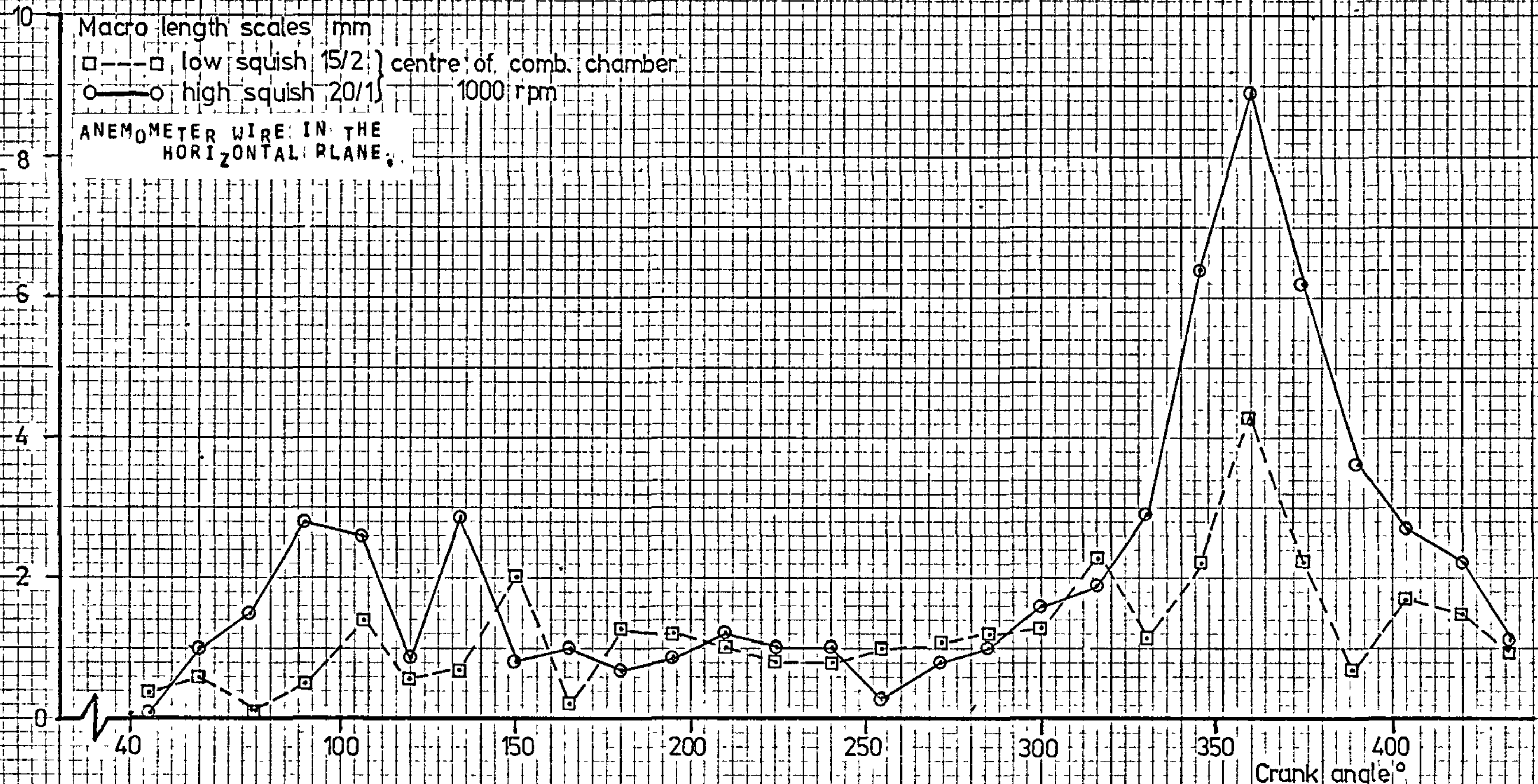

FIG8.15 EFFECT OF SQUISH ON MACRO LENGTH SCALES

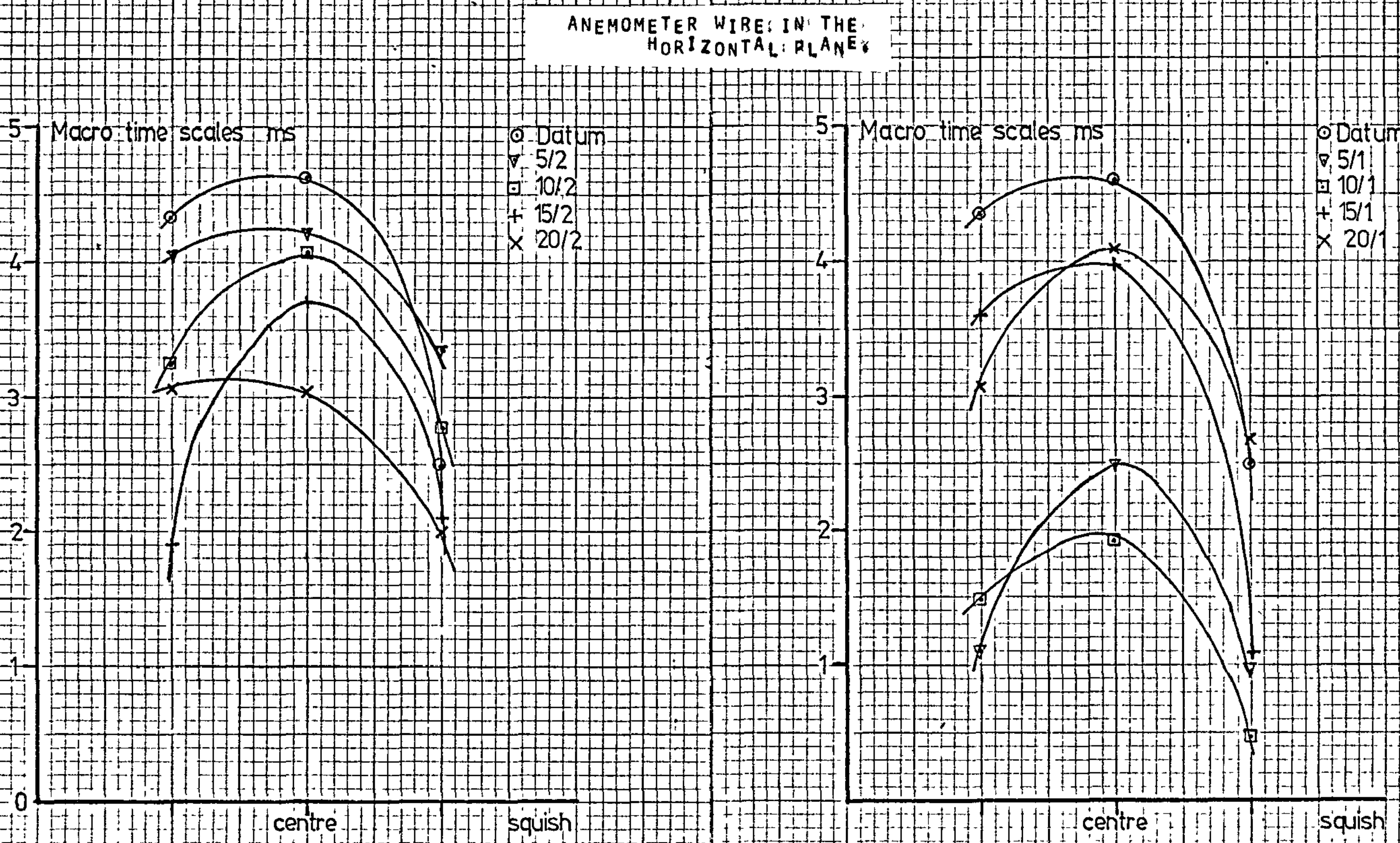

FIG8.16 MACRO TIME SCALES DISTRIBUTION 750 RPM AT TDC

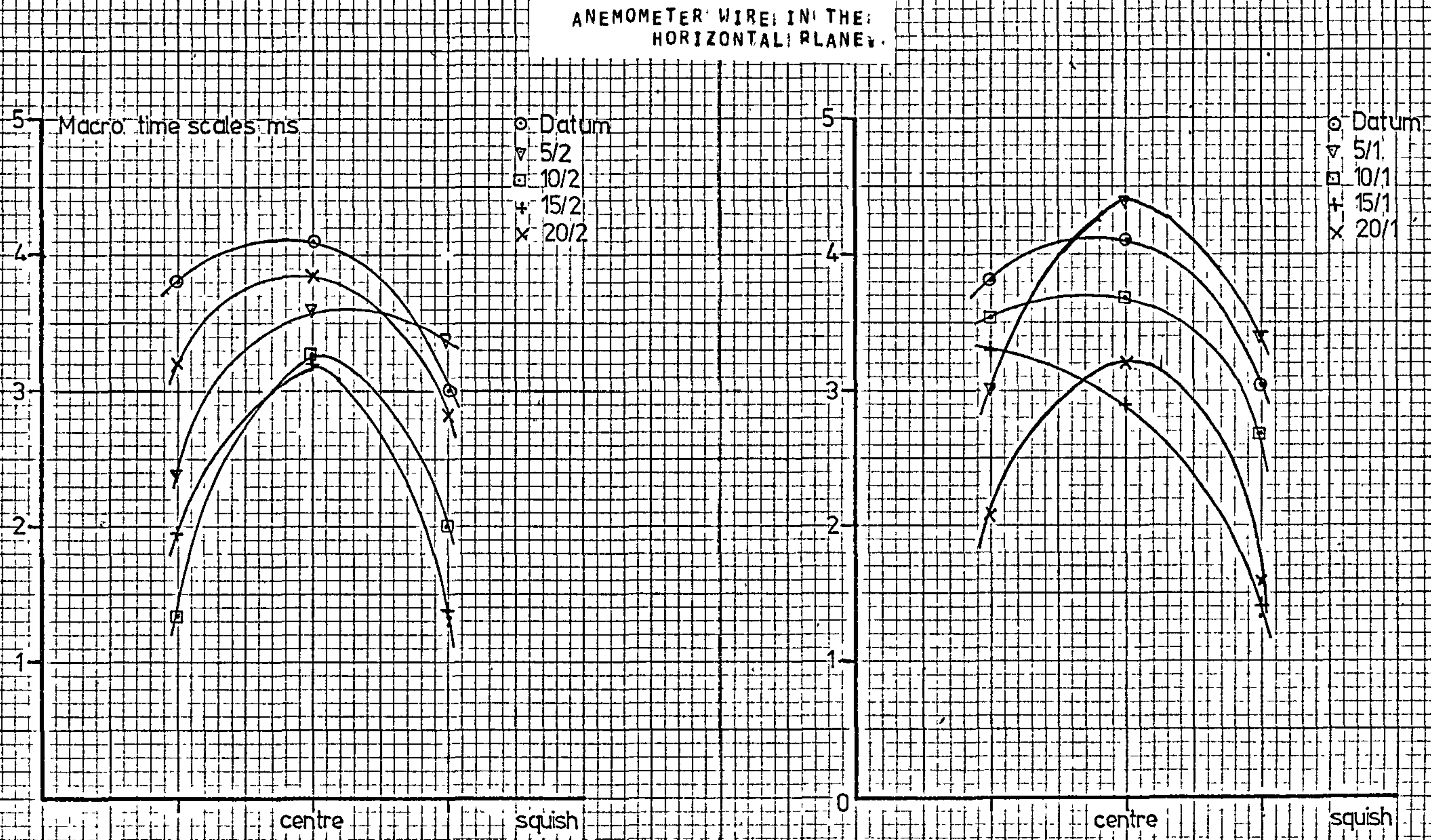

FIG 8.17 MACRO TIME SCALES DISTRIBUTION 1000 RPM AT TDC

ANEMOMETER WIRE IN THE HORIZONTAL PLANE.

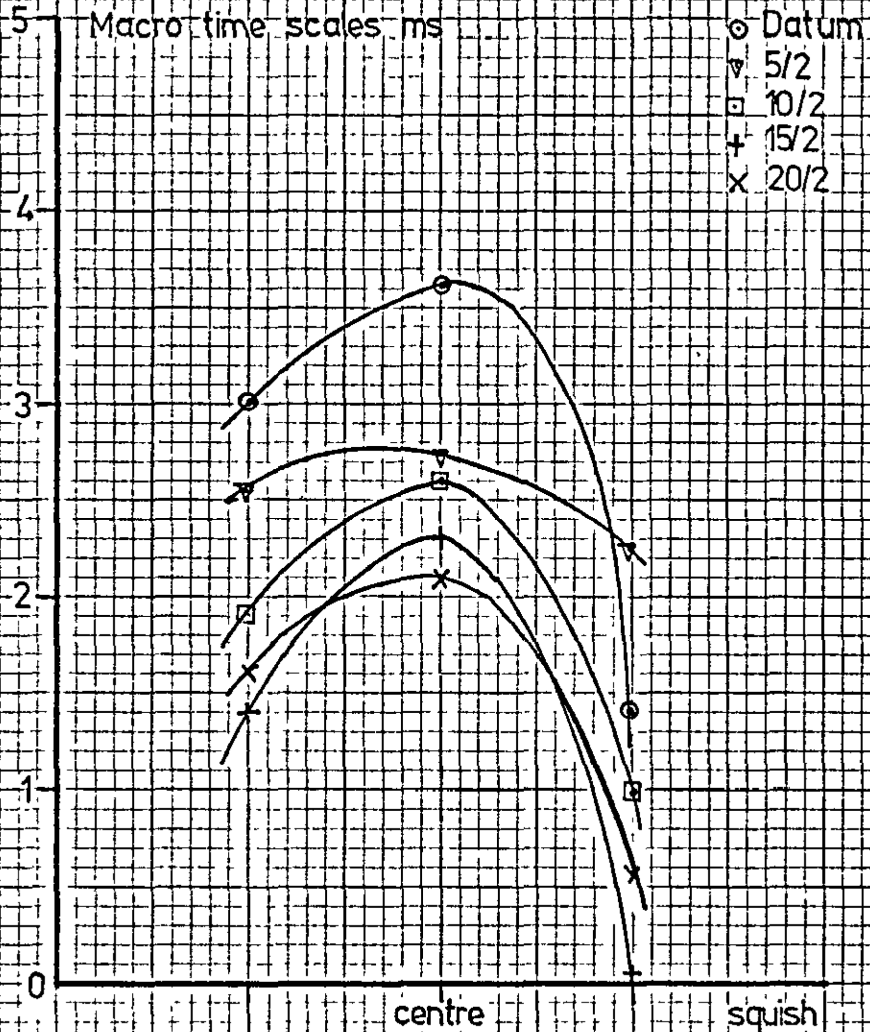

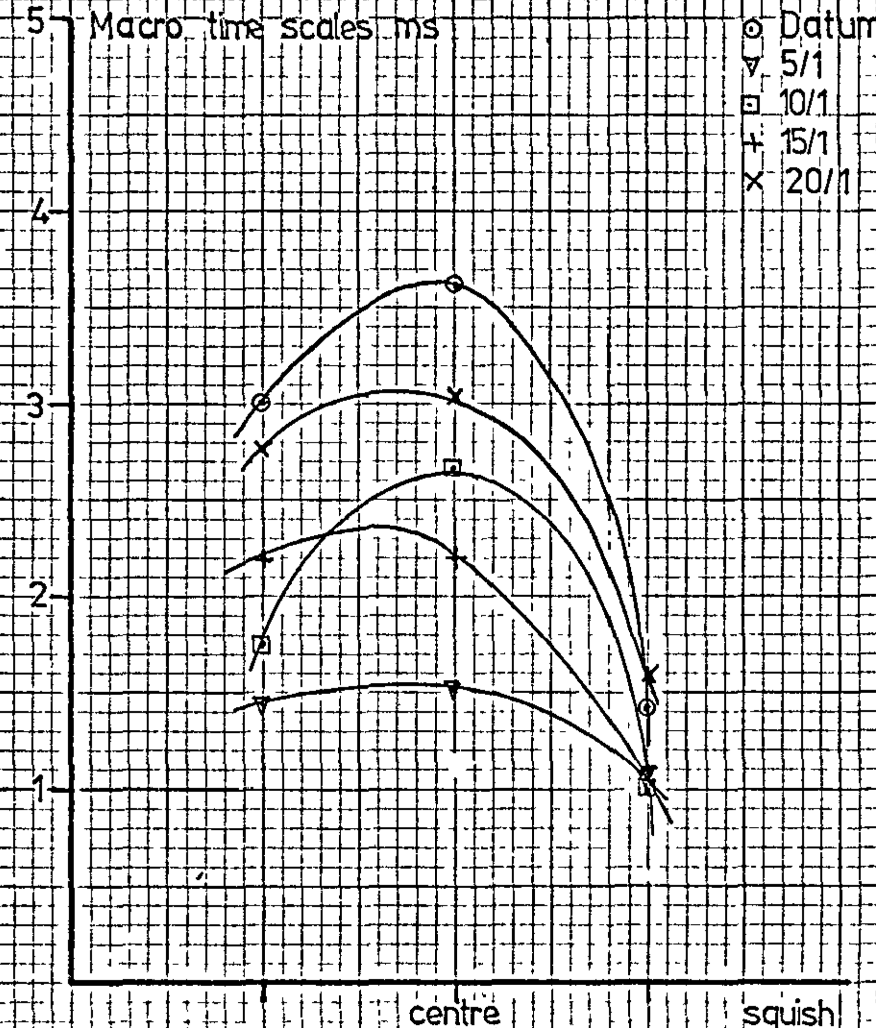

FIG 8.18 MACRO TIME SCALES OF TURBULENCE 1500 RPM AT TDC

CHAPTER 9

CONCLUSIONS

CONCLUSIONS

1. The mean air velocity increases with the engine speed.
2. The centre and the side of the combustion chamber opposite to the squish area are the areas influenced most by the squish velocities.
3. The propagation of the squish components depends on the magnitude of the squish area.
4. When no squish is present the air motion is a body swirl motion created by the intake jet. A local motion exists on the piston crown where a helical vortex is thought to form around the piston circumference.
5. For a given magnitude of squish area the effect on the air motion is more marked if the area is all in one place.
6. The turbulence intensity levels are not affected by the size of the squish area. From this point of view the turbulence structure is uniform through the combustion chamber.
7. The eddy size is only affected by large squish areas. In this case the eddies are large and are created as a result of the body motion imparted to the charge. Before this transition occurs their size does not vary with the amount of squish.
8. The eddy frequency increases with squish, more and faster eddies are created. This enhances the general level of turbulence.
9. The transition from turbulent isotropic motion to directional body motion occurs when more than 10 - 15% squish is present.
10. Eddies are largest and slowest in the centre of the c...

combustion chamber and smallest and fastest near the squish area. This is valid at all engine speeds.

CHAPTER 10

RECOMMENDATIONS

RECOMMENDATIONS

Future work should try to expand the scope of the work described here.

Squish chambers should be designed using the information already gained and with commercial production in mind. These should be studied in both motored and fired configurations. Valve timings and engine speeds closer to normal engine operations should be used.

There will be greater gains if the direction of the flow could be predicted. A multichannel anemometry system in conjunction with a multiwire probe could give the answer to these questions.

Also an investigation of the turbulence microscales could lead to higher accuracy in the prediction of the flow trends.

Future work should investigate the relationship between the effects of Squish on the flame propagation and the ability of an engine to run on lean mixtures.

A combustion model should be developed taking into account the specific effects of Squish on the flame propagation.

REFERENCES

1. Collis D.C. & Williams M.J.

Two Dimensional Convection from Heated Wires at Low Reynolds Numbers.

Journal of Fluid Mechanics. Vol. 6/1959.

2. Davies P.O.A.L. and Davis M.R.

The Hot Wire Anemometer.

I.S.A.V. Report No. 155 Oct. 1966.

3. Hassan H. and Dent J.C.

Correction for Temperature Loading and High Gas Pressure Effects for the Constant Temperature Hot Wire Anemometer.

British Journal for Applied Physics. 1969. Ser.2. Vol.2

4. D.R.Lancaster, Research Labs. G.M.Corp.

Effects of Engine Variables on Turbulence in a Spark Ignition Engine.

S.A.E. Paper No. 760159.

5. D.R. Lancaster, R.B.Krieger, Research Labs. G.M.Corp and S.C. Sorenson and W.L.Hull, Mech. Eng. Dept. Univ.of Illinois

Effects of Turbulence on Spark Ignition Engine Combustion.

S.A.E. Paper No. 760160

6. E.H. James.

Investigation of Turbulent Flow in the Combustion Chamber of a Spark Ignition Engine.

Ph. D. Thesis, L.U.T. 1972

7. Horvatin M., and Hussmann, A.W.

Measurement of Air Movements in Internal Combustion Engine Cylinders.

Disa Information No. 8 July 1969.

8. D.R. Lancaster, R.B.Krieger, J.H. Lienesch, Research Labs. G.M.Corp.

Measurement and Analysis of Engine Pressure Data.

S.A.E.Paper No. 750026.

9. Huebner, K.H. and McDonald A.T.

Experimental Determination of Airflow Patterns in Piston Engines with Induction Swirl.

S.A.E. Paper No. 720026.

10. Hassan H. and Dent J.C.

The Measurement of Air Velocity in a Motored Internal Combustion Engine Using a Hot Wire Anemometer.

Proceedings Inst. Mech. Eng. Vol. 185 50/75. 1975.

11. K.S. Varde, and G.G.Lucas.

Temperature History in the Combustion Chamber of a Spark Ignition Engine.

S.A.E. Paper No. 741017.

12. P.O. Witze.

Hot Wire Measurements of the Turbulence Structure in a Motored Spark Ignition Engine.

Sandia Laboratories 1975

13. E.H.James, G.G.Lucas.

Turbulent Flow in Spark Ignition Engine Combustion Chambers.

S.A.E. Paper No. 750885.

14. J.C.Dent, N. Salama.

Turbulence Structure in the Spark Ignition Engine.

I. Mech. E. paper No. C83/75

15. P.O.A.L. Davies, M.R.Davis, I. Wold.

Operation of the Constant Resistance Hot Wire Anemometer.

I.S.A.V. Report No. 189.

16. Instruction and Service Manual for Type 55D01 Anemometer Unit.

DISA.

17. Disa Probe Manual.

18. Davies P.O.A.L. and Fisher M.J.

Heat Transfer from Electrically Heated Cylinders.

Proceedings Royal Society. A280, 1964.

19. Lobo P.C.

The Determination of Velocity Patterns in Engine Cylinders by Means of the Hot Wire Anemometer.

P.H.D. Thesis London Univ. 1966

20. Horvatin M.

Some Problems Concerning the Analytical Evaluation of the Characteristics of Hot Wires Immersed in a Fluid of Variable Pressures and Temperatures.

Disa Information No. 8 July 1969.

21. Hinze J.O.

Turbulence

McGraw Hill New York 1959.

22. Hassan H.

Unsteady Heat Transfer in a Motored I.C.Engine.

Ph.D. Thesis 1968 L.U.T.

23. Salama N.S.

A study of Cyclic Variations in Gas Velocity and the Turbulence Structure in S.I.Engines.

Ph.D. Thesis L.U.T. 1974.

24. Davis M.R. and Davies P.O.A.L.

The Physical Characteristics of Hot Wire Anemometers.

I.S.A.V. Technical Report No. 2 /1968.

25. Russel V. Fisher and James P. Macey.

Digital Data Acquisition with Emphasis on Measuring Pressure Synchronously with Crank Angle

S.A.E. Paper No. 750028.

26. Semenov E.S.

Studies of Turbulent Gas Flow in Piston Engines.

N.A.S.A. Technical Translation F97.

27. Lancaster D.R.

The effects of Mixture Turbulence on Spark Ignition Engine Combustion.

Ph.D. Thesis. University of Illinois 1975.

28. Richard E. Winsor and Donald J. Patterson.

Mixture Turbulence - A Key to Cyclic Combustion Variation.

S.A.E. Paper No. 730086.

29. Tindal M.J., Williams T.J. and El Khafaji, A.H.A.

Gas Flow Measurements in Engine Cylinders.

S.A.E. Paper No. 740719.

29. P.O. Witze.

Hot Wire Measurements of the Turbulence Structure in a Motored Spark Ignition Engine.

Sandia Laboratories 1977

30. P.O. Witze.

Measurement of the Spatial Distribution and Engine Speed Dependence of Turbulent Air Motion in an I.C. Engine.

S.A.E. Paper No. 770220.

31. T.H. Ma,

Effect of Cylinder Charge Motion on Combustion.

I. Mech. E. Paper No. C81/75.

32. Andrews, C.E. D. Bradley, G.F. Hardy.

Hot Wire Anemometer Calibration for Measurement at Small Gas Velocities.

Int. J. Heat Mass Transfer. Vol. 15 pp 1765-1786. 1972.

33. Ohigashi, S. Hamamoto, Y. and Tanabe, S.

Technique of Measuring Gas Stream Velocity by Means of Electric Discharge.

Bulletin of the J.S.M.E. - Vol. 11, No.48, p. 1169, 1968

34. Ohigashi, S. Hamamoto, Y and Tanabe S,

Swirl - its Measurement and Effect on Combustion in a Diesel Engine.

Inst. Mech. E. Symposium on Air Pollution Control in Transport Engines, Nov. 9 - 11 1971.

35 Daneshyar H., Fuller D E., Decker E.L.

Vortex Motion Induced by the Piston of an Internal Combustion Engine

APPENDIX 1

EVALUATION OF THE POLYTROPIC INDEX OF COMPRESSION

Appendix 1

The gas temperatures which were measured as explained in Chapter were not used directly in the temperature compensation relationships. This was so because the wire response to the changes in temperature at around TDC of the compression stroke was observed to lag.

The alternative was to obtain the temperatures by using the polytropic relationship -

$$PV^n = K_1$$

or

$$P^{1-n} T^n = K_2$$

where K_1 and K_2 are constants and P, V and T are respectively the gas pressure, volume and temperature; n is the polytropic index of compression.

In the above relationship there is one variable which is not precisely known: the polytropic index n.

The literature survey revealed that the values of n used for similar purposes vary between 1.35 and 1.4. Some research workers allowed for the heat transfer, setting a low n, while others assumed or found that the heat transfer that takes place is not high enough to lower the value of γ below 1.4. It was thus desirable to find the relevant value of the index applicable specifically to the test in question. The polytropic law is based on the assumption that no mass transfer occurs and thus it is only applicable in this case when the valves are closed. It was therefore applied to the portion of the compression stroke that followed the closure of the intake valve.

Looking at the polytropic law

$$PV^n = K_1$$

and taking the logs of both sides of the equation the following relationship is obtained

$$\log P + n \cdot \log V = \log K_1 = C$$

This represents the equation of a straight line, of slope n and it provided the solution to the problem of finding the polytropic index applicable to the engine tests.

From the crank radius and connective rod geometry the volume of gas trapped above the piston can be calculated at any point in the engine cycle. This is given by:

$$V = \frac{\pi D^2}{4}\left(r + l + h - r \cdot \cos\alpha - \sqrt{l^2 - r^2 \sin^2\alpha}\right)$$

where

D = bore

R = crank radius = $\frac{\text{stroke}}{2}$

l = connecting rod length

h = combustion chamber height (applicable to disc chamber only)

α = angle of crank rotation (origin at TDC intake)

The above formula is likely to give erroneous results when used for piston positions very near the top dead centre. This is because the volume of air trapped between the piston and liner and situated above the top piston ring is not taken into account. This is negligible compared to the chamber volume when the piston is far from TDC. However near TDC, the neglected volume becomes higher compared to the combustion chamber volume and the induced error increases.

Following this consideration the last 30° of the compression stroke were not included in the analysis.

Consequently the pressures measured in the experimental runs and the corresponding gas volumes were tabulated at every 10° starting at 220° ABDC till 30° BTDC. The logs were taken of these and log V was plotted against log P. The plot was a straight line of slope - 1.4 and this value was used to calculate the gas temperature from the pressure data. Fig I.1

A reference point was necessary and this was the point at which the intake valve closes. During the exhaust stroke and the following intake stroke the gas temperature in a motored engine stays practically constant and a value for this can be confidently taken from the temperature readings. This was found to be $315^{\circ}K$. This value, coupled with the corresponding pressure at IVC provided the reference point. The gas temperatures in the rest of the cycle were found using these values and the current gas pressure value for which the temperature was calculated.

The value of $n = \gamma = 1.4$, proves that the heat transfer that exists in the engine is not high enough to create non isentropic conditions.

Pressure - Volume data used to determine the polytropic index of compression n.

α (ATDC)	V(cc)	P(N/cm ^{2})	Log V	Log P
220	578.37	9.1313	2.762	0.960
230	549.98	9.9605	2.740	0.998
240	515.87	10.8819	2.712	1.036
250	476.55	12.0797	2.678	1.082
260	432.80	13.8303	2.636	1.141
270	385.68	16.3181	2.586	1.212
280	336.52	19.8193	2.527	1.297
290	286.91	24.979	2.457	1.397
300	238.63	32.3501	2.377	1.509
310	193.58	43.1302	2.286	1.634
320	153.62	58.8859	2.186	1.77
330	120.49	80.999	2.81	1.908

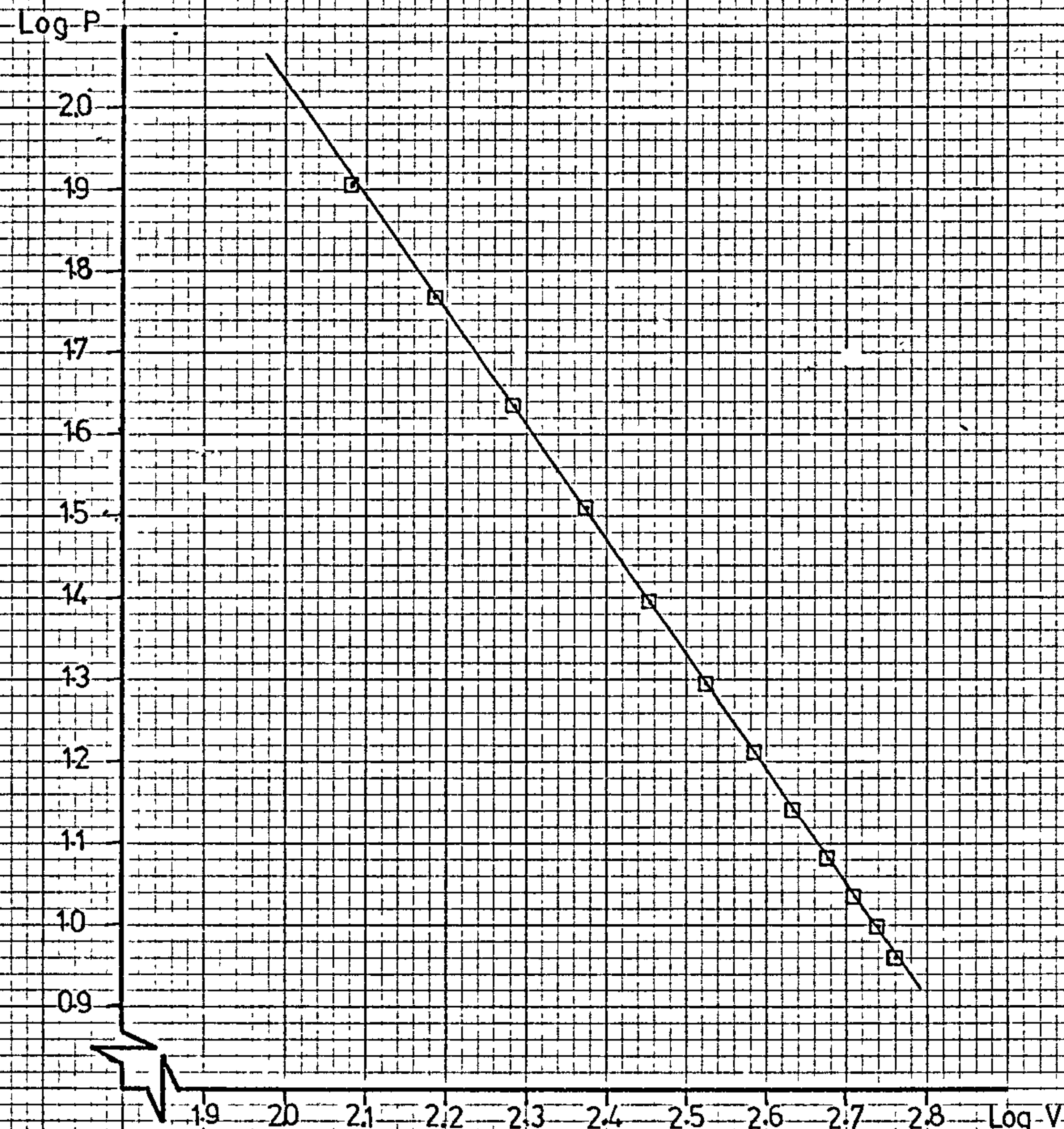

FIG I.1 THE POLYTROPIC INDEX OF COMPRESSION

APPENDIX 2

EXPERIMENTAL PROCEDURE

Experimental Procedure.

Prior to every test the anemometer was allowed to warm up for at least one hour. The probe was inserted in the combustion chamber with the cylinder head removed. It was ensured that the wire was perfectly aligned, and that the probe was accurately located in the axial direction. The cylinder head and rocker box were then replaced and the rig was started.

At the same position in the combustion chamber measurements were taken at three engine speeds: 750, 1000 and 1500 rpm. Following this the probe was traversed across the combustion chamber to its new position and the procedure was repeated.

The positions in the combustion chamber where recordings were made are shown in the diagram.

APPENDIX 3

COMPUTER PROGRAM FOR HOT WIRE PROBE CALIBRATION

```
      MASTER NURE
      DIMENSION TCNU(30),RE(30),REP(30),YCALC(30),ERROR(30),A(2)
      DIMENSION BRV(30),TPR(30),DP(30)
      READ(1,100)TAMB,ALPHA,RCOLD,RCOMP,RLEAD,ROP,WD,WL,PGAS
      TOP=TAMB+(ROP/RCOLD-1.0)/ALPHA
      WRITE(2,201)TAMB,RCOLD,ROP,WL,TOP,PGAS
      TFILM=(TOP+TAMB)/2.0
      T=TFILM-273.0
      Y=0.001*TFILM
      CONDG=2.41E-2+7.6397E-5*T-5.061E-8*(T**2.0)
      VISC=(0.43868+5.13195*Y-1.31065*(Y**2.0)-0.668597*(Y**3.0)+
     10.922798*(Y**4.0)-0.342237*(Y**5.0)+0.042674*(Y**6.0))/100000.0
      RHO=PGAS/(287.0*TFILM)
      DO 1 I=1,20
      READ(1,101)BRV(I),TPR(I),DP(I)
    1 CONTINUE
      DO 2 J=1,20
      TGRAD=TOP-TPR(J)
      BRI=BRV(J)/(ROP+RLEAD+RCOMP)
      QSUP=BRI**2.0*ROP
      QCOND=0.14264E-2-0.32763E-5*TGRAD+0.7251E-7*(TGRAD**2.0)-0.51078
     1E-10*(TGRAD**3.0)
      QRAD=1.788E-8*WD*WL*(TOP**4.0-TAMB**4.0)
      RNU=0.31831*(QSUP-QCOND-QRAD)/(WL*CONDG*(TOP-TAMB))
      TCNU(J)=RNU*(TAMB/TFILM)**0.17
      V=44.8218*SQRT((1.0-(1.0-DP(J)/PGAS)**0.2857)*TAMB)
      RE(J)=RHO*V*WD/VISC
    2 CONTINUE
      P=0.4
    4 WRITE(2,202)P
      DO 3 K=1,20
      REP(K)=RE(K)**P
    3 CONTINUE
      CALL E02ACF(REP,TCNU,20,A,2,REF)
      WRITE(2,203)
      DO 6 J=1,20
      YCALC(J)=A(1)+A(2)*REP(J)
      ERROR(J)=100.0*(TCNU(J)-YCALC(J))/TCNU(J)
      WRITE(2,200)REP(J),TCNU(J),YCALC(J),ERROR(J)
    6 CONTINUE
      WRITE(2,204)A(1),A(2)
      P=P+0.01
      IF(P-0.55)4,4,5
    5 CONTINUE
  100 FORMAT(F6.2,F9.7,F5.3,F5.2,F6.4,F6.3,F9.7,F8.6,F10.3)
  101 FORMAT(F7.4,F6.2,F9.4)
  200 FORMAT(2X,F7.4,10X,F6.4,10X,F6.4,10X,F6.2)
  201 FORMAT(///////,30H AMBIENT TEMPERATURE(DEG K)=   ,F6.2/,30H COLD RE
     1SISTANCE(OHMS)=          ,F5.3/,30H OPERATING RESISTANCE(OHMS)=  ,F6.
     23/,30H HOT WIRE LENGTH(M)=              ,F8.6/,30H OPERATING TEMPERAT
     3URE(DEG K)=,F6.2/,30H GAS PRESSURE(N/SQM)=          ,F10.3)
  203 FORMAT(3X,5HRE**P,12X,4HTCNU,11X,5HYCALC,12X,5HERROR/)
  202 FORMAT(/////,2X,2HP=,F4.2,//)
  204 FORMAT(/,2X,5HA(1)=,F10.5,5X,5HA(2)=,F10.5)
      STOP
      END
```

APPENDIX 4

COMPUTER PROGRAM FOR FLOW CHARACTERISTICS EVALUATION

```
JB FLOW;B;RA2889
JBCORE 40K
LERK $TT
REATE FRED,LIMSIZE=200K
ET CR1,/ARPRESS
ET CR2,/ARTEMP
JFORTRAN
N TRO(NON-STANDARD),ONLINE
SE MTO,FRED
UN CRO(DATA);;1700
***
```

```
OMPILATION BY #XFAT MK 6A    DATE  19/12/77  TIME  19/42/20
```

```
      LIST
      SEND TO (ED,SEMICOMPUSER.AXXX)
      DUMP ON (ED,PROGRAM USER)
      WORK (ED,WORKFILEUSER)
      RUN
      LIBRARY(ED,SUBGROUPGINO)
      PROGRAM(FLOW)
      INPUT 1 = CRO
      INPUT 2 = MT1/FORMATTED(GUSTAV9)/1284
      INPUT 3 = CR1
      INPUT 4 = CR2
      CREATE 5 = MTO/UNFORMATTED (FRED  (1;4095))/1030
      OUTPUT 6 = LPO
      END
```

```
      MASTER FLOW
      INTEGER E,BC
      DIMENSION IDAT(512),U(512)
      DIMENSION PGAS(512),TPR(512),TGAS(512),CONDG(512),RHO(512)
      DIMENSION QCOND(512);QRAD(512),UMEAN(512),TURB(512);RTURB(512)
      DIMENSION TSCA(30),ALSCA(30),FI(512);PHI(30),VISC(512),TFILM(512)
      CALL LU1934
      CALL WINDOW(2)
      READ(1,107)NCYCL
      WRITE(6,203)NCYCL
      ANCYCL=NCYCL
      READ(1,108)SPEED
      WRITE(6,204)SPEED
      FI(1)=0.0
      DO 16 K=2,510
      FI(K)=FI(K-1)+1.0
   16 CONTINUE
      PHI(1)=45.0
      DO 17 K=2,28
      PHI(K)=PHI(K-1)+15.0
   17 CONTINUE
C
C GENERAL DATA REFERING TO ANEMOMETER OPERATION
```

```
      READ(1,102)TAMB,ALPHA,RCOLD,RCOMP,RLEAD,ROP,WD,WL
      TOP=TAMB+(ROP/RCOLD-1.0)/ALPHA
      WRITE(6,201)TAMB,RCOLD,ROP,WL,TOP
      READ(1,103)A,B,P
      WRITE(6,202)A,B,P
C
C COMPUTATION OF GAS CHARACTERISTICS DURING CYCLE
C
      READ(1,104)TBDC,PBDC
      READ(3,105)(PGAS(I),I=1,512)
      READ(4,109)(TPR(I),I=1,512)
      DO 3 J=1,510
      TGAS(J)=TBDC*((PGAS(J)/PBDC)**0.2857)
      TFILM(J)=(TOP+TGAS(J))/2.0
      T=TFILM(J)-273.0
      Y=0.001*TFILM(J)
      CONDG(J)=2.41E-2+7.6397E-5*T-5.061E-8*(T**2.0)
      VISC(J)=(0.43868+5.13195*Y-1.31065*(Y**2.0)-0.668597*(Y**3.0)+
     10.922798*(Y**4.0)-0.342237*(Y**5.0)+0.042674*(Y**6.0))/100000.0
      RHO(J)=PGAS(J)/(287.0*TFILM(J))
      TGRAD=TOP-TPR(J)
      QCOND(J)=0.14264E-2-0.32763E-5*TGRAD+0.7251E-7*(TGRAD**2.0)
     1-0.51078E-10*(TGRAD**3.0)
      QRAD(J)=1.788E-8*WD*WL*(TOP**4.0-TGAS(J)**4.0)
    3 CONTINUE
C
C INPUT OF BRIDGE VOLTAGE DATA ON MAGNETIC TAPE STORE
C
      READ(2,100)E,BC
      E=E/64
      CONST=8.0*BC*(10.0**E)/(32767.0**2.0)
      NSKIP=800
      DO 19 K=1,NSKIP
      READ(2,101)(IDAT(J),J=1,512)
   19 CONTINUE
      DO 1 N=1,NCYCL
      READ(2,101)(IDAT(J),J=1,512)
      DO 2 K=1,510
      BRV=IDAT(K)*CONST
      BRI=BRV/(ROP+RLEAD+RCOMP)
      QSUP=BRI**2*ROP
      RNU=0.31831*(QSUP-QCOND(K)-QRAD(K))/(WL*CONDG(K)*(TOP-TGAS(K)))
      UFACT=(RNU*((TGAS(K)/TFILM(K))**0.17)-A)/B
      U(K)=(ABS(UFACT))**(1.0/P)*VISC(K)/(RHO(K)*WD)
    2 CONTINUE
      U(2)=(U(1)+U(3))/2.0
      U(258)=(U(257)+U(259))/2.0
      WRITE(5)(U(M),M=1,510)
    1 CONTINUE
C
C COMPUTATION OF GAS MEAN VELOCITIES
C
      REWIND 5
      DO 4 M=1,NCYCL
      READ(5)(U(I),I=1,510)
      DO 4 K=1,510
      IF(M-1)5,5,6
    5 UMEAN(K)=U(K)/ANCYCL
      GO TO 4
    6 UMEAN(K)=UMEAN(K)+U(K)/ANCYCL
    4 CONTINUE
```

```
      WRITE(6,211) (UMEAN(I),I=1,510)
      CALL AXISCA(1,17,0,0,510.0,1)
      CALL AXISCA(1,10,0,0,100.0,2)
      CALL GRID(0,1,1)
      CALL GRAPOL(FI,UMEAN,510)
      CALL PICCLE
C
C COMPUTATION OF TURBULENCE INTENSITY
C
      REWIND 5
      DO 7 M=1,NCYCL
      READ(5)(U(I),I=1,510)
      DO 7 K=1,510
      IF(M-1)8,8,9
    8 TURB(K)=SQRT((U(K)-UMEAN(K))**2)/ANCYCL
      GO TO 7
    9 TURB(K)=TURB(K)+SQRT((U(K)-UMEAN(K))**2)/ANCYCL
    7 CONTINUE
      WRITE(6,212)(TURB(I),I=1,510)
      CALL AXISCA(1,17,0.0,510.0,1)
      CALL AXISCA(1,15,0.0,30.0,2)
      CALL GRID(0,1,1)
      CALL GRAPOL(FI,TURB,510)
      CALL PICCLE
C
C COMPUTATION OF RELATIVE TURBULENCE INTENSITY
C
      DO 10 I=1,510
      RTURB(I)=TURB(I)/UMEAN(I)
   10 CONTINUE
      WRITE(6,213)(RTURB(I),I=1,510)
      CALL AXISCA(1,17,0.0,510.0,1)
      CALL AXISCA(1,10,0.0,1.0,2)
      CALL GRID(0,1,1)
      CALL GRAPOL(FI,RTURB,510)
      CALL PICCLE
C
C COMPUTATION OF AUTOCORRELATION COEFFICIENTS
C
      REWIND 5
      DO 11 M=1,NCYCL
      READ(5)(U(I),I=1,510)
      J=0
      DO 11 K=45,450,15
      J=J+1
      ACOR=0
      FLREF=U(K)-UMEAN(K)
      DO 12 N=1,40
      FLPAST=U(K-N)-UMEAN(K-N)
      ACOR=ACOR+(FLREF*FLPAST)/(TURB(K)*TURB(K-N))
   12 CONTINUE
C
C COMPUTATION OF TURBULENCE MACRO SCALES
C
      IF(M-1)13,13,14
   13 TSCA(J)=0.16666*ACOR/(ANCYCL*SPEED)
      GO TO 11
   14 TSCA(J)=TSCA(J)+0.16666*ACOR/(ANCYCL*SPEED)
   11 CONTINUE
      DO 18 K=1,28
      TSCA(K)=ABS(TSCA(K))
   18 CONTINUE
```

```
      WRITE(6,214)(TSCA(I),I=1,28)
      CALL AXISCA(1,9,45.0,450.0,1)
      CALL AXISCA(1,10,0.0,0.0080,2)
      CALL GRID(0,1,1)
      CALL GRAPOL(PHI,TSCA,28)
      CALL PICCLE
      K=45
      DO 15 I=1,28
      ALSCA(I)=TSCA(I)*UMEAN(K)
      K=K+15
   15 CONTINUE
      WRITE(6,215)(ALSCA(I),I=1,28)
      CALL AXISCA(1,9,45.0,450.0,1)
      CALL AXISCA(1,15,0.0,0.150,2)
      CALL GRID(0,1,1)
      CALL GRAPOL(PHI,ALSCA,28)
      CALL PICCLE
      CALL DEVEND
  100 FORMAT(10X,2I10,22X)
  101 FORMAT(256I10)
8    IS THIS LARGE A REPEAT COUNT INTENDED AT ABOUT COLUMN 15, LINE 0181

  102 FORMAT(F6.2,F9.7,F5.3,F5.2,F6.4,F6.3,F9.7,F8.6)
  103 FORMAT(3F6.4)
  104 FORMAT(F6.2,F9.2)
  105 FORMAT(8(1X,F9.1))
  107 FORMAT(I3)
  108 FORMAT(F6.1)
  109 FORMAT(8(1X,F9.3))
  201 FORMAT(1X,27HAMBIENT TEMPERATURE(DEG K)=,F6.2/
     1,1X,22HCOLD RESISTANCE(OHMS)=,F5.3/
     2,1X,27HOPERATING RESISTANCE(OHMS)=,F6.3/
     3,1X,19HHOT WIRE LENGTH(M)=,F8.6/
     4,1X,29HOPERATING TEMPERATURE(DEG K)=,F6.2)
  202 FORMAT(1X,28HCALIBRATION CONSTANTS      A=,F6.4/,27X,2HB=,F6.4/,
     127X,2HN=,F6.4)
  203 FORMAT(////////,1X,30HNUMBER OF CYCLES INVESTIGATED=,I3)
  204 FORMAT(1X,18HENGINE SPEED(RPM)=,F6.1)
  211 FORMAT(///,51X,18HMEAN VELOCITY(M/S)//,10(1X,F11.3))
  212 FORMAT(///,47X,25HTURBULENCE INTENSITY(M/S)//,10(1X,F11.3))
  213 FORMAT(///,45X,29HRELATIVE TURBULENCE INTENSITY//,10(1X,F11.4))
  214 FORMAT(///,42X,36HTIME MACRO-SCALES OF TURBULENCE(SEC)//,
     14(15X,F11.8))
  215 FORMAT(///,42X,36HLENGTH MACRO-SCALES OF TURBULENCE(M)//,
     14(15X,F11.5))
      STOP
      END

MENT, LENGTH  1022, NAME  FLOW  -   COMMENTS


      FINISH

PILATION -  NO ERRORS   1 COMMENT

E:      27 BUCKETS USED
```